Calhoun: The NPS Institutional Archive

DSpace Repository

Theses and Dissertations 1. Thesis and Dissertation Collection, all items

1981

A numerical study of the role of air-sea fluxes in extratropical cyclogenesis.

Sandgathe, Scott Alphonse

Monterey, California. Naval Postgraduate School

http://hdl.handle.net/10945/20621

Downloaded from NPS Archive: Calhoun

Calhoun is the Naval Postgraduate School's public access digital repository for research materials and institutional publications created by the NPS community. Calhoun is named for Professor of Mathematics Guy K. Calhoun, NPS's first appointed -- and published -- scholarly author.

Dudley Knox Library / Naval Postgraduate School
411 Dyer Road / 1 University Circle
Monterey, California USA 93943

http://www.nps.edu/library

A NUMERICAL STUDY OF THE ROLE OF AIR-SEA FLUXES IN EXTRATROPICAL CYCLOGENESIS

Scott Alphonse Sandgathe

NAVAL POSTGRADUATE SCHOOL
Monterey, California

THESIS

A NUMERICAL STUDY OF THE ROLE OF AIR-SEA FLUXES IN EXTRATROPICAL CYCLOGENESIS

by

Scott Alphonse Sandgathe

September 1981

Thesis Advisor: R.L. Elsberry

Approved for public release; distribution unlimited.

T200705

REPORT DOCUMENTATION PAGE		READ INSTRUCTIONS BEFORE COMPLETING FORM
1. REPORT NUMBER	2. GOVT ACCESSION NO.	3. RECIPIENT'S CATALOG NUMBER
4. TITLE (and Subtitle) A Numerical Study of the Role of Air-Sea Fluxes in Extratropical Cyclogenesis		5. TYPE OF REPORT & PERIOD COVERED Ph.D. Thesis; September 1981
		6. PERFORMING ORG. REPORT NUMBER
7. AUTHOR(s) Scott Alphonse Sandgathe		8. CONTRACT OR GRANT NUMBER(s)
9. PERFORMING ORGANIZATION NAME AND ADDRESS Naval Postgraduate School Monterey, California 93940		10. PROGRAM ELEMENT, PROJECT, TASK AREA & WORK UNIT NUMBERS
11. CONTROLLING OFFICE NAME AND ADDRESS Naval Postgraduate School Monterey, California 93940		12. REPORT DATE September 1981
		13. NUMBER OF PAGES 134
14. MONITORING AGENCY NAME & ADDRESS (if different from Controlling Office)		15. SECURITY CLASS. (of this report) Unclassified
		15a. DECLASSIFICATION/DOWNGRADING SCHEDULE

16. DISTRIBUTION STATEMENT (of this Report)

Approved for public release; distribution unlimited.

17. DISTRIBUTION STATEMENT (of the abstract entered in Block 20, if different from Report)

18. SUPPLEMENTARY NOTES

19. KEY WORDS (Continue on reverse side if necessary and identify by block number)

Cyclogenesis; Extratropical Cyclogenesis; Air-sea Fluxes; Surface Fluxes; Ocean Cyclogenesis; Polar Low; Diabatic Processes

20. ABSTRACT (Continue on reverse side if necessary and identify by block number)

This study uses a numerical model to investigate the effect of the air-sea fluxes of sensible heat and moisture in extratropical cyclogenesis over the open ocean. The model is a sectorized version of the UCLA general circulation model including the Arakawa-Schubert cumulus parameterization scheme and the Randall version of the Deardorff planetary boundary layer parameterization. Idealized initial conditions are specified in the atmosphere and ocean that are typical of open-ocean fall and spring conditions.

DD FORM 1 JAN 73 1473 EDITION OF 1 NOV 65 IS OBSOLETE
S/N 0102-014-6601

#20 - ABSTRACT - (CONTINUED)

Adiabatic and diabatic model results are compared over a 15-day integration period. Diabatic processes, including the surface fluxes, cause a large reduction in low-level static stability during the initial cyclone growth period. This reduction in static stability, as well as the latent heat release, leads to the rapid growth of wave numbers 12 and 18 in the diabatic model experiment, while only wave number 6 is present in the adiabatic experiment. The growth of the cyclones is much more rapid in the diabatic experiment. However, cyclones in the adiabatic experiment attain similar maximum intensities as in the diabatic experiment, and undergo an analogous decay period. After development of the initial cyclone, a variety of secondary low developments occur in the diabatic experiments that are similar to those observed over the open ocean.

The role of the air-sea fluxes is studied by selectively removing the surface fluxes at various stages of the cyclone development. Removal of the air-sea fluxes produces significant changes in the evolution of the diabatic model cyclones. Removal of the surface sensible heat flux results in an intensified low-level temperature gradient in the developing cyclone. The enhanced low-level temperature advection increases large-scale lifting, and therefore latent heat release, resulting in an intensification of the cyclone. Removal of the surface moisture flux prevents the development of secondary lows which might otherwise eventually replace the primary cyclone, as occurs in the complete diabatic model. These model results are not verifiable with observations, however, they show a mechanism by which some disturbances over the ocean could develop while other seemingly similar disturbances would not.

A Numerical Study of the Role of Air-Sea Fluxes in Extratropical Cyclogenesis

by

Scott Alphonse Sandgathe
Lieutenant, United States Navy
B.S., Oregon State University, 1972

Submitted in partial fulfillment of the
requirements for the degree of

DOCTOR OF PHILOSOPHY

from the

NAVAL POSTGRADUATE SCHOOL

Thesis
S7185
c.1

ABSTRACT

This study uses a numerical model to investigate the effect of the air-sea fluxes of sensible heat and moisture in extratropical cyclogenesis over the open ocean. The model is a sectorized version of the UCLA general circulation model including the Arakawa-Schubert cumulus parameterization scheme and the Randall version of the Deardorff planetary boundary layer parameterization. Idealized initial conditions are specified in the atmosphere and ocean that are typical of open-ocean fall and spring conditions.

Adiabatic and diabatic model results are compared over a 15-day integration period. Diabatic processes, including the surface fluxes, cause a large reduction in low-level static stability during the initial cyclone growth period. This reduction in static stability, as well as the latent heat release, leads to the rapid growth of wave numbers 12 and 18 in the diabatic model experiment, while only wave number 6 is present in the adiabatic experiment. The growth of the cyclones is much more rapid in the diabatic experiment. However, cyclones in the adiabatic experiment attain similar maximum intensities as in the diabatic experiment, and undergo an analogous decay period. After development of the initial cyclone, a variety of secondary low developments occur in the diabatic experiments that are similar to those observed over the open ocean.

The role of the air-sea fluxes is studied by selectively removing the surface fluxes at various stages of the cyclone development. Removal of the air-sea fluxes produces significant changes in the evolution of the diabatic model cyclones. Removal of the surface sensible heat flux results in an intensified low-level temperature gradient in the developing cyclone. The enhanced low-level temperature advection increases large-scale lifting and therefore latent heat release, resulting in an intensification of the cyclone. Removal of the surface moisture flux prevents the development of secondary lows which might otherwise eventually replace the primary cyclone, as occurs in the complete diabatic model. These model results are not verifiable with observations, however, they show a mechanism by which some disturbances over the ocean could develop while other seemingly similar disturbances would not.

TABLE OF CONTENTS

I. INTRODUCTION ---------------------------------- 14

II. THE ATMOSPHERIC MODEL ------------------------ 20

- A. FINITE DIFFERENCE SCHEME ------------------ 20
- B. DIABATIC PARAMETERIZATION ----------------- 25
- C. MODEL VARIATIONS -------------------------- 28
- D. INITIALIZATION ---------------------------- 29

III. LARGE SCALE RESPONSE ------------------------- 37

- A. DIABATIC-ADIABATIC COMPARISON ------------- 39
- B. SURFACE FLUX MODIFICATION TO THE PRIMARY LOW DEVELOPMENT ------------------ 48

IV. INITIAL DEVELOPMENT -------------------------- 57

- A. DIABATIC CONTRIBUTIONS TO WAVE GROWTH ----- 58
- B. SURFACE FLUX MODIFICATION OF GROWTH ------- 68

V. SECONDARY LOW DEVELOPMENT EXPERIMENT ---------- 80

- A. CASE A--FALL HEMISPHERE DAYS 6-8 ---------- 84
- B. CASE B--FALL HEMISPHERE DAYS 10-12 -------- 103
- C. CASE C--SPRING HEMISPHERE DAYS 10-12 ------ 107
- D. CASE D--SPRING HEMISPHERE DAYS 9-11 ------- 111
- E. SUMMARY ----------------------------------- 121

VI. CONCLUSIONS ---------------------------------- 124

LIST OF REFERENCES ------------------------------- 128

INITIAL DISTRIBUTION LIST ------------------------ 132

LIST OF TABLES

TABLE PAGE

2-1. Summary of the model features ------------ 26

3-1. Experiments for the large-scale study ---- 38

3-2. Central pressures (mb) for the primary cyclone/anticyclone by experiment for days 4, 6 and 8 -------------------------- 49

4-1. Experiments for the initial development study --------------------------------------- 57

4-2. Surface fluxes of zonal mean sensible heat (S) and moisture (Q) in W/m^2 at day 2. (Q is in latent heat equivalent.) ---- 68

5-1. Experiments for the secondary development study ------------------------ 81

LIST OF FIGURES

FIGURE PAGE

2-1. Vertical distribution of model large-scale prognostic variables. Pressure values of sigma levels vary with surface pressure. A surface value of 1000 mb is assumed in this figure. -- 22

2-2. Horizontal distribution of model large-scale prognostic variables. $\pi\dot{\sigma}$ which is not shown is carried at T-points. (Arakawa scheme C) ---- 24

2-3. Initial zonal wind (solid) and temperature (dash) profiles. Contours 10 m/s (dot-dash 5 m/s) and 10°C. ------------------------------------ 31

2-4. Model (solid) and climatological (dash) sea-surface temperatures. Climatology adapted from Robinson (1976) at approximately 160°W for April (southern hemisphere) and October (northern hemisphere). ------------------------- 33

2-5. Model initial specific humidity at sigma levels 6, 5 and 4 (approximately 900, 700 and 500 mb) compared with climatological northern hemisphere zonal mean values from Oort and Rasmussen (1971) for April (southern hemisphere) and October (northern hemisphere). ----------------- 35

3-1. Surface pressure for A after six days of integration for a. northern hemisphere and b. southern hemisphere. Contour interval 4 mb. Southern hemisphere inverted with pole (south) at top (east remains toward right). ------------ 40

3-2. As in Fig. 3-1 except for diabatic model (D). -- 40

3-3. Vertical phases of wavenumber 6 mode along 40°S for A after 2 days of integration. V is meridional wind, T is temperature, and $\dot{\sigma}$ is vertical velocity. ----------------------------------- 41

3-4. Surface pressure for DR after five days of integration for a. northern hemisphere and b. southern hemisphere. Contour interval 4 mb. -- 44

3-5. Position of streamline troughs at sigma level 3 (300 mb) in the southern hemisphere for a. A and b. D. ------------------------------- 45

3-6. As in Fig. 3-2 except after four days of integration. ---------------------------------- 46

3-7. Northern hemisphere surface pressure at day 6 for a. D-FS, b. D-FQ and c. D-FSQ. Contour interval 4 mb. ----------------------------------- 50

3-8. Northern hemisphere surface moisture flux rate at day 6 for D. Contour interval 4 mm/day. -- 51

3-9. Northern hemisphere specific humidity fields at sigma level 6 (900 mb) at day 6 for a. D, b. D-FS, c. D-FQ and d. D-FSQ. Contour interval 2 g/kg. -------------------------------- 53

3-10. As in Fig. 3-9 except for temperature fields. Contour interval 5°C. Also shown (next page) e. experiment F. -------------------------------- 54

4-1. Exponential growth rate between days 2.5 and 3.5 for the meridional velocity perturbation by wavenumber (see text for description) for a. sigma level 3 (300 mb), 36°S, b. sigma level 3, 46°N, c. sigma level 6 (900 mb), 36°S and d. sigma level 6, 46°N. Experiments D, A and A36 are compared. --------------- 59

4-2. Location of streamline troughs at day 3 for a. A and b. D. ---------------------------------- 61

4-3. Change in potential temperature differences with pressure between sigma levels 4 and 6 (500 to 900 mb) in °C/100 mb for a. 36°S and b. 46°N. ---------------------------------- 64

4-4. As in Fig. 4-3. S and Q represent experiments D-FS and D-FQ respectively. -------------- 69

4-5. Amplitude (m/s) of the meridional wind perturbation by wavenumber for day 2 (stippled) and day 3 (hatched) for a. 46°N and b. 36°S. D, S and Q as in Fig. 4-4. -------------------- 71

4-6. Amplitude (m/s) at day 3 of the meridional wind perturbation summed over wavenumbers 6 through 30 for a. 46° N and b. 36° S. Experiments D, S(D-FS), Q(D-FQ) and A are compared. -- 74

4-7. As in Fig. 4-6 except for temperature perturbation (°C). ------------------------------ 76

4-8. As in Fig. 4-6 except for vertical velocity perturbation ($10^{-4}m^2$ mb/s). -------------------- 77

5-1. Surface pressure maps for D for a. Case A, day 6.5, b. Case B, day 11, c. Case C, day 11 and d. Case D, D-FSQ, day 10.5. Contour interval 4 mb. Secondary low for case study indicated by an arrow in each figure. --------- 83

5-2. Expanded surface pressure maps of the secondary low for Case A at day 6 in the fall hemisphere for a. D, b. D-FS, c. D-FQ and d. D-FSQ. Contour interval 2 mb. -- 85

5-3. As in Fig. 5-2 except for day 6.25. ----------- 86

5-4. As in Fig. 5-2 except for day 6.5. ------------ 87

5-5. As in Fig. 5-2 except for day 8. -------------- 88

5-6. Temperature field with vector winds at lowest sigma level (900 mb) for day 6.25 using the expanded region as in Fig. 5-3 for a. D, b. D-FS, c. D-FQ and d. D-FSQ. Contour interval 2°C. X indicates position of secondary low. Vector length proportional to square root of wind speed. Speed also given at vector head (m/s). Direction of vector toward wind speed value. ------------------ 90

5-7. Precipitation rate for day 6 and expanded region as in Fig. 5-2 for a. D and b. D-FS. Contour interval 2 cm/day. Experiments D-FQ and D-FSQ not shown as rate less than 2 cm/day. ------------------------------------- 91

5-8. Precipitation rate for day 6.25 and expanded region as in Fig. 5-3 for a. D, b. D-FS, c. D-FQ and d. D-FSQ. ------------------------ 92

5-9. Specific humidity at the lowest model sigma level (900 mb) for day 6 and expanded region as in Fig. 5-2 for a. D, b. D-FS, c. D-FQ and d. D-FSQ. Contour interval 1 g/kg. ------ 93

5-10. Term D of the Petterssen development equation for day 6.25 and an expanded region as in Fig. 5-3 for a. D, b. D-FS, c. D-FQ and d. D-FSQ. Contour interval 5 x 10^{-5} °C/s (4.3 °C/day). Position of secondary low indicated by X. See text for discussion. ----- 98

5-11. As in Fig. 5-10 except for term E. ------------ 99

5-12. As in Fig. 5-10 except for term F. ------------ 101

5-13. As in Fig. 5-10 except for term C. Contour interval 5 x 10^{-9}. ---------------------------- 102

5-14. Expanded surface pressure maps of the secondary low for Case B at day 10.5 in the fall hemisphere for a. D, b. D-FS, c. D-FQ and d. D-FSQ. Contour interval 2 mb. -- 104

5-15. As in Fig. 5-14 except for day 11. ------------ 105

5-16. As in Fig. 5-14 except for day 11.25. --------- 106

5-17. Term D of the Petterssen development equation for day 11 and an expanded region as in Fig. 5-15 for a. D, b. D-FS, c. D-FQ and d. D-FSQ. Contour interval 5 x 10^{-5} °C/s. ---- 108

5-18. As in Fig. 5-17 except for term E. ------------ 109

5-19. As in Fig. 5-17 except for term F. ------------ 110

5-20. Expanded surface pressure maps of the secondary low for case C at day 10.5 in the spring hemisphere for a. D, b. D-FS, c. D-FQ and d. D-FSQ. Contour interval 2 mb. -- 112

5-21. As in Fig. 5-20 except for day 10.75. --------- 113

5-22. As in Fig. 5-20 except for day 11. ------------ 114

5-23. Term D of the Petterssen development equation for day 10.75 and an expanded region as in Fig. 5-21 for a. D, b. D-FS, c. D-FSQ and d. D-FSQ. Contour interval 5 x 10^{-5} °C/s. ---- 115

5-24. As in Fig. 5-23 except for term E. ------------ 116

5-25. As in Fig. 5-23 except for term F. ------------ 117

5-26. Expanded surface pressure maps of secondary low in F in the spring hemisphere for a. day 10.5 and b. day 11. Region as in Figs. 5-20 and 5-22, respectively. Contour interval 2 mb. -- 119

5-27. Southern hemisphere temperature fields at sigma level 6 (900 mb) at day 10.5 for a. D and b. F. Contour interval 5°C. Location of secondary low indicated by X. -------------- 119

5-28. As in Fig. 5-27 except for expanded region as in Fig. 5-26a. Contour interval 2°C. ------ 120

5-29. Term D of the Petterssen development equation for day 10.5 and an expanded region as in Fig. 5-26a for a. D and b. F. Contour interval 5 x 10^{-5} °C/s. ------------------------ 120

ACKNOWLEDGMENTS

The author expresses his sincere thanks to Dr. Russell Elsberry for his time, guidance and true dedication to his role as a teacher throughout this research.

The author also thanks Dr. Robert Haney for many helpful discussions as well as Dr. Thomas Rosmond, Mr. Edward Barker and Mr. Steve Payne for numerous consultations and for providing the NOGAPS model and initialization routines.

The author expresses his gratitude to the personnel of the Fleet Numerical Oceanographic Center for their excellent service and support, and especially to Mrs. Kris Francum for her encouragement and more than efficient service. Thanks, also, to Mr. James Peak and Mr. William Thompson for their daily encouragement.

Most importantly, the author expresses his deepest gratitude to his family (Gail, Joel and Erin), who supported, encouraged, and gently prodded this research to completion.

This research was partially supported by the Naval Postgraduate School Foundation. Computing facilities were provided by the Fleet Numerical Oceanographic Center and the Pacific Missile Test Range.

I. INTRODUCTION

Extratropical cyclones are responsible for the meridional transport of heat and momentum as well as for most significant weather in the mid-latitudes. Simpson (1969) estimates that 75% to 85% of the mid-latitude transfer of heat, momentum and moisture through the ocean surface occurs during the passage of extratropical cyclones. Understanding the general circulation of the atmosphere and oceans, therefore, requires an accurate knowledge of these large-scale eddies and how they utilize the large amounts of energy transferred to them from the world oceans. These storms also cause considerable destruction (Gyakum, 1980; Rasmussen, 1979) and disruption of commerce. Current numerical models frequently fail to predict these systems accurately beyond one to two days, possibly due to the inadequate parameterization of the diabatic processes (Sanders and Gyakum, 1980). The success of medium and extended range forecasting may depend on the proper understanding and modelling of the role of the air-sea fluxes in the development of the extratropical cyclones.

Extensive circumstantial evidence indicates that the air-sea fluxes play a major role in ocean cyclogenesis. Petterssen et al., (1962) described the evolution of the cyclone based on a composite of 51 cases of western North Atlantic Ocean storms. They found that initial storm development over the ocean appears to be due mainly to low-level thermal advection. This

is in contrast to development over land where upper-level vorticity advection is the dominant development mechanism. Nitta and Yamamoto (1974) studied open ocean cyclogenesis over the East China Sea. They also found cases of cyclogenesis occurring with zonal flow aloft, which implies that low-level thermal advection is the dominant development mechanism over the ocean. Other case studies (e.g., Winston, 1955; Pyke, 1965; Sanders and Gyakum, 1980) of explosive cyclogenesis over the oceans suggest that air-sea exchanges are responsible for the observed rapid rates of development. More indirect evidence has been obtained recently from studies of cyclogenesis over the southern oceans. In a review of air-sea interaction in the southern hemisphere, Baker (1979) cites studies that show the highest frequency of cyclone development occurs over the oceanic polar front. Carleton (1981) obtained the same result using satellite data to locate the initial positions of developing storms in the southern hemisphere. These studies are only able to postulate that air-sea exchanges are important in over-ocean cyclogenesis. Sanders and Gyakum (1980) support this observation and also find a positive correlation between the intensity of the cyclogenesis and the strength of the ocean temperature gradient.

Conflicting evidence regarding the importance of air-sea fluxes has been reported from several numerical model investigations and one observational study. Spar and Atlas (1975) investigated the response to sea-surface temperatures using

the Goddard Institute for Space Studies general circulation model. They found the model to be insensitive to the specification of sea-surface temperatures for both short- and extended-range forecasts. Danard and Ellenton (1979) studied the role of the air-sea fluxes based on real data predictions with an eight-level primitive equation model. They also found that the air-sea fluxes are unimportant to modelled cyclogenesis along the east coast of North America. Wei (1979) presents the only contrary observational study. She investigated the energetics of an East China Sea storm using the Air Mass Transformation Experiment (AMTEX) data. She found that surface sensible heat fluxes and latent heat release contribute very little to the total available potential energy of the system, and concludes that the diabatic processes are unimportant in ocean cyclogenesis.

The mechanisms by which air-sea fluxes could enhance ocean cyclogenesis are also in question. Petterssen _et_ _al_., (1962) suggest the modification of low-level thermal advection as a mechanism. Pyke (1965) and Simpson (1969) propose an indirect enhancement by increasing cumulus convection which, in turn, increases the vorticity of the cyclone. Baker (1979) suggests that ocean temperature gradients induce thermally direct mean meridional circulations, enhancing the jet stream in their location and thereby determining the region of cyclogenesis. Recent studies of intermediate-scale cyclones developing over the ocean reveal similar controversies. Rasmussen (1979)

analyzes case studies of polar lows over the eastern North Atlantic Ocean. His studies indicate that these lows are convectively driven, implying a role for the air-sea fluxes similar to the one of Pyke (1965) and Simpson (1969). Reed (1979) and Mullen (1979) presented case studies of similar polar lows in the eastern North Pacific Ocean. They found the lows are driven by baroclinic instability processes with the air-sea fluxes contributing mainly to the reduction of low-level static stability and thereby enhancing development. Mullen (1979) and Reed (1979) encourage model studies to resolve these controversies.

The fundamental hypothesis of this study is that the surface fluxes of moisture and sensible heat significantly modify the planetary boundary layer and the lower atmosphere on a time scale of one to four days. These effects change the low-level baroclinicity and static stability of the atmosphere as well as the moisture availability for latent heat processes. These processes may account for the observed differences between land and ocean cyclogenesis.

This study should be viewed as the first in a series of numerical experiments at the Naval Postgraduate School that are designed to investigate the role of air-sea interaction in the development of extratropical cyclones. Its purpose is to examine open-ocean cyclogenesis in an idealized atmosphere that is in quasi-equilibrium with the underlying ocean-surface temperatures. The study does not include a land-sea boundary and is not intended to treat the more energetic

cyclogenesis which occurs near the coast, presumably as a result of extreme air-ocean imbalances. The specific objectives of this study are to:

1. determine the contribution of the surface fluxes to the growth of an unstable baroclinic wave during the early linear growth phase;
2. show the mechanisms through which these fluxes modify the growth and decay of a baroclinic wave; and
3. investigate the role of these fluxes in the development of secondary small-scale cyclones.

A basic assumption of this research is that the scarcity of conventional observations over the ocean, and the complex interactions of the physical processes involved, require the use of a numerical model. In particular, the model should include a sophisticated planetary boundary layer parameterization and analytic initial conditions to avoid uncertainties due to incomplete or incorrect observations over the oceans. Previous observational studies (see Pyke, 1965; Laevastu, 1965; Simpson, 1969) were severely hampered by a lack of both conventional observations and measurements of boundary layer fluxes required to investigate these interactions. Previous numerical studies (Spar and Atlas, 1975; Gambo, 1976; Danard and Ellenton, 1979) used either conventional observations or numerical models in which the parameterizations of the diabatic processes were greatly simplified. This experiment

utilizes a version of the UCLA general circulation model that is being developed by the Naval Environmental Prediction Research Facility (NEPRF) for use as the Navy Operational Global Atmospheric Prediction System (NOGAPS). The NOGAPS model has one of the most complete parameterizations of the interactions between the planetary boundary layer and the free atmosphere. This model provides a state-of-the-art tool for investigating the role of the air-sea fluxes. However, this is only a model study and must be validated when adequate atmospheric observations become available.

Chapter II of this paper describes the NOGAPS prediction model used in this research, and the atmosphere and ocean conditions chosen to initialize the model. The analysis of the experimental results is divided into three parts for ease of interpretation. These are:

1. Chapter III--the adiabatic-diabatic comparison and the large-scale response to the surface fluxes,
2. Chapter IV--the initial growth phase of the cyclone waves, and
3. Chapter V--the development of the secondary cyclones.

Chapter VI is a discussion of the results of this investigation in terms of the three objectives.

II. THE ATMOSPHERIC MODEL

The model chosen for this study is a state-of-the-art operational forecast model. Extensive evaluation and verification of the model has been performed by research groups at the Naval Oceanography Command (Paine, 1980) and at UCLA (Mechoso *et al.*, 1978). The model has been chosen by the Naval Oceanography Command to replace their current operational atmospheric prediction model. Any model is an idealization of the real world limited both by parameterizations of real world processes and by initial conditions. By using a numerical model in this study it is hoped that the results will aid in the interpretation of future observational studies and also provide insight into the difficulties of current forecast models in handling open-ocean cyclogenesis (Sanders and Gyakum, 1980).

The following sections describe the NOGAPS forecast model, the method of removing diabatic processes from the model and the method of initializing the model.

A. FINITE DIFFERENCE SCHEME

The adiabatic portion of the model is described in detail by Arakawa and Lamb (1977), and thus only a brief review is presented here. The NOGAPS code for this study was kindly provided by Dr. T. Rosmond of the Naval Environmental Prediction Research Facility (NEPRF) and contains all modifications made to the system through July, 1980. A smoothing of

the meridional wind component on the latitude rings immediately adjacent to the poles has been added to maintain model stability when computing on the fine resolution grid (2° lat by 2.5° long).

The prognostic variables for the model are the horizontal velocity, V, temperature, T, a form of the surface pressure, π, and specific humidity, q. Additional prognostic variables associated with the planetary boundary layer (PBL) will be described in the next section. The model uses a sigma coordinate system defined as

$$\sigma = \frac{p - p_I}{\pi} \qquad (2\text{-}1)$$

where:

$p_I = 50$ mb

$\pi = p_s - p_I$;

p is pressure and p_s is the pressure at the earth's surface. In this study the lower boundary of the model is open ocean. The top of the model atmosphere, p_I, is 50 mb. No stratospheric physics are contained in this version (NOGAPS) of the model. The vertical distribution of the six model layers, assuming an arbitrary surface pressure of 1000 mb, is protrayed in Fig. 2-1. The vertical velocity, $\dot{\sigma}$, is carried at the layer interfaces, with V, T and q defined at the layer mid-levels. Simmons and Hoskins (1976) investigated the sensitivity of atmospheric numerical predictions to the number

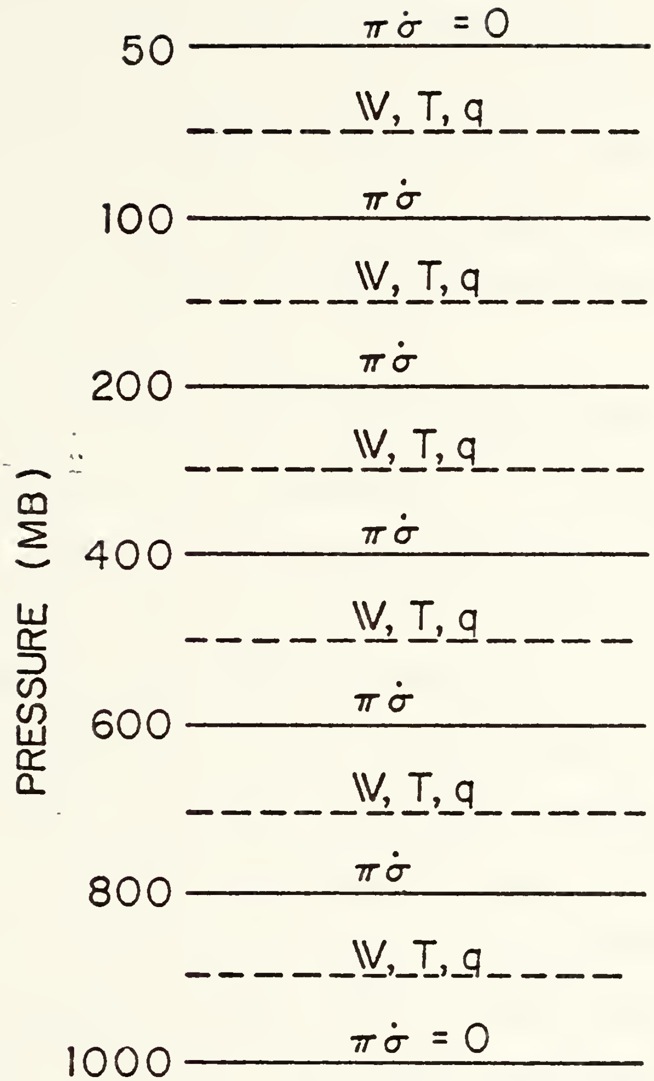
PRESSURE (MB)
50
$\pi\dot{\sigma}=0$
$\mathbb{V}, T, q$
100
$\pi\dot{\sigma}$
$\mathbb{V}, T, q$
200
$\pi\dot{\sigma}$
$\mathbb{V}, T, q$
400
$\pi\dot{\sigma}$
$\mathbb{V}, T, q$
600
$\pi\dot{\sigma}$
$\mathbb{V}, T, q$
800
$\pi\dot{\sigma}$
$\mathbb{V}, T, q$
1000
$\pi\dot{\sigma}=0$

Figure 2-1. Vertical distribution of model large-scale prognostic variables. Pressure values of sigma levels vary with surface pressure. A surface value of 1000 mb is assumed in this figure.

of model layers in the vertical. They compared results from two-, five-, eight- and 16-layer versions of the same model. They found the five-layer model accurately represented phase speeds to wave number 16 (the limit of their study) and growth rates to wave number 12. For waves shorter than zonal wave number 12, the five-layer version overestimates growth rates while the eight-layer version accurately predicts phase speed and growth rates to the limit of their study, wave number 16. Six layers is adequate for this study, however a greater resolution in the lower atmosphere would be preferable for future studies dealing with small-scale waves.

The variables are staggered in the horizontal (Fig. 2-2) such that the meridional wind component, v, is carried at points north and south of the center point and the zonal wind component, u, is carried at points east and west of the center point. The u and v components are averaged to the center (T) point for diabatic and frictional computations. A coarse-model resolution of 4° lat by 5° long was used during initial model development to reduce integration time. This resolution was increased to 2° lat by 2.5° long for the experiments described below to properly handle growth rates and phase speeds of the large-scale cyclones. The finer resolution results in grid distances of 222 km by 196 km at 45°N/S, which is also sufficient to resolve secondary systems with a wavelength of 1500 to 2000 km.

The experiments are performed on a 60 degree pole-to-pole sector having 24 grid points east-west and 91 grid points

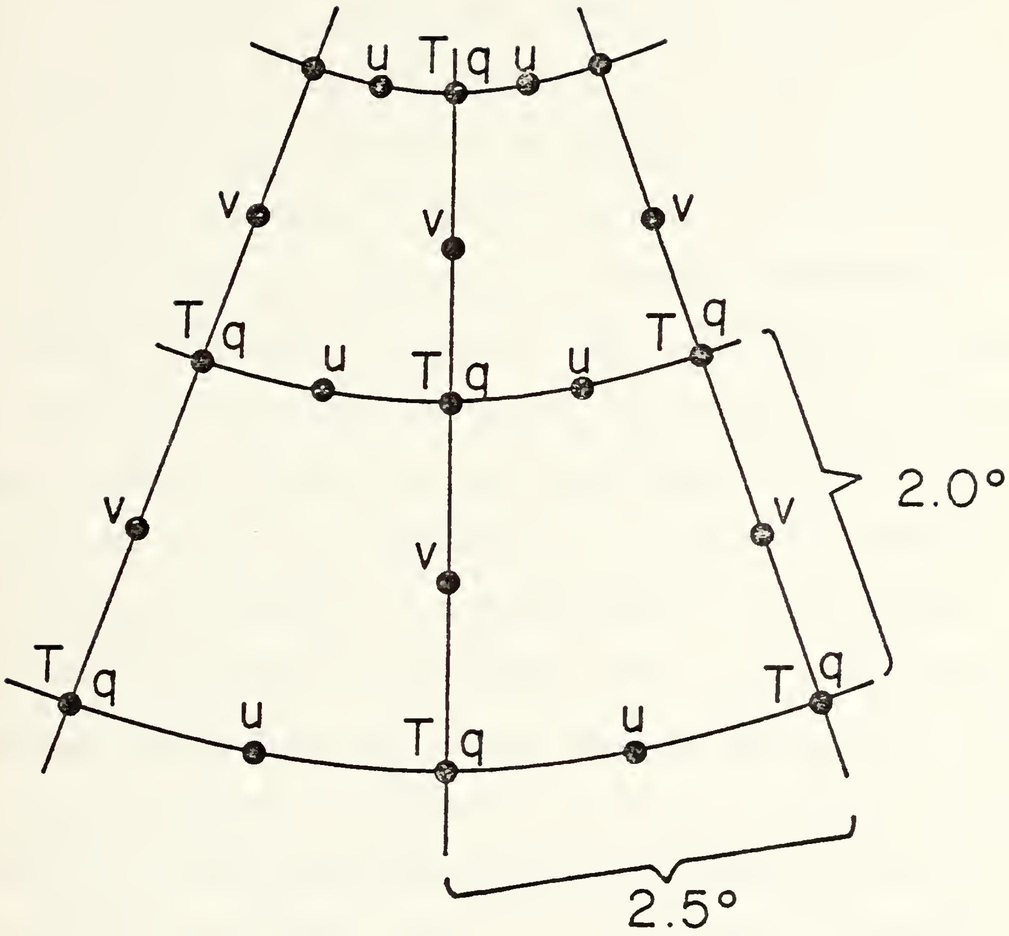
u
T
q
u
v
v
v
T
q
u
T
q
u
T
q
2.0°
v
v
v
T
q
u
T
q
u
T
q
2.5°

Figure 2-2. Horizontal distribution of model large-scale prognostic variables. $\pi\dot{\sigma}$ which is not shown is carried at T-points. (Arakawa scheme C)

north-south. The model uses cyclic east-west boundary conditions, which allow a continuous over-ocean propagation. The 60 degree sector was chosen to reduce computation time and space requirements. Adiabatic model studies by Simmons and Hoskins (1978) have shown simultaneous development of identical waves around the globe when the model was initialized by a normal-mode, wave number six perturbation as in these experiments. Although this may not be strictly true for this diabatic model study, the differences are only due to small time differences in solar heating and should not affect the qualitative aspects of the model experiments.

The model utilizes a leap-frog time differencing scheme with a time step of three minutes in the fine mesh version. The model diabatic package is executed every 30 minutes, and is followed by a Matsuno time step to control the computational mode and to assist in assimilation of the diabatic effects (see Haltiner and Williams, 1980). To avoid using an extremely short time step to maintain computational stability near the poles, a smoothing technique is used on the zonal mass flux and east-west pressure gradient terms in that region (Arakawa and Lamb, 1977). An additional smoothing of the meridional component immediately adjacent to the poles is required for the fine-mesh version.

B. DIABATIC PARAMETERIZATION

One of the assumptions of this research is that a sophisticated PBL parameterization (Table 2-1) is required to

Table 2-1

Summary of the Model Features

Model Dynamics

60° pole-to-pole sector

Δx = 2.5° long (213 km at 40°N/S)

Δy = 2.0° lat (240 km)

Cyclic east-west boundary conditions

Staggered grid (Arakawa scheme C)

σ vertical coordinate

6 model layers in troposphere

Model Diabatics

Planetary boundary layer (Deardorff/Randall)

- diagnostic determination of surface fluxes
- variable depth
- stratus cloud layer parameterization

Arakawa-Schubert cumulus parameterization (Lord)

Large-scale precipitation

Moist convective adjustment

Radiation (Katayama/Schlesinger)

- diurnal and seasonal variation
- cloud and water modifications

adequately simulate the direct and indirect effects of the surface fluxes on extratropical cyclone development. The PBL treatment in this model follows Deardorff (1972), as implemented in the UCLA model by Randall (1976). It allows for interactions between the PBL and cumulus cloud ensembles and/or a stratus cloud layer at each model gridpoint. Surface fluxes of momentum, heat and moisture are diagnostically determined using a bulk Richardson number based on the sea-surface temperature and the values of V, T and q from the dynamic portion of the model. These values are then used to predict a new PBL depth and the strength of the inversion jumps of V, T and q at the top of the PBL. The NOGAPS PBL differs from that described in Arakawa and Lamb (1977) in that it is constrained to remain within the lowest model layer, i.e., beneath approximately 800 mb, to avoid the unrealistic PBL depths which occurred in previous versions tested at NEPRF and UCLA.

Cumulus parameterization follows the scheme of Arakawa and Schubert (1974) as introduced into the model by Lord (1978). The base of the cumulus cloud ensembles is taken as the top of the PBL and provides communication between the PBL and the higher model layers through detrainment of mass and moisture at the cloud top level. Condensation also occurs at grid points where the air becomes supersaturated, and in a moist convective adjustment procedure that has been added to remove moist convective instability between layers not associated with the PBL. The radiational heating computation

which follows Katayama (1972) includes the effects of water vapor and also cloud distributions predicted by the PBL and cumulus parameterizations and by large-scale precipitation processes.

C. MODEL VARIATIONS

The approach used in these experiments is to selectively withdraw the physical processes from the complete diabatic model. This results in much less model shock during the first few hours of integration than in experiments where physical processes are added to the adiabatic model integration. In the adiabatic case, the air-sea differences and surface winds can become abnormally large. This can result in excessive surface heat, moisture or momentum fluxes as those processes are added to the model. In the diabatic model, the air-sea fluxes are in quasi-equilibrium at the time that the physical processes are withdrawn from the model. Thus, there is almost no shock generated and the wave cyclone is only gradually modified.

The experiments are based on six different model configurations. The nomenclature to be used in describing these basic configurations is

1. D--the full diabatic model as described above;
2. A--an adiabatic model created by removing the physical parameterization package which contains all diabatic effects and friction, and by adding dry convective adjustment to maintain stability;

3. F--an adiabatic model with friction represented in the PBL parameterization, but not allowing any heat or moisture transfer to the large-scale variables;
4. D-FS--the full diabatic model without surface sensible heat fluxes, created by setting the surface heat transfer to zero within the PBL calculations;
5. D-FQ--the full diabatic model without surface moisture fluxes, created as in (4) but for the moisture transfer;
6. D-FSQ--the full diabatic model without surface fluxes of moisture or sensible heat, created as in (4) and (5).

It should be emphasized that this is intended to be a study of physical processes, not of a model parameterization scheme or of an initialization test of questionable or erroneous data. These experiments start with a system in which the surface fluxes are relatively small. Removing the surface heat flux does not remove radiative sources and sinks of heating, nor does removing the surface moisture flux prevent condensation of or the redistribution of the existing moisture by the various cloud parameterizations within the model. These experiments are similar to "spin-down" experiments and as such they require time before the absence of the surface transfer processes is felt.

D. INITIALIZATION

The model initial conditions have been chosen to study the air-ocean fluxes during the spring and fall regimes over

the open ocean. The model start time has been selected as 1 October. This makes the northern sector a fall regime and the southern sector a spring (April) regime with respect to the solar fluxes.

The model atmosphere initial conditions are analytically specified following Simmons and Hoskins (1977,1978). Zonal jets are centered at 35°S and 45°N with a maximum of 52 m/s in the southern or spring hemisphere and 35 m/s in the northern or fall hemisphere (see Fig. 2-3). The wind profiles follow the function $u(\sigma,\phi) = U_0(\sigma)M(\mu)$ where:

ϕ = latitude

σ = vertical coordinate

μ = $\sin \phi$

$$M(\mu) = \begin{cases} \sin^3(\pi\mu^2) & 45°\text{N jet} \\ \sin^4(\pi\mu^{1.247}) & 35°\text{S jet} \end{cases}$$

and $U_0(\sigma)$ is a polynomial function approximation of the January mean zonal wind profile at 30°N taken from Oort and Rasmussen (1971). This polynomial function is $U_0(\sigma)$ for the fall profile but is multiplied by a factor of 1.5 at all levels to create $U_0(\sigma)$ for the spring profile.

The jet locations and intensities are intended only to represent conditions which could exist during those seasons. April jet speeds frequently exceed 80 m/s, the maximum attained in these experiments, and jet latitudes are highly variable (Palmen and Newton, 1969). The mean latitudes are

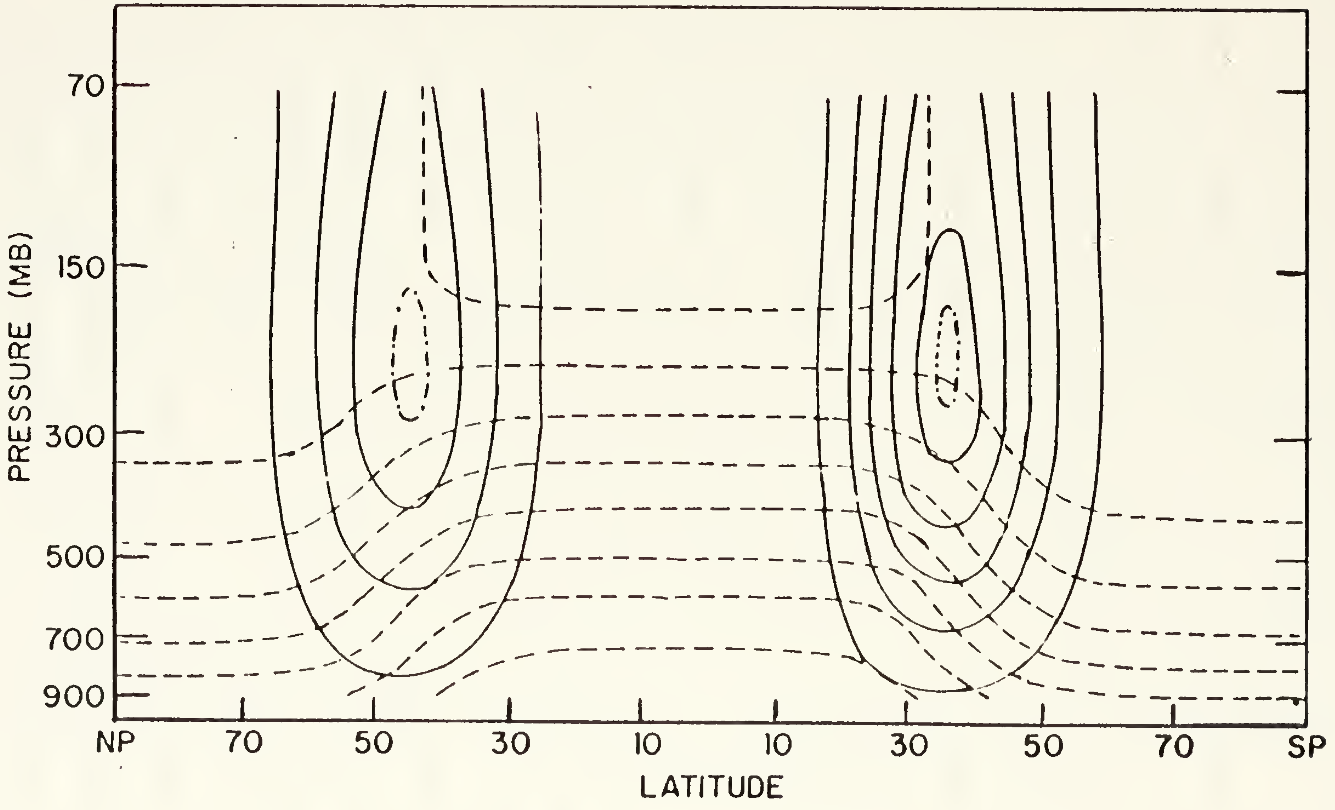

Figure 2-3. Initial zonal wind (solid) and temperature (dash) profiles. Contours 10 m/s (dot-dash 5 m/s) and 10°C.

representative of spring and fall conditions as given in Oort and Rasmussen (1971). In addition, these jets guarantee the growth of baroclinically unstable waves, as found by Simmons and Hoskins (1977,1978).

Temperature fields are derived using the nonlinear balance routine developed by Mr. E. Barker of NEPRF. The mean January geopotential heights at 30°N from Oort and Rasmussen (1971) are used as the reference profile to solve for the geopotential field from the above analytic wind field using the nonlinear balance equation. The initial temperature field is then determined from the geopotential field using the hydostatic equation. The reference geopotential profile is specified at 30°S (spring regime) in the balance routine to match the temperature field as closely as possible to the climatological sea-surface temperature gradient.

In order to avoid large initial surface fluxes, emphasis has been placed on the specification of low-level temperature and moisture profiles. In these experiments, the ocean surface temperatures are independent of longitude and fixed in time. Ocean surface temperatures are derived from the model surface air temperatures, so that initially the lowest model layer is near neutral stability. Some adjustments are made to achieve both a realistic sea-surface temperature gradient and a field that is consistent with the simple atmospheric structure represented by the specified jet intensity/location in each hemisphere. In Fig. 2-4 the model sea-surface temperatures are compared with smoothed values at approximately 160°W

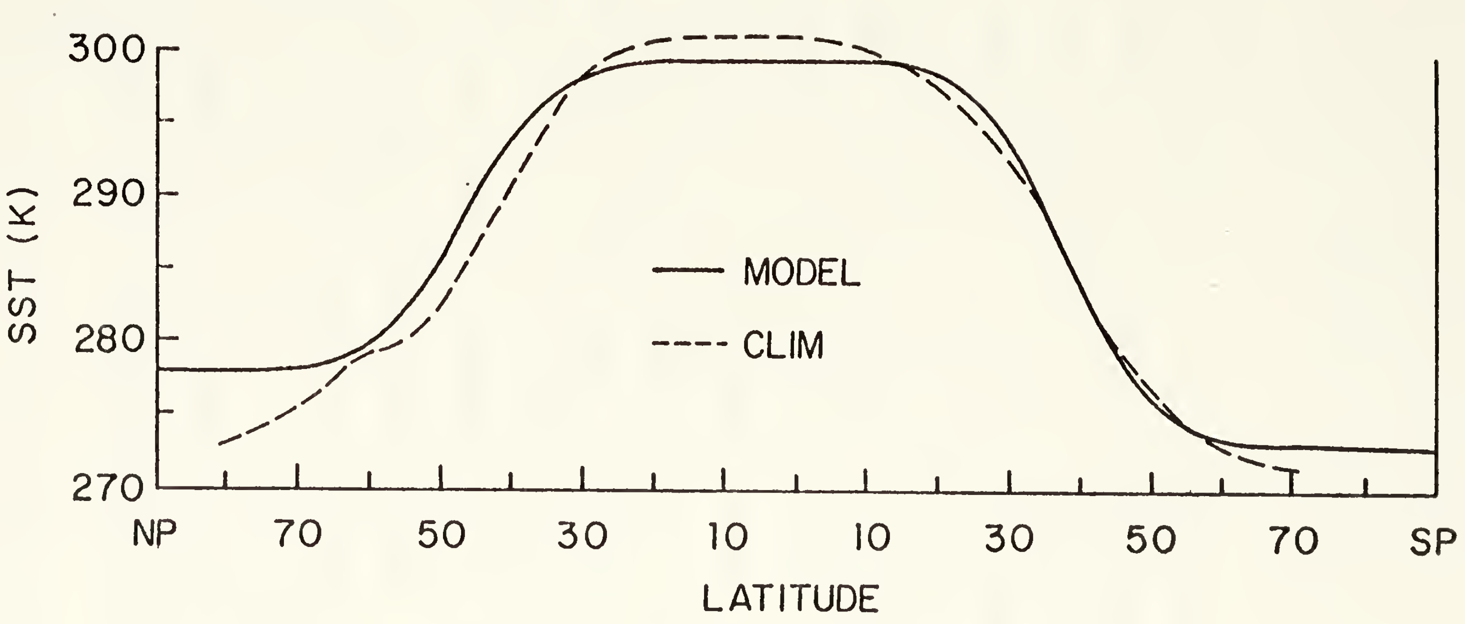

Figure 2-4. Model (solid) and climatological (dash) sea-surface temperatures. Climatology adapted from Robinson (1976) at approximately 160°W for April (southern hemisphere) and October (northern hemisphere).

taken from Robinson (1976). Climatological values for the southern hemisphere (spring) are April northern hemisphere values. The lower equatorial temperatures are desirable to reduce the influence of the convectively-driven Hadley circulation. The specification of open-ocean conditions (no sea ice) is responsible for the temperature differences near the poles.

Realistic moisture profiles for the marine atmosphere are more difficult to specify. The intent in this experiment is to represent open-ocean conditions, i.e., mid-Pacific or eastern Atlantic. Therefore, it is natural to assume much higher relative humidity values in the lower model levels than the global mean values. Initial moisture fields for the model were specified with a 90% relative humidity at 900 mb, and a linear decrease to 40% at the highest model level (70 mb). Fig. 2-5 is a comparison of model relative and specific humidities with zonal mean values from the global climatology by Oort and Rasmussen (1971) for the three lowest model levels. Model relative humidities compare favorably with climatology when considered as open-ocean versus global means. Mullen (1979) found low-level relative humidities of 80% to 85% over the eastern North Pacific Ocean. Specific humidities are significantly different near the equator and the poles due to differences between mean atmosphere and model temperatures in those regions.

The low-level winds are initially less than 3 m/s. This helps to prevent an initial shock or imbalance due to large

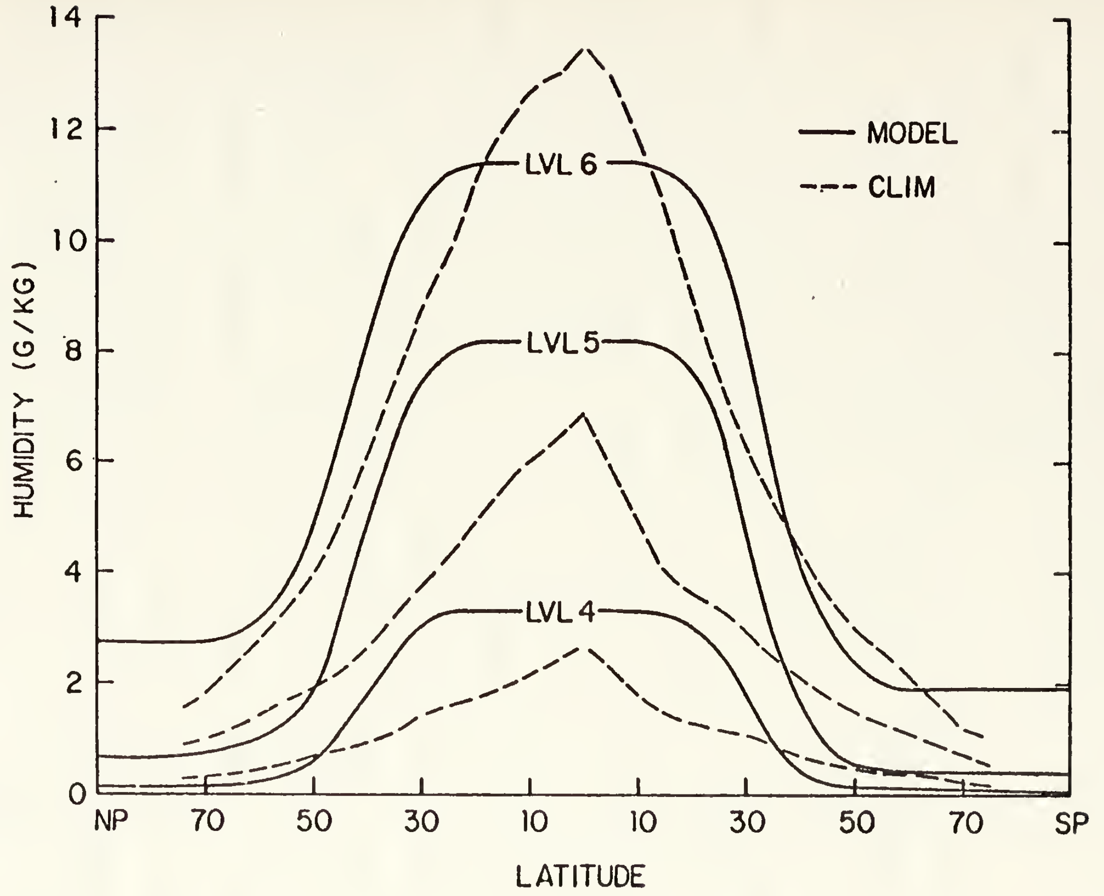

Figure 2-5. Model initial specific humidity at sigma levels 6, 5 and 4 (approximately 900, 700 and 500 mb) compared with climatological northern hemisphere zonal mean values from Oort and Rasmussen (1971) for April (southern hemisphere) and October (northern hemisphere).

air-sea fluxes. Consequently, the PBL is set to a very shallow depth (10 mb) with no temperature, moisture or velocity jumps at the top. Rather than attempt to specify these values, it is intended that both the low-level wind field and the PBL will evolve to realistic values as the initial perturbation develops.

The conditions discussed above are used for all experiments with unperturbed initial conditions (hereafter referred to as Z for zonal), and as the basis for creating two different perturbed initial conditions. The first perturbed case (S) is created following Simmons and Hoskins (1977). A small amplitude sinusoidal perturbation is added to the meridional wind component at all levels prior to balancing. This perturbation is in zonal wave number six with maximum values of .5 m/s at 45°N/S, and equal to zero at the equator and the poles. The associated surface pressure perturbation is approximately 1 mb. These initial conditions are used for the extratropical cyclone evolution experiments. The second perturbed case (R) is created by inserting similar small amplitude perturbations into the zonal initial conditions (Z) after the fields are balanced. In this case, perturbations with a maximum value of .1 m/s in wave numbers 6, 12, 18, 24, 30 and 36 are added to the meridional wind component.

III. LARGE SCALE RESPONSE

The experimental results have been divided into three parts. This chapter describes the large-scale, baroclinic wave growth in the diabatic model atmosphere, and how this compares to the adiabatic model experiment. The adiabatic experiment is also verified with a similar model experiment by Simmons and Hoskins (1978). This chapter introduces the surface flux experiments and describes their results in terms of large-scale cyclone development. The next chapter considers the effects of the individual diabatic processes during the linear growth phase (first 72 h) of the baroclinically unstable waves. In the following chapter, the development of secondary cyclone waves in the diabatic model experiment is discussed. In particular, the effect of the surface fluxes of sensible heat and moisture on the development of the secondary cyclone waves is examined based on these model experiments.

The experiments are of two basic types--those starting at day 0, and those initialized at day 4 using fields from the full diabatic model integration (Table 3-1). The objective of the first group is to establish the magnitude of the model atmosphere response to the diabatic parameterizations. The second group of experiments is performed to study the influence of the individual diabatic processes. These experiments employ the technique (described in Section II.C) of selectively

Table 3-1

Experiments for the Large-scale Study

Exp.	Initial Fields*	Integration Period	Model Version*
	Experiments Initialized from Day 0		
D	S (wave no. 6)	15 days	complete diabatic
A	S	15 days	adiabatic
DZ	Z-zonal	3 days	complete diabatic
DR	R-multiwave	5 days	complete diabatic
	Experiments Initialized from Day 4		
F	S4 (fields from D at day 4)	6 days	adiabatic with model friction
D-FS	S4	6 days	diabatic w/o surface sensible heat flux
D-FQ	S4	6 days	diabatic w/o surface moisture flux
D-FSQ	S4	6 days	diabatic w/o surface moisture or sensible heat fluxes

*See Sections II.C and II.D for a more complete discussion of model variations and initial conditions.

removing the model parameterizations to investigate the contributions of the surface fluxes of sensible heat and moisture.

A. DIABATIC-ADIABATIC COMPARISON

The adiabatic model experiment (A) compares very closely with the results of a similar study by Simmons and Hoskins (1978). Surface pressure maps for experiment A at day 6 are displayed in Figs. 3-1 a-b. The northern hemisphere case (3-1a), which employs initial conditions adapted from Simmons and Hoskins (1978), is essentially the same as in their study (see their Fig. 1). The surface pressure field exhibits a pure wave number six pattern in each hemisphere. The growth of the cyclone-anticyclone pair is much greater in the spring (southern) hemisphere, as would be expected with the more intense initial jet in that hemisphere. Southern hemisphere maps in Fig. 3-1b and below are presented in inverted form (south at top, east remains toward right) for ease of comparison with the northern hemisphere results. The positions of the cyclone centers also reflect the more equatorward initial latitude of the upper-level jet maximum in the spring hemisphere. The vertical structure of the growing cyclone (Fig. 3-3) is that of a typical growing baroclinic wave as seen in observational studies (Palmen and Newton, 1969). This structure also follows closely that obtained by Hoskins (1978) in a theoretical study of baroclinic waves. In agreement with Simmons and Hoskins (1978), the wave cyclone in A reaches

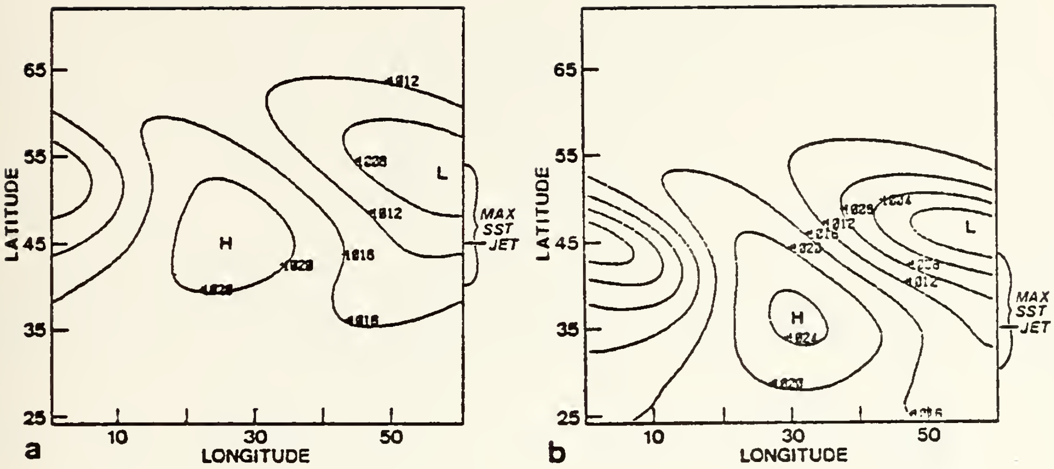
65
55
45
35
25
LATITUDE
10
30
50
LONGITUDE
a
b
H
L
1012
1028
1016
MAX SST JET
1024

Figure 3-1. Surface pressure for A after six days of integration for a. northern hemisphere and b. southern hemisphere. Contour interval 4 mb. Southern hemisphere inverted with pole (south) at top (east remains toward right).

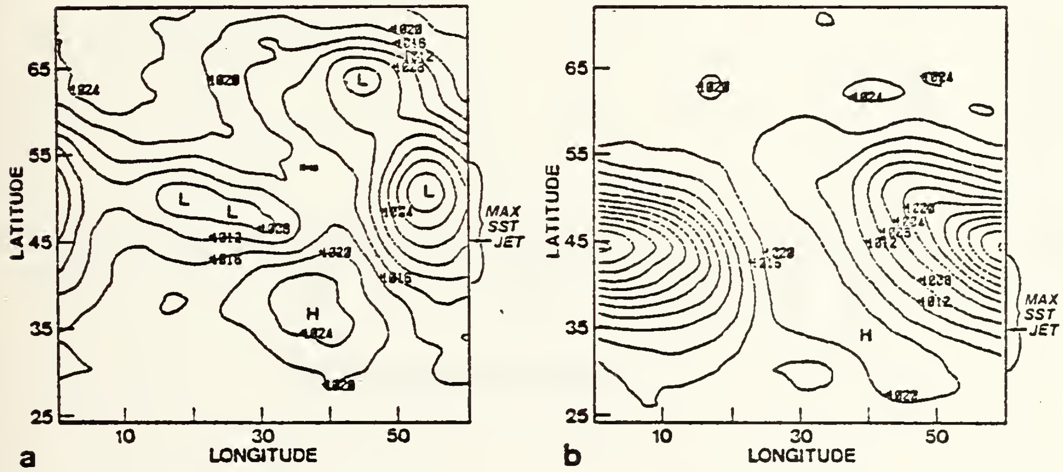
65
55
45
35
25
LATITUDE
10
30
50
LONGITUDE
a
b
H
L
1024
1028
1012
1016
1020
MAX SST JET

Figure 3-2. As in Fig. 3-1 except for diabatic model (D).

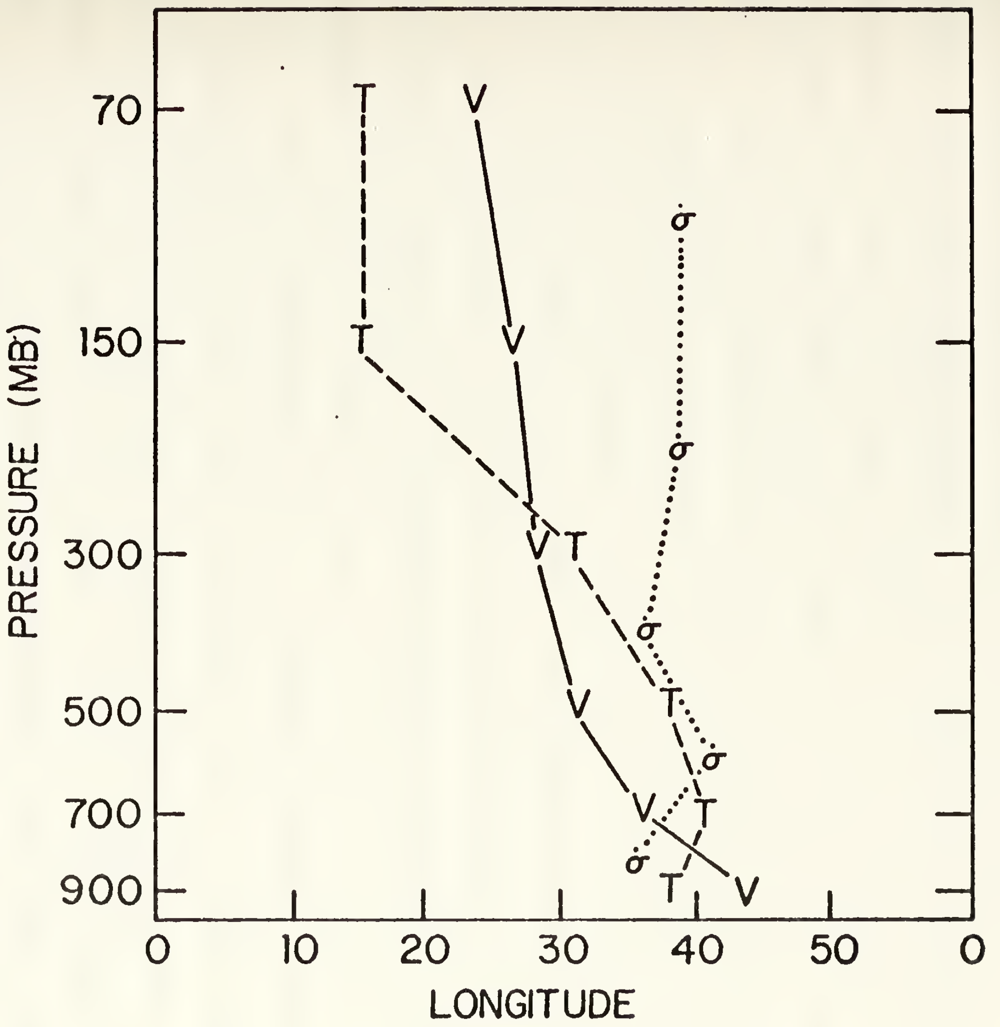

Figure 3-3. Vertical phases of wavenumber 6 mode along 40°S for A after 2 days of integration. V is meridional wind, T is temperature, and σ is vertical velocity.

a maximum intensity at about day 9 and then decays slowly through day 15 of the model experiment. Simmons and Hoskins (1978) demonstrated that this decay was brought about by barotropic processes which became dominant during the later part of the forecast period.

The full diabatic model experiment, D, is used for adiabatic-diabatic comparisons and as the control case for the surface flux model experiments. The inclusion of diabatic processes in this experiment results in much more rapid development of the primary low by day 6 (see Figs. 3-2 a-b and 3-1 a-b). In addition, shorter wavelength disturbances grow in the diabatic experiment as found by Haltiner (1967). Although shorter wavelengths are not apparent at day 6 in the spring case (Fig. 3-2b), they are present at earlier (see Fig. 3-6b below) and later times (see Chapter V) in the diabatic model run. Secondary cyclone waves are more prevalent in the fall hemisphere, but they are an important feature of both hemispheres in the diabatic model experiments.

Experiments A and D are initialized with a wave number six perturbation. Following Simmons and Hoskins (1978) and other studies of baroclinic wave growth, it was assumed that wave number six would be the most unstable for these experiments. Instead, the initial period of one to three days is dominated by wave number 18 growth. As mentioned above, a wave number 6 disturbance eventually evolves. To estimate the sensitivity to the use of wave number 6 in the initial

conditions, a second diabatic experiment (DR) was performed using the multi-wave initial conditions described in Section II.D. Wave number 18 again dominates the early growth period, but a distinct wave number 6 pattern evolves by day 5 (Figs. 3-4 a-b). Haltiner (1967) conjectured that the evolution of large-scale waves in the atmosphere was more the result of a change in scale of shorter wavelengths, than the growth from a small amplitude perturbation of large-scale dimensions. This is apparently true in D and DR. This aspect of the diabatic model experiments and the growth of the smaller scale waves is discussed in detail in the following chapters.

The primary trough in D exhibits a larger phase speed than that of the primary trough in A during the period of strongest development (Figs. 3-5 a-b). This speed difference is approximately 5° long per day (450 km at 35°S) at its maximum; however, the phase speeds are approximately the same after day 5.

The release of latent heat narrows and strengthens by several fold the zone of upward motion. This increases the conversions of eddy available potential energy to eddy kinetic energy, and enhances the growth of the baroclinic wave (Palmen and Newton, 1969; Haltiner, 1971). This more rapid growth is evident in D. A result not anticipated from previous work is that the cyclones in A eventually (about day 9) become nearly as intense, 980 mb/980 mb (northern/southern hemisphere) central pressure versus 982 mb/976 mb, as in D.

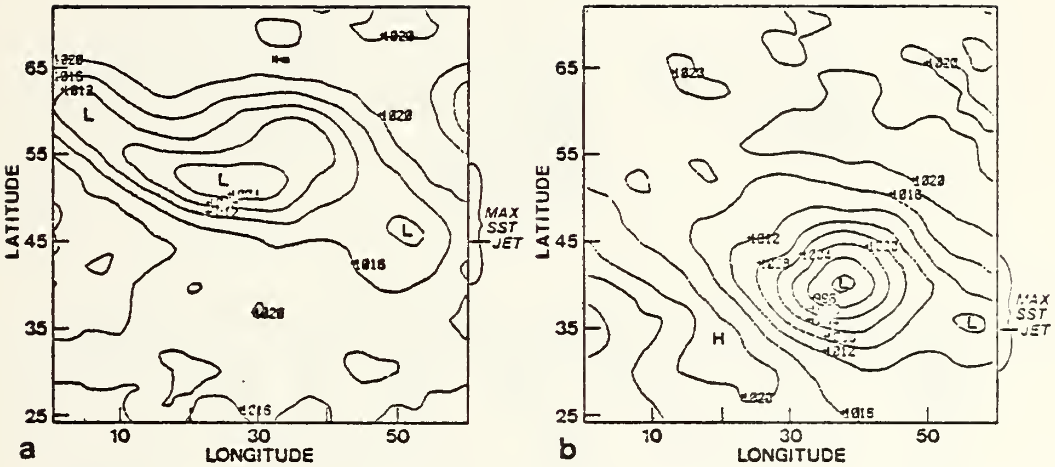

Figure 3-4. Surface pressure for DR after five days of integration for a. northern hemisphere and b. southern hemisphere. Contour interval 4 mb.

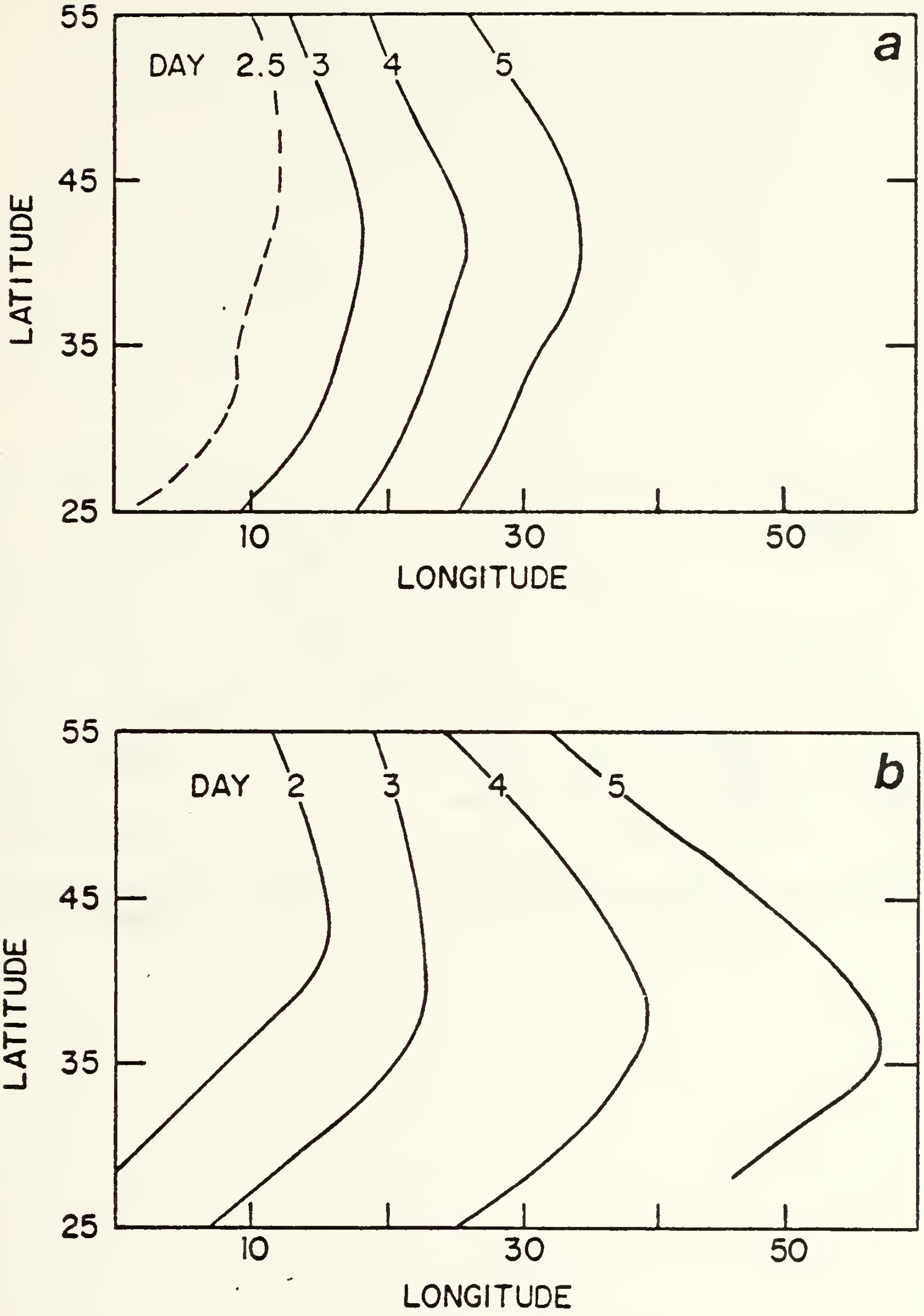

Figure 3-5. Position of streamline troughs at sigma level 3 (300 mb) in the southern hemisphere for a. A and b. D.

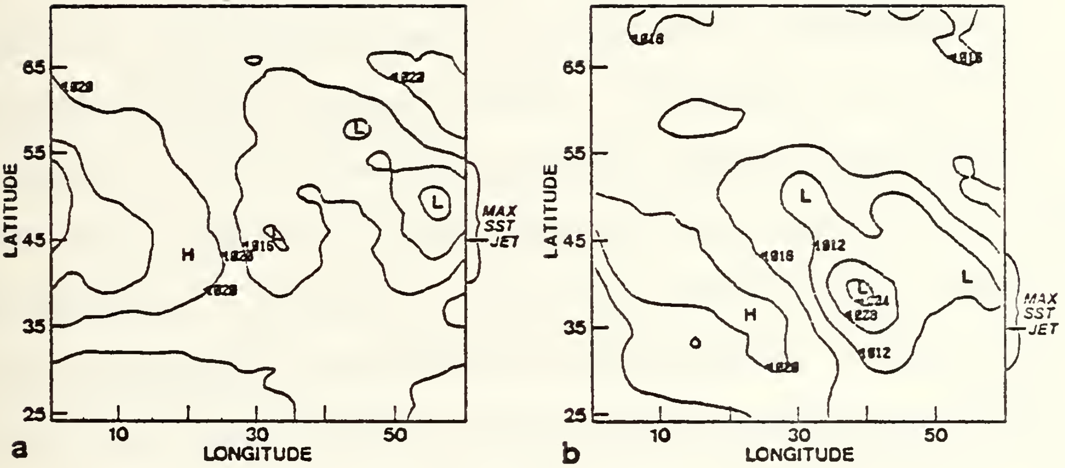

Figure 3-6. As in Fig. 3-2 except after four days of integration.

Beyond day 8, the primary lows begin a gradual decay in intensity as in A. The barotropic decay process appears to control the diabatic experiment as in the adiabatic experiment. Thus, although the minimum surface pressure appears to depend on the large-scale baroclinic and barotropic processes, the diabatic processes greatly affect the timing and rate of development of the primary lows.

In summary, the adiabatic model experiment is consistent with previous studies, notably Simmons and Hoskins (1978). The primary cyclones attain approximately the same maximum intensity in the diabatic as in the adiabatic experiments and undergo a similar decay period. The growth of the primary cyclone is much more rapid in the diabatic experiment, however, and involves interactions with wave scales not present in the adiabatic experiment. Also, in the adiabatic experiment the hemispheric differences are primarily in the intensity of the primary cyclone. The diabatic experiment demonstrates a stronger tendency toward shorter wavelengths in the fall hemisphere as well. These results agree closely with observational studies. Sanders and Gyakum (1980) found a greater frequency of rapidly deepening storms over the oceans where diabatic processes are more dominant. Also, there is a greater tendency for shorter wavelength cyclones to develop over the mid- and high-latitude oceans than over land (Reed, 1979; Nitta and Yamamoto, 1974).

B. SURFACE FLUX MODIFICATION TO THE PRIMARY LOW DEVELOPMENT

Four model versions are initialized with fields from day 4 of D (Figs. 3-6 a-b) to study the contributions of the diabatic processes (Table 3-1). The broad areas of low pressure on the right side of each figure evolved into intense cyclones (see Figs. 3-2 a-b) during the next two days of integration in all model versions. Removal of the surface fluxes produced relatively minor changes in the intensity of the primary cyclones and anticyclones (Table 3-2) and very slight changes in phase speed (not shown) by day 6, which is two days after removal of the fluxes. Removal of the surface sensible heat flux (D-FS) leads to an additional 1-3 mb deepening of the primary cyclone. The largest effect occurs in the northern or fall hemisphere with the warmer SST and weaker upper-level jet. The removal of the surface moisture flux (D-FQ) leads to 4-5 mb less deepening of the primary cyclone in two days. No further deepening occurred beyond day 6 in D-FQ and D-FSQ. Thus, there are differences of 9-10 mb in central pressure by day 8, four days after initialization. These minor changes are expected from previous observational studies (see Palmen and Newton, 1969) and also from numerical model studies (Haltiner, 1971; Spar and Atlas, 1975).

The surface pressure fields at day 6 of the no surface flux experiments (Figs. 3-7 a-c) are very similar to those of the diabatic experiment (Fig. 3-2a). However, large surface fluxes of moisture (Fig. 3-8) which are present in D and D-FS, but are not present in D-FQ and D-FSQ, lead to

Table 3-2

Central pressures (mb) for the primary cyclone/anticyclone by experiment for days 4, 6 and 8.

Model Exp.	Hemisphere	Time Day 4	Day 6	Day 8
D	Fall	1012/1020	988/1028	983/1024
	Spring	1002/1020	975/1022	981/1024
D-FS	Fall	initialized with fields from D above	987/1027	980/1022
	Spring	"	974/1024	980/1028
D-FQ	Fall	initialized with fields from D above	992/1024	992/1024
	Spring	"	979/1022	985/1024
D-FSQ	Fall	initialized with fields from D above	992/1024	993/1024
	Spring	"	978/1024	985/1024
F	Fall	initialized with fields from D above	997/1029	992/1028
	Spring	"	997/1026	981/1025

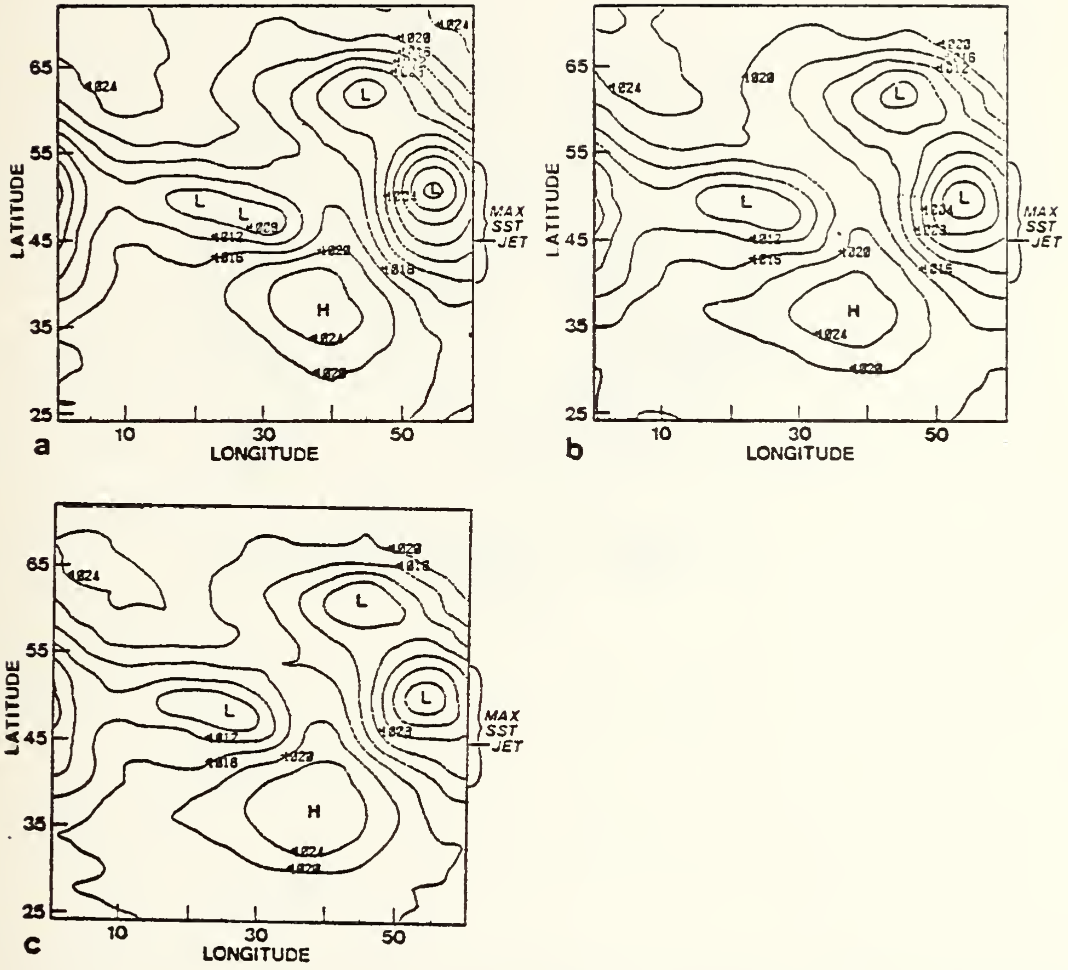
a
b
c
LATITUDE
LONGITUDE
25
35
45
55
65
10
30
50
L
H
MAX SST JET
1024
1020
1016
1012

Figure 3-7. Northern hemisphere surface pressure at day 6 for a. D-FS, b. D-FQ and c. D-FSQ. Contour interval 4 mb.

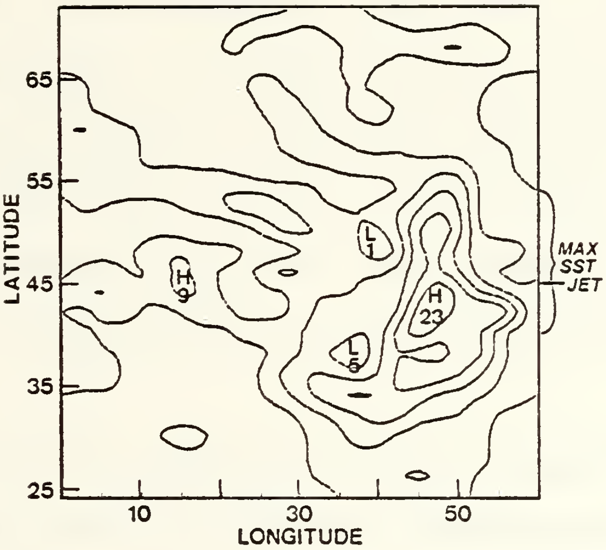

Figure 3-8. Northern hemisphere surface moisture flux rate at day 6 for D. Contour interval 4 mm/day.

different cyclone evolutions in these experiments. The largest moisture fluxes, which are equivalent to approximately 1200 cal/cm^2/day of latent heat, are located in the southwest quadrant of the primary cyclone in D and in D-FS (similar to D but not shown). These values are consistent with previous observational studies (e.g., Petterssen _et_ _al_., 1962 and others). After two days, the loss of the moisture flux has led to large changes in the distribution of low-level moisture (Figs. 3-9 a-d). Very dry air is advected into the primary cyclone in D-FQ and D-FSQ (Figs. 3-9 c-d) as a result of the lack of the surface moisture flux. This results in a decrease in latent heat release in the primary cyclone and a large reduction in its growth after day 6 (Table 3-2).

It is generally accepted that the temperature gradient associated with the cold front of a developing cyclone is greater than that of the warm front. For the low-level temperature fields of the experiments performed here (Figs. 3-10 a-e) this is only true in the adiabatic experiment, F, and possibly the no surface flux experiment, D-FSQ. Both the surface sensible heat flux and the surface moisture flux reduce the strengthening of the low-level temperature gradient by thermal advection. D-FS and D-FQ have a larger temperature gradient in the region of the primary cyclone than in D. This gradient is even larger in D-FSQ, and approaches that of the adiabatic experiment, F. Although this does not

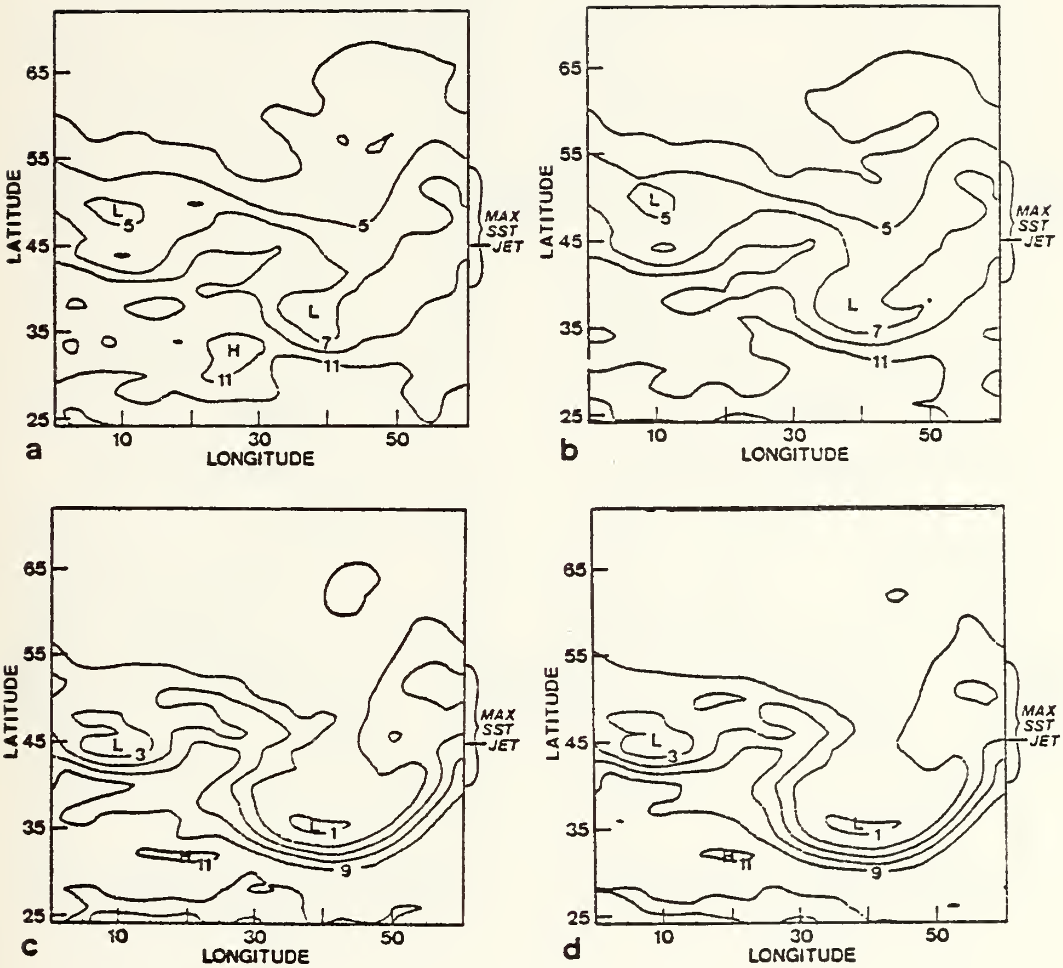

Figure 3-9. Northern hemisphere specific humidity fields at sigma level 6 (900 mb) at day 6 for a. D, b. D-FS, c. D-FQ and d. D-FSQ. Contour interval 2 g/kg.

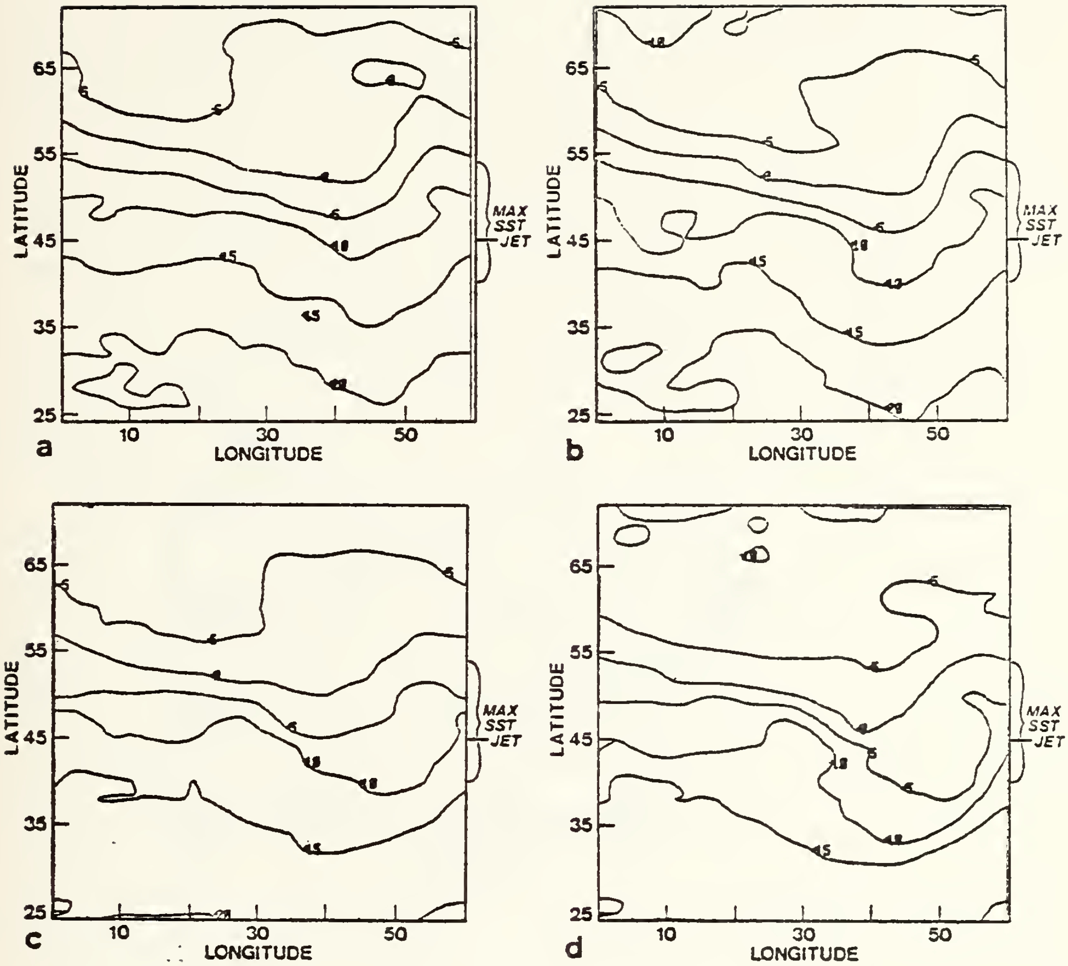
a
b
c
d
LATITUDE
LONGITUDE
65
55
45
35
25
10
30
50
MAX SST JET
5
10
15
20

Figure 3-10. As in Fig. 3-9 except for temperature fields. Contour interval 5°C. Also shown (next page) e. experiment F.

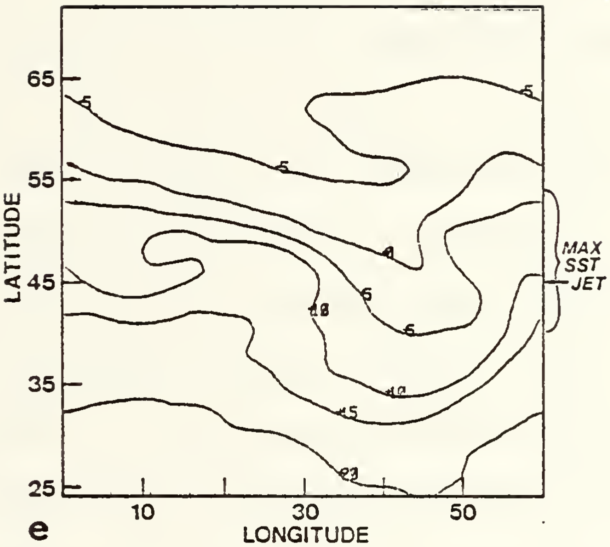
65
55
45
35
25
LATITUDE
10
30
50
LONGITUDE
e
5
5
5
8
6
6
18
10
15
23
MAX
SST
JET

apparently affect the evolution of the primary cyclone on a two-to-three day time scale, it could have significant effects on the development of secondary or subsequent cyclones.

Diabatic processes play a greater role in the growth of the primary cyclone in the fall hemisphere with the weaker jet and higher SST. Over the open ocean, the surface fluxes of moisture and sensible heat only weakly modify the development of the primary cyclones on a time scale of less than two days, as found in the case studies of Mullen (1979). The modifications of the low-level temperature and moisture distributions are significant, however. In particular, the surface fluxes tend to weaken the temperature and moisture gradients associated with strong advection, especially in the western sector of the cyclone where the surface fluxes are largest (Petterssen et al., 1962). This results in more intense gradients in the eastern sector than in the western sector of the primary cyclone in the model marine atmosphere. This is in contrast to that found in the adiabatic experiments or in typical over-land examples of cyclogenesis. Beyond two days, these modifications affect the development of the primary cyclone. The response of secondary or subsequent cyclones may also be affected, as presented in Chapter V.

IV. INITIAL DEVELOPMENT

A major feature of the diabatic experiment is the evolution of multiple lows and secondary lows (see Fig. 3-2a). A cyclone scale initially much shorter than wave number six expected from the adiabatic experiment predominates during the first three to four days of the diabatic experiment. Beyond day 4, as seen in Figs. 3-6 and 3-2, these multiple lows gradually evolve into an intense primary low with associated secondary wave cyclones. The evolution of these secondary cyclones is addressed in Chapter V. This chapter describes the initially linear growth phase and the reasons why the smaller-scale cyclones occur.

Table 4-1 lists the model experiments viewed in this chapter. The initial conditions and model configurations used for these experiments are presented in Chapter II.

Table 4-1

Experiments for the initial development study

Exp.	Initial Fields[*]	Integration Period	Model Version[*]
D	S--wave no. 6	15 days	complete diabatic
A	S	15 days	adiabatic
A36	S1.5 (fields from D at day 1.5)	2 days	adiabatic
D-FS	S	3 days	diabatic w/o surface sensible heat flux
D-FQ	S	3 days	diabatic w/o surface moisture flux

[*] See sections II.C and II.D for a more complete discussion of model variations and initial conditions.

A. DIABATIC CONTRIBUTIONS TO WAVE GROWTH

Growth rates by wavenumber at 300 and 900 mb for experiments A, A36 and D are displayed in Figs. 4-1 a-d. The growth rates are obtained by performing a Fourier analysis of the meridional wind components for two time periods. The exponential growth rate for each wave number is then obtained from

$$\varepsilon = (t_2 - t_1)^{-1} \ln\left(\frac{v_{\ell k}(t_2)}{v_{\ell k}(t_1)}\right) , \qquad (4\text{-}1)$$

where:

ε = growth rate

v = meridional wind component

k = wavenumber (6,12,18,24)

ℓ = model sigma level (~ 900 mb and 300 mb)

t_1 = initial time, and

t_2 = final time.

The most obvious difference between experiments A and D is that only wave number 6 grows in A. This has already been described and is most clearly seen in the surface pressure fields displayed in Figs. 3-1 and 3-6. Experiment A36 was included to incorporate any changes in the model basic flow that may have occurred due to slight imbalances in the initial conditions, or due to the adjustment of the diabatic model to

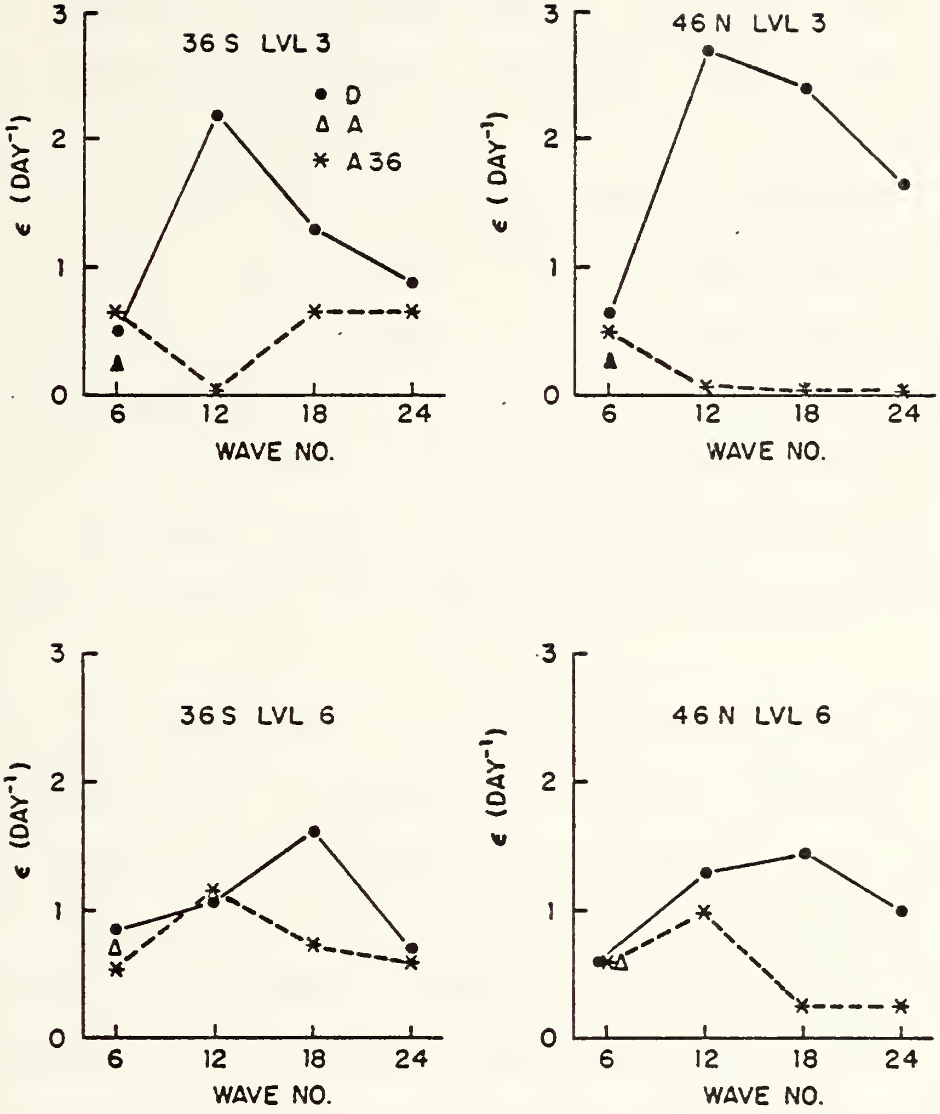

Figure 4-1. Exponential growth rate between days 2.5 and 3.5 for the meridional velocity perturbation by wavenumber (see text for description) for a. sigma level 3 (300 mb), 36°S, b. sigma level 3, 46°N, c. sigma level 6 (900 mb), 36°S and d. sigma level 6, 46°N. Experiments D, A and A36 are compared.

the underlying sea-surface temperatures. Experiments A and A36 use the same adiabatic version of the model--the only difference is that A36 is initialized using fields from day 1.5 of the diabatic experiment while A uses the day 0 fields. In A36, wave number 12 grows more rapidly than wave number 6 in the lower atmosphere (900 mb). At higher levels, wave number 12 exhibits no growth in A36. Another readily evident feature is the north/south variation in the A36 experiment at higher wave numbers. Wave numbers 18 and 24 grow weakly at low levels and not at all in upper levels in the weaker jet/ higher SST fall hemisphere. In the spring hemisphere, these wave numbers exhibit a growth comparable to wave number 6 at both levels. The last feature to note relative to A36 is that wave number 6 grows more rapidly in this experiment than in A.

The diabatic experiment D, exhibits a definite shift of the most unstable wave to shorter wavelengths. At upper levels, wave number 12 is the most rapidly growing wave in both hemispheres, while at low levels wave number 18 dominates. This is a distinctly different result from that of the adiabatic experiments. Wave number 6 also grows more rapidly in D than A everywhere except at low-levels in the northern or fall hemisphere. Figs. 4-2 a-b give the streamline troughs versus height and longitude for A and D. These figures provide a clearer picture of the actual wave number/height relationships described in the growth rate calculations, although variations in intensity are not indicated.

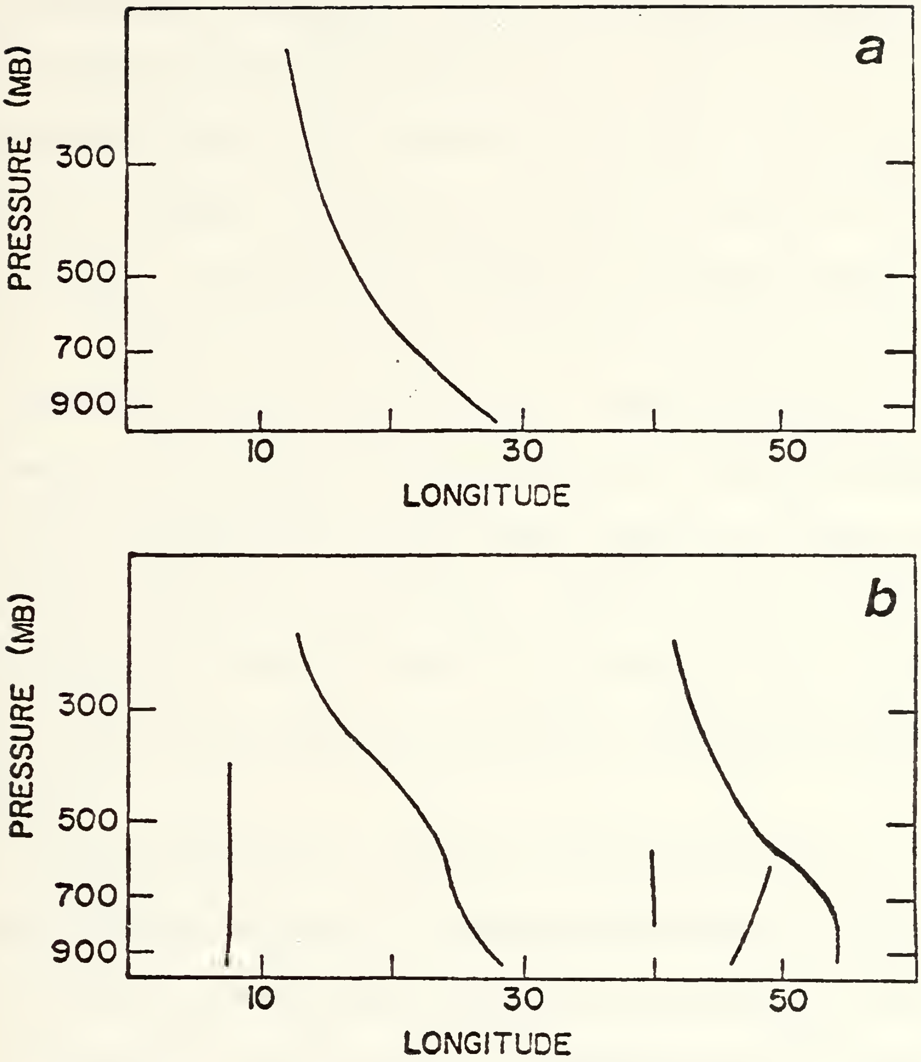

Figure 4-2. Location of streamline troughs at day 3 for a. A and b. D.

Several model studies, e.g., Staley and Gall (1977) and Blumen (1979), have found that the wavelength of the most unstable wave in the atmosphere is very sensitive to changes in low-level static stability. In addition, Rao and Ferreira (1979) performed a numerical study of intermediate-scale (less than 2000 km) waves using a moist model with a CISK-type parameterization of convective heating. They found that the use of a standard atmosphere value for static stability of .02 $m^2s^{-2}mb^{-2}$ produced two modes of unstable waves. The first was a conventional, long baroclinic wave in which latent heating was relatively unimportant. The second was an intermediate-scale disturbance in which latent heating-induced vertical velocities were of the same order or larger than those of the baroclinic processes. When a small value of static stability (.002 $m^2s^{-2}mb^{-2}$) was used, only a conventional baroclinic wave was found, but with an intermediate-scale wavelength.

The above study and a similar one by Gambo (1976) suggest that there are two modes of intermediate-scale unstable waves:

1. a latent heat-driven mode with energetics similar to a tropical system but not dependent on low values of static stability; and,
2. a conventional baroclinic mode which arises due to very low values of static stability.

Clearly only the conventional, baroclinic mode can occur in the adiabatic experiments. While the diabatic model does not

have a CISK latent heat parameterization, the more complete parameterizations of convective, PBL and large-scale latent heating processes should allow the formation of either intermediate-scale mode. In the discussion below, differences in wave growth among experiments A, A36 and D are explained in terms of these two unstable modes.

Static stability is defined as

$$S \equiv - \frac{\alpha}{\theta} \frac{\partial \theta}{\partial p} \qquad (4\text{-}2)$$

where:

α = specific volume

θ = potential temperature and

p = pressure.

Figs. 4-3 a-b give the variation of $\partial\theta/\partial p$ as a function of time for experiments A, A36 and D for the 900-500 mb layer. The corresponding values of static stability range from .015 to .012 $m^2s^{-2}mb^{-2}$. Values of static stability are computed separately for the 900 mb-surface (D only), and 900-700 mb and 700-500 mb layers. The lowest values are found in the 900-700 mb layer (.011 to .013 $m^2s^{-2}mb^{-2}$), but the greatest temporal variability is found in the 700-500 mb layer (.015 to .022 $m^2s^{-2}mb^{-2}$). The averaging of the two model layers seems to describe the variability of static stability in the lower model atmosphere better.

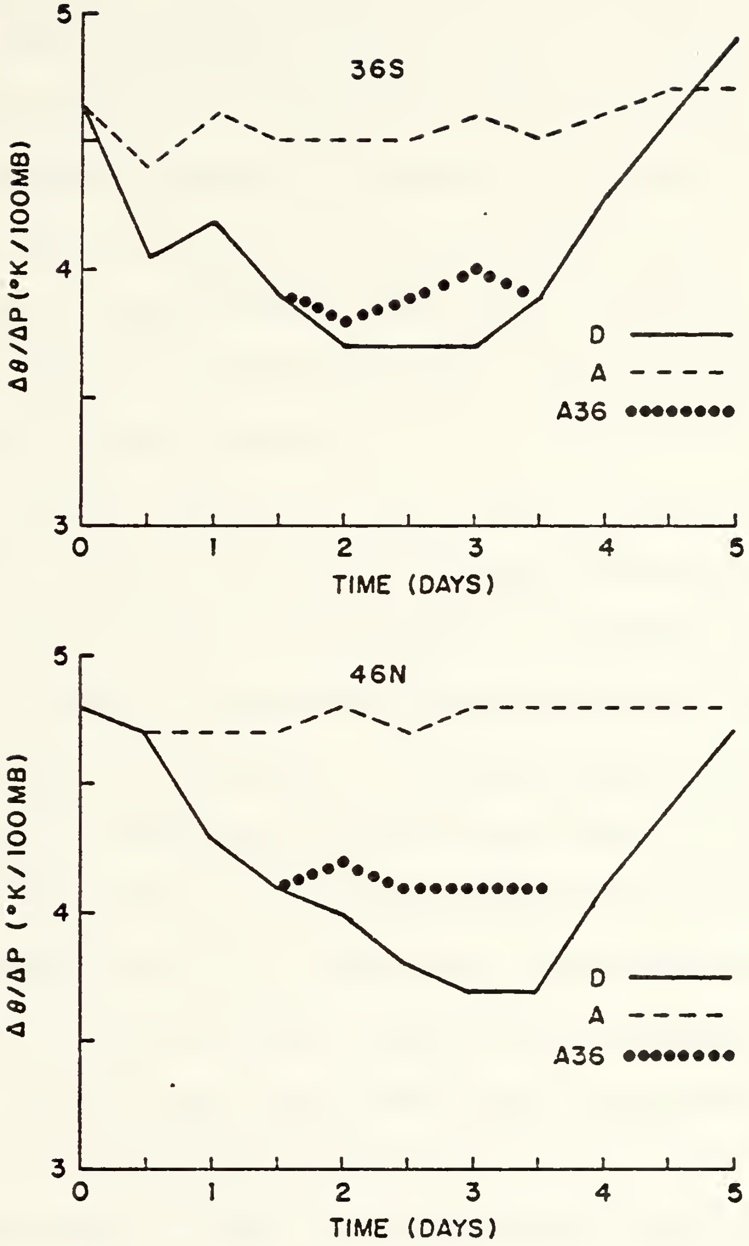

Figure 4-3. Change in potential temperature differences with pressure between sigma levels 4 and 6 (500 to 900 mb) in °C/100 mb for a. 36°S and b. 46°N.

In the region of the jets in both hemispheres, the zonally-averaged static stability reduces rapidly during the first two to three days of integration in D. The trend then reverses around day 3 to 3.5, and the static stability increases to a value comparable to A by day 5. Both experiments A and A36 maintain a relatively constant static stability throughout the period being considered, with the A36 case having a much smaller value due to the initialization at day 1.5 from D. It is important to note that the value of static stability is similar in experiments A36 and D, particularly in the southern or spring sector.

Low-level static stability (Fig. 4-3) and the growth rates of wave numbers 6 and 12 (Fig. 4-1) appear to be associated, especially in the adiabatic experiments. The only energy source for the waves in the adiabatic experiment is baroclinic instability. No changes in static stability due to air-sea fluxes or latent heat release can occur in the adiabatic experiments. Thus, it appears significant that wave number 12 develops in A36 at low-levels, but does not develop in A which has a larger static stability (by a factor of 40%). Also, Mullen (1979) found that small-scale cyclones in the north Pacific Ocean generally have very small values of static stability. As noted in Gambo (1976) and Rao and Ferreira (1979), the intermediate-scale baroclinically unstable mode is a shallow wave, and it is not present at 300 mb in A36. The deeper and longer (wave number 6) wave is relatively insensitive to low-level static stability changes and its growth

rate in A36 increases only slightly over that of wave number 6 in A. The variations in growth rates of wave numbers 18 and 24 at the 900 mb level in A36 may be similarly explained in terms of low-level static stability. However, the growth of these waves at 300 mb (southern case only) is nearly identical to that of wave number 6 in A36. Because these waves (18 and 24) are expected to be shallow waves, their occurrence at 300 mb is likely due to nonlinear effects (Williams, 1965).

Low-level static stability in D is not significantly difference from that of A36. Nevertheless the wavelength of the fastest growing wave is shifted to shorter wavelengths in D at all levels. Wave number 12 dominates at 300 mb and wave number 18 dominates at 900 mb. However, wave number 6 grows only slightly faster in D than in A. Static stability is not likely to be the cause for this additional shift, and the only model differences are in the diabatic processes. This implies a latent heating process is responsible for the enhanced growth of the shorter wavelength waves, in agreement with the second unstable mode of Gambo (1976) and Rao and Ferreira (1979). Another fact supporting this reasoning is the much larger growth rates at 300 mb in the northern or fall case. In terms of baroclinic instability processes, the much stronger baroclinically unstable jet is located in the southern case. Consequently, the largest growth rates should be present there, which is true for the shorter waves of A36. If, however, latent heat release is responsible for the larger

growth rates, the lower vertical wind shear and higher sea-surface temperatures in the northern case should produce the largest growth. Also, as is shown below, wave number 18 commences rapid growth at the onset of D, when the low-level static stability is comparable to that in A. This growth appears to be in response to low-level precipitation or latent heat release occurring due to the very moist initial atmosphere, and also due to surface heat fluxes.

Fig. 4-2b also depicts a more vertical structure associated with the shallower wave in D than in the deep waves, or in wave number 6 (Fig. 4-2a) of A. The east-west tilt of the deeper waves is more typical of a growing baroclinic wave, while the lack of tilt of wave number 18 is more suggestive of a latent heat-driven wave (Palmen and Newton, 1969).

To summarize this section, much shorter wavelength waves are present in the diabatic experiment than in the adiabatic experiments. Two processes seem to be responsible for the growth of the shorter wavelength waves. The first is the reduction of the low-level static stability by the diabatic processes. The second is the release of latent heat. The growth rates in the fall case with higher sea-surface temperatures and a weaker jet responded to these diabatic effects more strongly than in the spring case with the stronger baroclinically unstable jet. These results are in close agreement with the case studies of Reed (1979) and Rasmussen (1979). Reed observed small values of low-level static stability

associated with the development of intermediate-scale cyclones while Rasmussen observed strong latent heat release and a tropical structure. Both observed characteristics are present in the diabatic experiment and appear to contribute to the growth of the intermediate-scale waves.

B. SURFACE FLUX MODIFICATION OF GROWTH

The surface fluxes during the initial growth phase are very small in terms of normal atmospheric values (Table 4-2). This is due to the specification of the initial fields and also because the surface wind speed associated with the small amplitude perturbation is still small. However, it will be shown that these small surface fluxes, through interaction of the PBL with the model diabatic processes, have a significant effect on the model atmosphere.

Table 4-2

Surface fluxes of zonal mean sensible heat (S) and moisture (Q) in W/m^2 at day 2. (Q is in latent heat equivalent.)

Latitude	Flux	Experiment		
		D	D-FS	D-FQ
46°N	S	18.3	-	25.6
	Q	48.3	42.0	-
36°S	S	15.2	-	39.5
	Q	42.5	34.4	-

The static stability of the surface flux experiments decreases in the same sense as in D (Fig. 4-4 a-b). D-FS

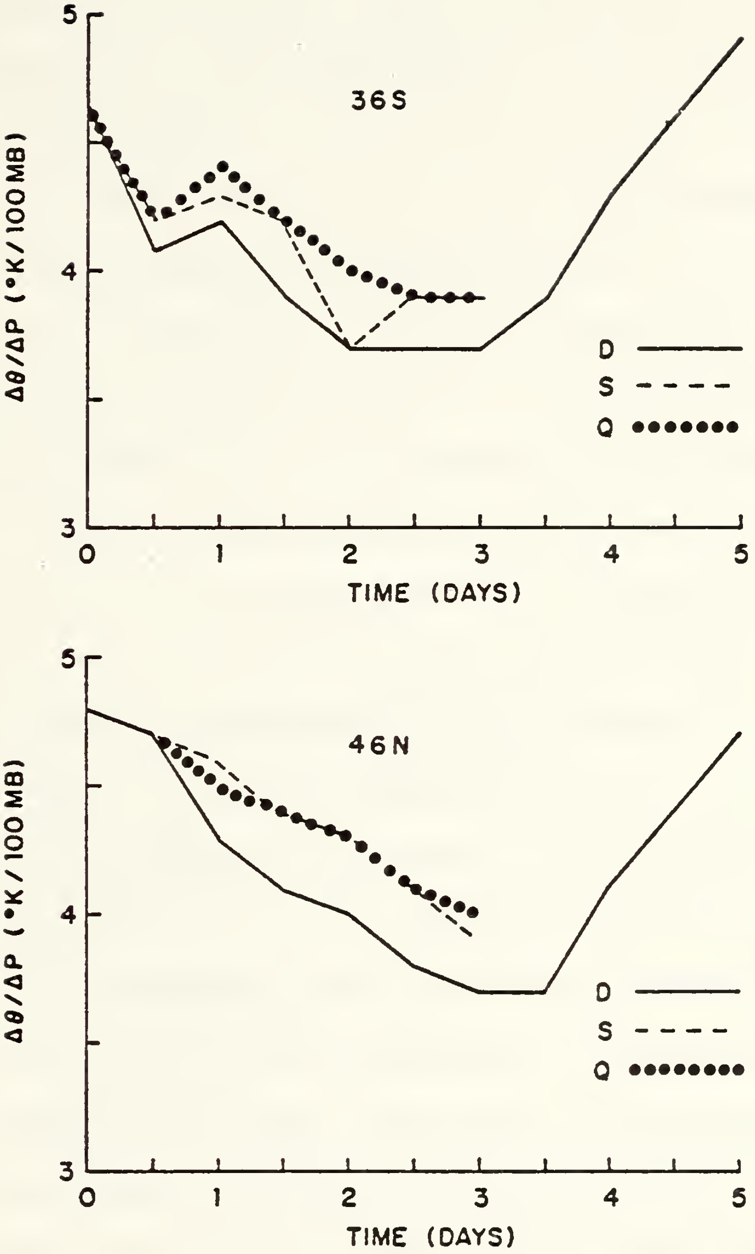

Figure 4-4. As in Fig. 4-3. S and Q represent experiments D-FS and D-FQ respectively.

(no surface sensible heat flux) follows D closer than does D-FQ (no surface moisture flux). Comparison with experiments A and A36 (Fig. 4-3) indicates that static stability in experiments D-FS and D-FQ follows that of A36 more closely than that of A. Consequently, the reduction in static stability should increase the growth of the shorter waves in D-FS and D-FQ to a level at least comparable to A36. This shift, however, should occur gradually as static stability is reduced and not during the initial 24 to 48 h of integration.

Figs. 4-5 a-b give the amplitudes of the meridional wind components at day 2 and day 3 by wavenumber for the diabatic experiments. In the preceding section wave growth rates between days 2.5 and 3.5 are derived for the adiabatic/diabatic comparison. Here the actual amplitudes indicate the temporal change of wave growth in response to static stability and other factors. Note also that values given in Fig. 4-5 are vertically averaged, whereas the values in Fig. 4-1 are at a single level. The values for wave number 6 are much larger than the other wave numbers at day 2 because the model was initialized with a value of approximately .5 m/s in wave number 6. This results in a larger amplitude for this wavenumber even though it may have a smaller growth rate than the higher wave numbers. The exponential growth rates, which depend on the ratios of the day 3 to the day 2 amplitudes, are not shown here.

The largest scale wave, wave number 6, is relatively insensitive to the removal of the surface fluxes. D-FS (no

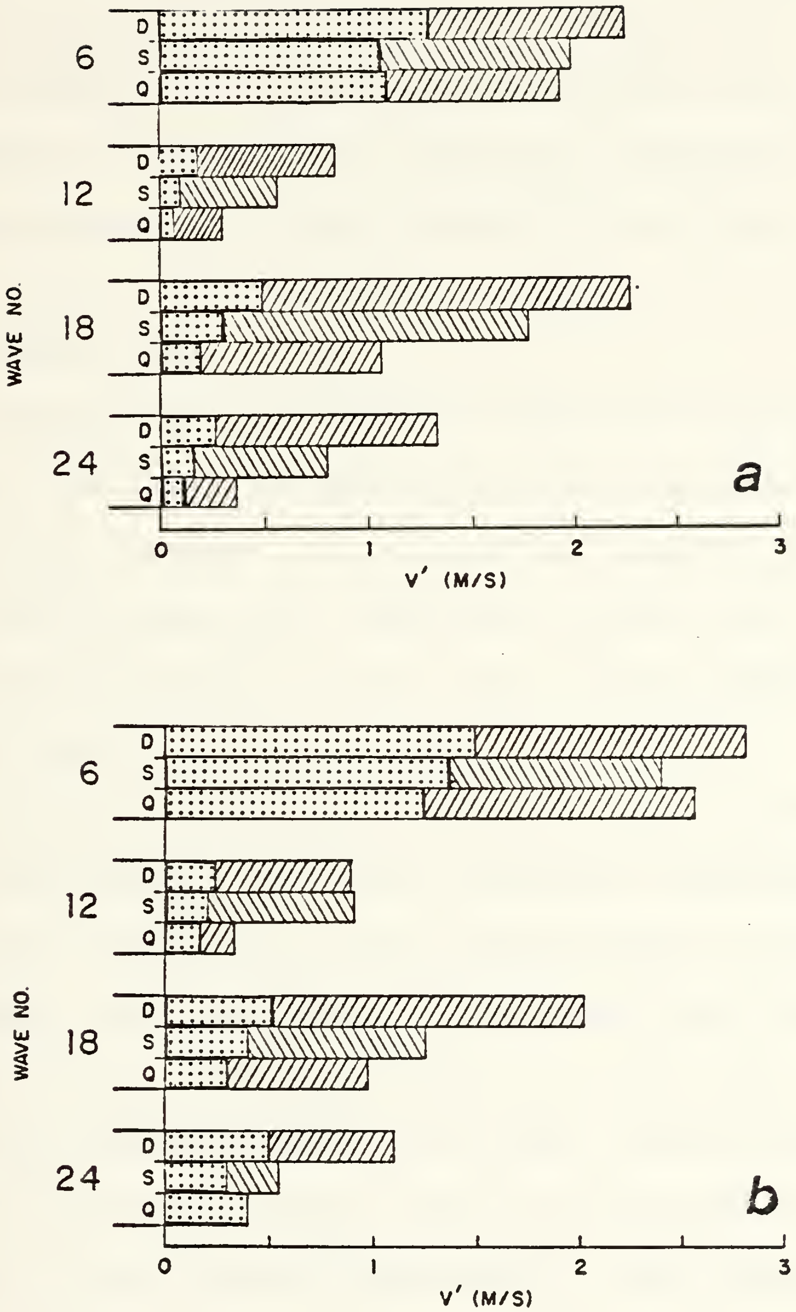

Figure 4-5. Amplitude (m/s) of the meridional wind perturbation by wavenumber for day 2 (stippled) and day 3 (hatched) for a. 46°N and b. 36°S. D, S and Q as in Fig. 4-4.

surface sensible heat flux) and D-FQ (no surface moisture flux) exhibit 10% to 15% less amplitude in wave number 6 than does D. There is also a smaller growth rate in the fall case compared to the spring case with the stronger jet. The reduction in amplitude in D-FS differs from the study of diabatic effects on baroclinic instability discussed in Chapter III. This may be due to the cooperative reduction in surface moisture flux in this experiment as noted in the results presented in Table 3-2.

Wave number 12 is the slowest growing wave during the first one to two days in all the diabatic experiments. Beyond this time, however, it becomes the fastest growing wave in experiments D and D-FS. Referring to Fig. 4-4, the correlation with the decrease in low-level static stability appears to be very high.

Wave number 18 shows the greatest initial growth in the diabatic experiments. This wavelength and wavenumber 24 are also the most sensitive to the surface fluxes of sensible heat and moisture. The amplitude of wavenumber 18 at days 2 and 3 in D-FS is 20% to 40% less than in D. For D-FQ, the amplitudes in both hemispheres are less than 50% of those in D. Wave number 18 growth is more rapid in the fall or weaker jet hemisphere in the diabatic experiments. This behavior is opposite to that of wave number 6, which grows more rapidly in the spring hemisphere. This difference of growth could be either a response to lower values of vertical wind shear as

found by Rao and Ferreira (1979), or a response to higher sea-surface temperatures. Considering changes in growth rate of wavenumber 18, the greatest decrease from loss of the surface sensible heat flux during the first two days occurs in the fall sector. However, wavenumber 18 grows at the same rate between days 2 and 3 in the fall case for all three experiments, which implies that some other process has become dominant.

The vertical distribution of the meridional velocity perturbation for experiments D, D-FS, D-FQ and A is given in Figs. 4-6 a-b. A Fourier analysis routine is used to filter out the mean meridional velocity and all perturbation components with a wavenumber higher than 30. Several tendencies already noted in Figs. 4-1 and 4-5 are present here. The largest amplitude in A is in the spring hemisphere, whereas it is in the fall hemisphere for the diabtaic experiments. The stronger spring jet controls the growth in A. The perturbation in A is much smaller than that found in the diabatic experiments--as much as a factor of 10 smaller than D at 900 mb at 46°N. Removal of the surface fluxes, D-FS and D-FQ, makes the amplitude of the perturbation approach that of the adiabatic experiment. Withholding the surface moisture flux, D-FQ, has a larger effect than removal of the surface sensible heat flux. The contributions of the higher wave numbers (see Fig. 4-5), which grow more rapidly in the fall hemisphere, are responsible for the larger amplitude in that hemisphere of the diabtaic experiments.

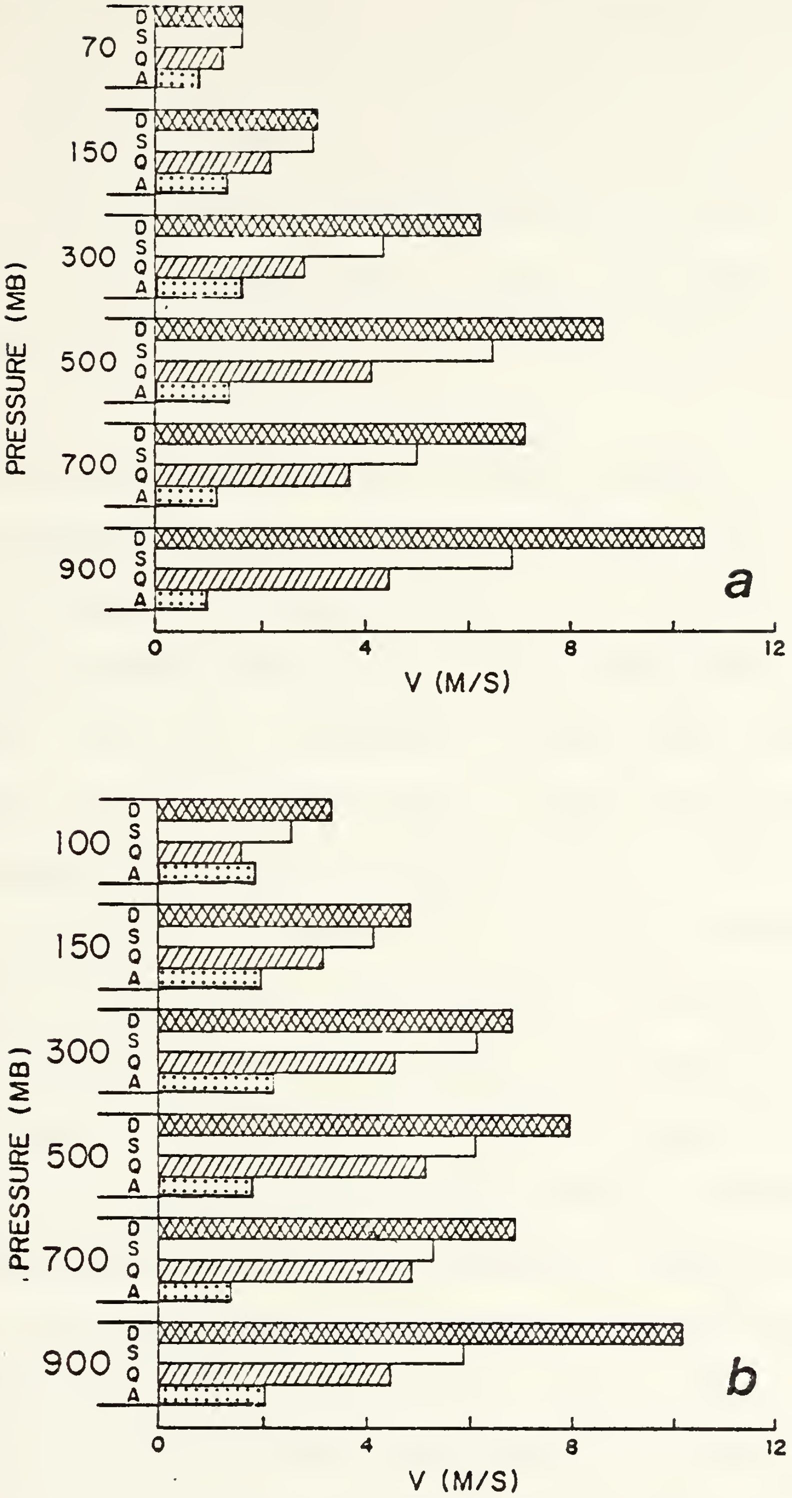

Figure 4-6. Amplitude (m/s) at day 3 of the meridional wind perturbation summed over wavenumbers 6 through 30 for a. 46°N and b. 36°S. Experiments D, S(D-FS), Q(D-FQ) and A are compared.

The largest amplitude in D is at the lowest model level. This is due to the contributions of the high wavenumber components which tend to be associated with shallow systems. In D-FQ and D-FS, the greater response of the shorter waves to the loss of the surface fluxes causes the greatest reduction in growth at the lowest level. Again, D-FS and D-FQ tend toward the adiabatic experiment which has its largest amplitude at 300 mb.

The temperature perturbations are much larger in the diabatic experiments than in A (Figs. 4-7 a-b). The inclusion of the surface fluxes increases the amplitude of the perturbations. The percentage decrease in the temperature perturbation of D-FS, D-FQ and A relative to D does not reflect the larger decrease in wave growth that is found for the meridional velocity perturbation. The implication here is that the contribution to growth of the wave is not in direct response to the addition of low-level heat through the surface fluxes. These fluxes must also indirectly cause the greater wave growth exhibited by the meridional velocity component.

The vertical velocity perturbations (Figs. 4-8 a-b, derived as for the meridional velocity perturbation) appear to be the link between the temperature perturbations and the wave growth as seen in the velocity perturbations. The vertical velocity perturbation in D is 10 to 20 times that of A. Haltiner (1971) describes how larger vertical velocities resulting from diabatic heating lead to a greater conversion of eddy

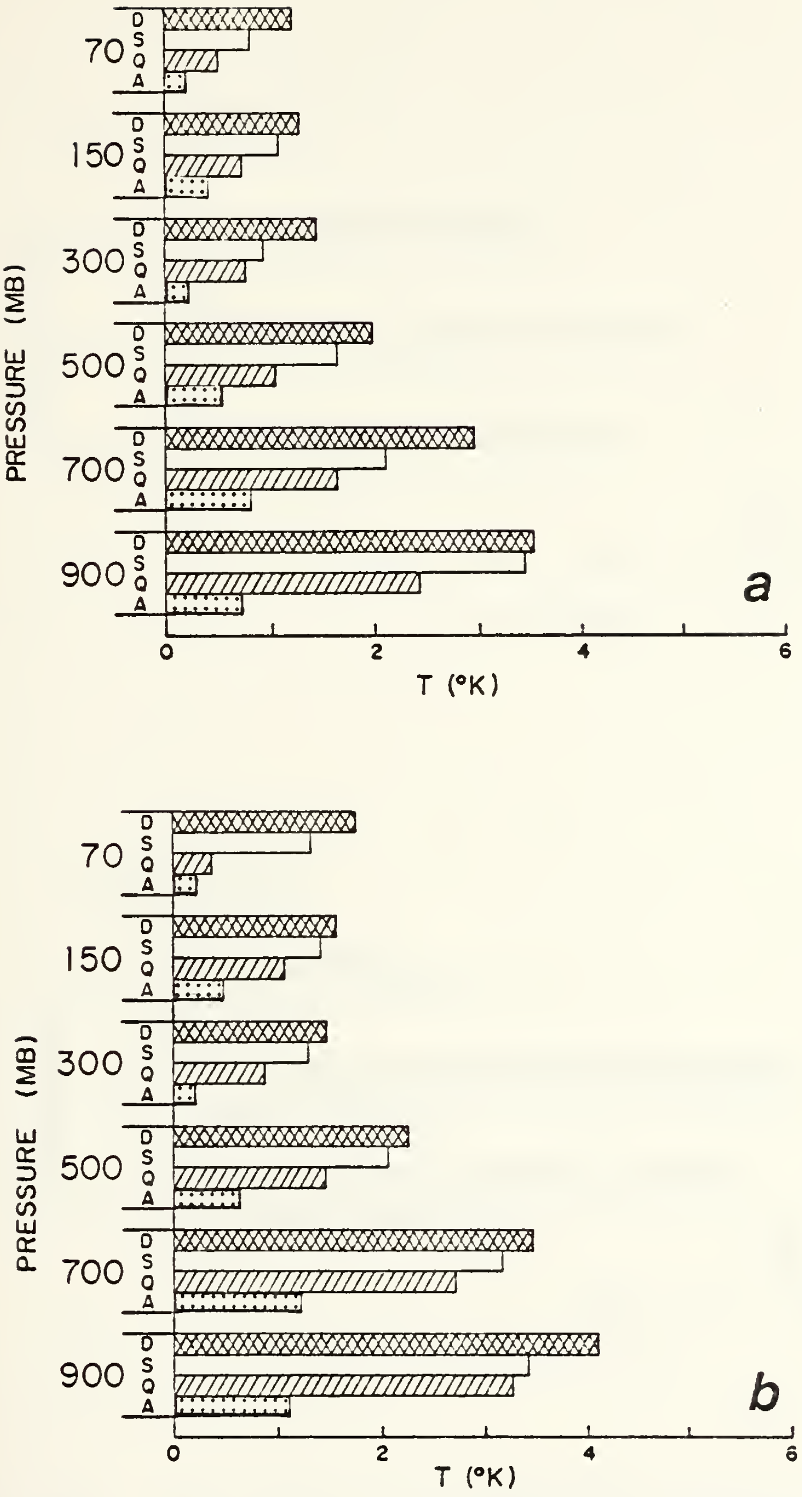

Figure 4-7. As in Fig. 4-6 except for temperature perturbation (°C).

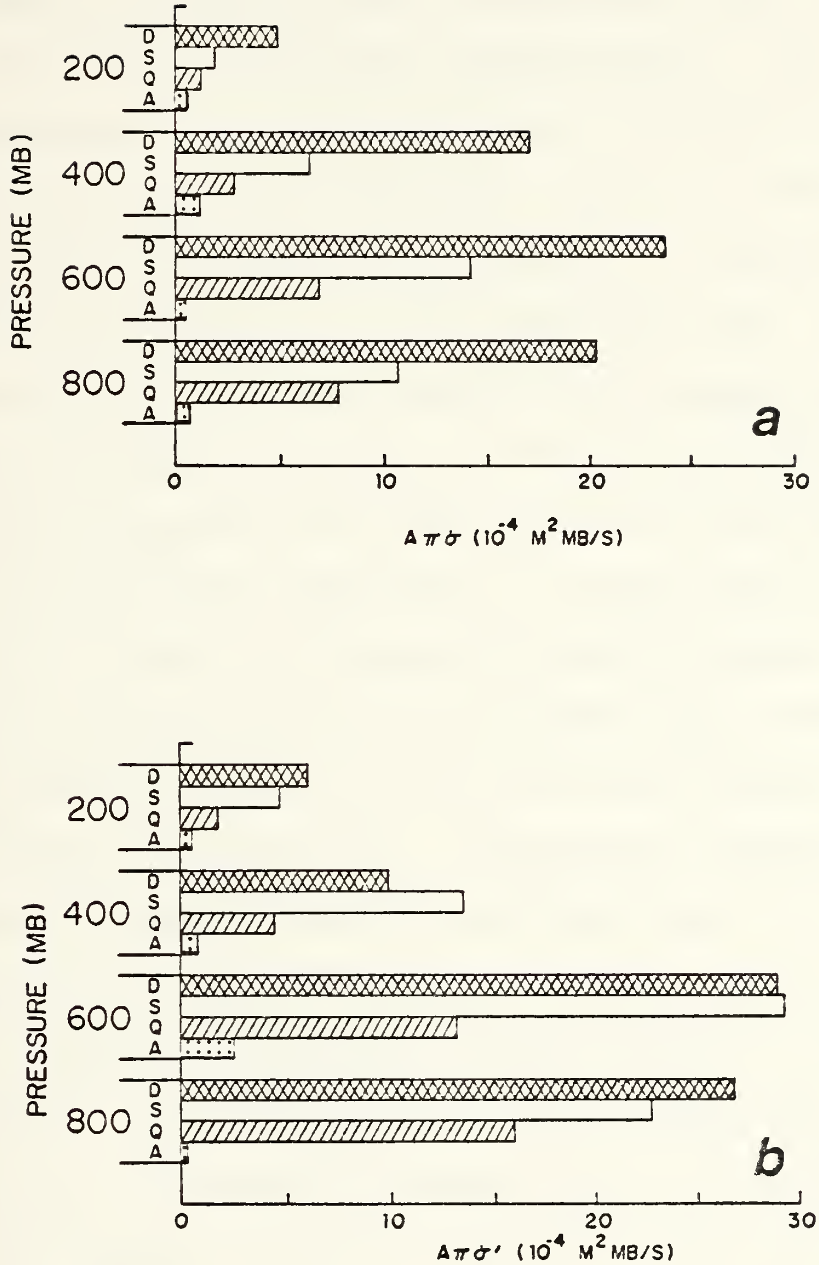

Figure 4-8. As in Fig. 4-6 except for vertical velocity perturbation (10^{-4} m^2 mb/s).

available potential energy to eddy kinetic energy, resulting in enhanced wave growth. A large portion of the difference between vertical velocities in D and A is clearly due to the surface fluxes of sensible heat and moisture, with surface moisture flux (D-FQ) having the greatest effect. The hemispheric difference is also evident here. At 46°N with a higher SST and weaker jet, D-FS has a vertical velocity perturbation 40% to 50% less than that in D. In the spring hemisphere, the difference is less than about 10%. The slightly larger value at 400 mb in the spring case becomes slightly less than in D when the values are averaged over 34° to 36°S. In the spring hemisphere, vertical velocities associated with the stronger jet may be sufficient to trigger the release of latent heat. In the fall hemisphere with the weaker jet, the contribution of the larger surface sensible heat fluxes in generating vertical velocities may be a major factor in triggering the release of latent heat. Hemispheric differences are also evident in D-FQ (no surface moisture flux). In the fall case, vertical velocity perturbations range from an approximately 85% reduction from those in D at 200 mb to a 65% reduction at 800 mb. The corresponding spring case range is 70% to one of 40%. The surface sensible heat and moisture fluxes appear to be cooperative (as in Table 4-2), and the lower SST of the spring hemisphere results in a smaller moisture flux or influence by the moisture flux.

The contributions of the surface fluxes to the distribution of the vertical velocity is not the same for both moisture

flux and sensible heat flux. In D-FQ, the largest perturbation is in the lowest layer, 800 mb, in both hemispheres. This is due to the surface sensible heat flux causing the greatest heating at this level. In D-FS, the maximum is at 600 mb, due to heating caused by the release of latent heat at higher levels. Again, a cooperation between the two surface fluxes may be required to produce the large vertical velocities associated with D.

In summary, the surface fluxes of sensible heat and moisture contribute to a reduction in low-level static stability in the diabatic model atmosphere. This reduction is sufficient to shift the wavelength of maximum growth in the model atmosphere to shorter wavelengths than those found in the adiabatic model atmosphere. In addition, latent heating in the diabatic experiments enhances the development of shorter wavelengths. This latent heating is very sensitive to the availability of low-level moisture and, to a lesser degree, surface sensible heat fluxes. The fall case with a weaker jet and higher sea-surface temperatures is much more sensitive to changes in the surface fluxes.

V. SECONDARY LOW DEVELOPMENT EXPERIMENT

Several observational studies of secondary lows or polar lows have been performed. Nitta and Yamamoto (1974) and others investigated the development of weak, small-scale cyclones over the East China Sea. Mullen (1979) and Reed (1979) have completed case studies of polar lows which form in polar outbreaks associated with major frontal systems or large-scale cyclones over the eastern Pacific Ocean. Rasmussen (1979) has investigated small-scale, intense cyclones in the North Atlantic Ocean which he also terms polar lows. These systems have two common features. They are small or intermediate scale (zonal wavelength of 1000 to 2000 km), and they originate over the ocean. Reed (1979) has also noted that very few intermediate-scale cyclones occur over land. Because these lows appear mainly over the ocean, it is felt that air-sea fluxes are likely to be important during their evolution.

Intermediate-scale waves are present throughout the diabatic model experiments, although they are dominated by the large-scale primary cyclone. This chapter examines the evolution of the secondary cyclones using the technique described above of selectively removing the surface flux processes from the diabatic model. Table 5-1 is a list of the integrations performed for this experiment. Fields from the full diabatic experiment are used to initialize the other model experiments at day 4 (S4) and day 9 (S9).

Table 5-1

Experiments for the secondary development study

Exp.	Initial Fields[*]	Integration Period	Model Version[*]
D	S (wave no. 6)	15 days	complete diabatic
D-FS(4)	S4 (fields from D at day 4)	6 days	diabatic w/o surface sensible heat flux
D-FQ(4)	S4	6 days	diabatic w/o surface moisture flux
D-FSQ(4)	S4	6 days	diabatic w/o surface moisture or sensible heat fluxes
F(4)	S4	6 days	adiabatic w/friction
D-FS(9)	S9 (fields from D at day 9)	3 days	diabatic w/o surface sensible heat flux
D-FQ(9)	S9	3 days	diabatic w/o surface moisture flux
D-FSQ(9)	S9	3 days	diabatic w/o surface moisture or sensible heat fluxes
F(9)	S9	3 days	adiabatic w/friction

[*] See Sections II.C and II.D for a more complete discussion of model variations and initial conditions.

Four cases involving development of a secondary cyclone wave are examined. Surface pressure maps for an illustrative time from each case are presented in Figs. 5-1 a-d. The first three maps are from D and the last is from D-FSQ. A common feature of the first three cases is that the secondary lows develop in the equatorward flow over warmer water, similar to the polar lows studied by Reed (1979) and Rasmussen (1979). The first two cases examined (see Figs. 5-1a and b) are fall hemisphere developments, while the last two cases (Figs. 5-1c and d) are spring hemisphere developments. Intermediate-scale waves grow more readily in the initial development experiments. Not only is the number of secondary lows larger in the fall hemisphere than in the spring hemisphere of the diabatic experiment, they are also more intense. It will be shown that the secondary lows in the fall case may evolve into the next primary cyclone. In the spring case, the secondary lows remain relatively weak compared to the primary cyclone and dissipate more rapidly.

Expanded analyes of various model atmosphere parameters and derived quantities are presented below. Analyses cover an area of 18° lat by 22.5° long or 10 x 10 model grid points. The expansion is about the same center point for any given time and hemisphere, and is chosen as approximately the position of the center of the secondary cyclone in D-FS, except as noted. Southern hemisphere analyses are inverted with south at the top of the map for ease of comparison with the northern hemisphere cases.

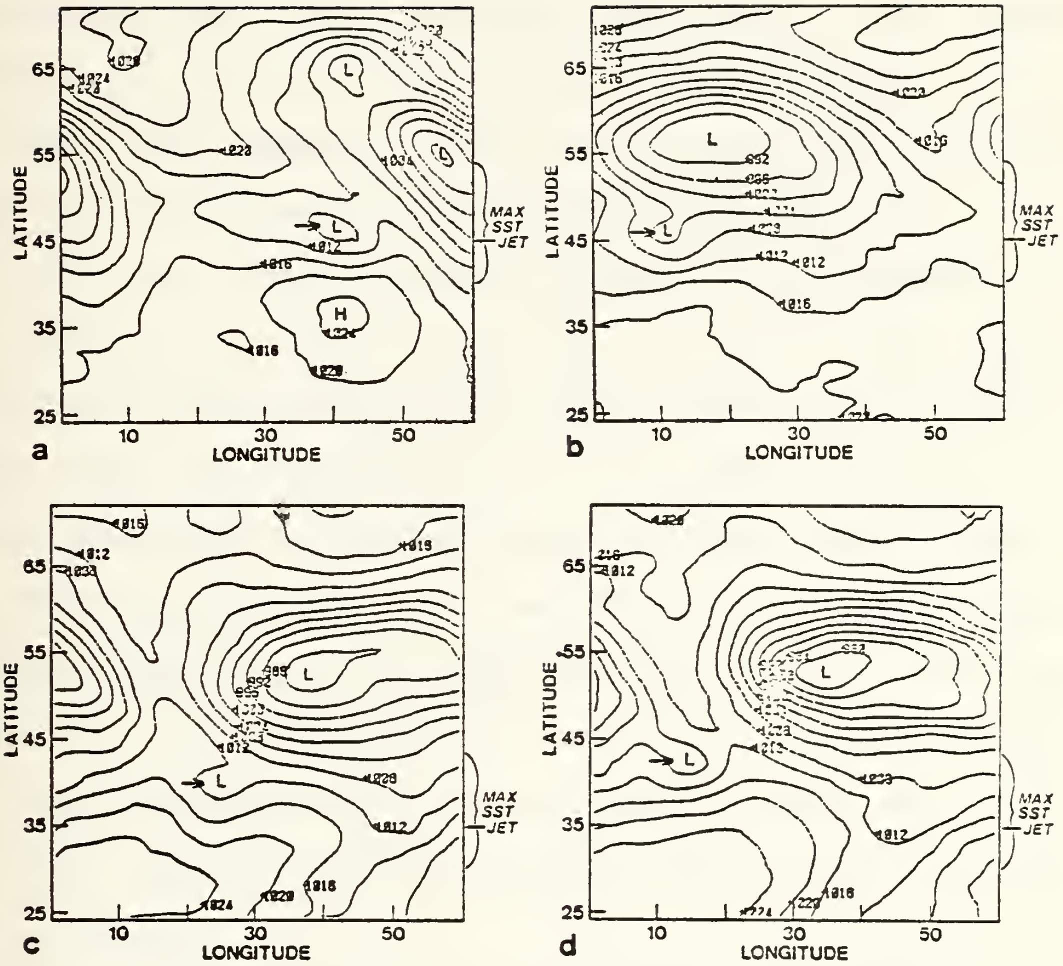
a
LATITUDE
LONGITUDE
65
55
45
35
25
10
30
50
L
H
1012
1016
1020
MAX SST JET
b
LATITUDE
LONGITUDE
L
992
1012
1016
MAX SST JET
c
LATITUDE
LONGITUDE
L
1012
1016
1020
1024
MAX SST JET
d
LATITUDE
LONGITUDE
L
1012
1016
MAX SST JET

Figure 5-1. Surface pressure maps for D for a. Case A, day 6.5, b. Case B, day 11, c. Case C, day 11 and d. Case D, D-FSQ, day 10.5. Contour interval 4 mb. Secondary low for case study indicated by an arrow in each figure.

A. CASE A--FALL HEMISPHERE DAYS 6-8

Case A gives an example of selective development of a secondary low. At day 6 of D a double low exists approximately 35 degrees west of the main primary low (see position in Fig. 3-2a). A very similar system exists in the same location in experiments D-FS, D-FQ and D-FSQ (see Figs. 3-7 a-c, respectively). At day 6 all four diabatic experiments, D, D-FS, D-FQ and D-FSQ, exhibit a dual low structure with a 1004 mb central pressure (see expanded surface pressure analyses Figs. 5-2 a-d). These secondary lows evolve differently during the next 12 h (Figs. 5-3 a-d and 5-4 a-d). The cyclones in D-FS and D-FSQ (no surface sensible heat flux) are more intense than their counterparts, D and D-FQ. In addition, in D-FQ and D-FSQ (no surface moisture flux) the westward lobe of the initial dual low (see Fig. 5-2a) has developed, causing a phase lag of 9° long behind the lows in D and D-FS after 12 h. A slight phase lag (1° long) is also associated with the addition of the surface sensible heat flux. The low in D lags that in D-FS and, similarly, the low in D-FQ lags that in D-FSQ.

In D and D-FS, the secondary cyclone intensifies as it moves into the northerly flow region of the primary cyclone (see Figs. 5-5 a-d), and eventually absorbs and replaces the primary cyclone. This is not true in D-FQ and D-FSQ. In the latter experiments the secondary cyclone gradually weakens and is absorbed by the primary cyclone. The secondary lows are relatively sensitive to the air-sea fluxes. Therefore,

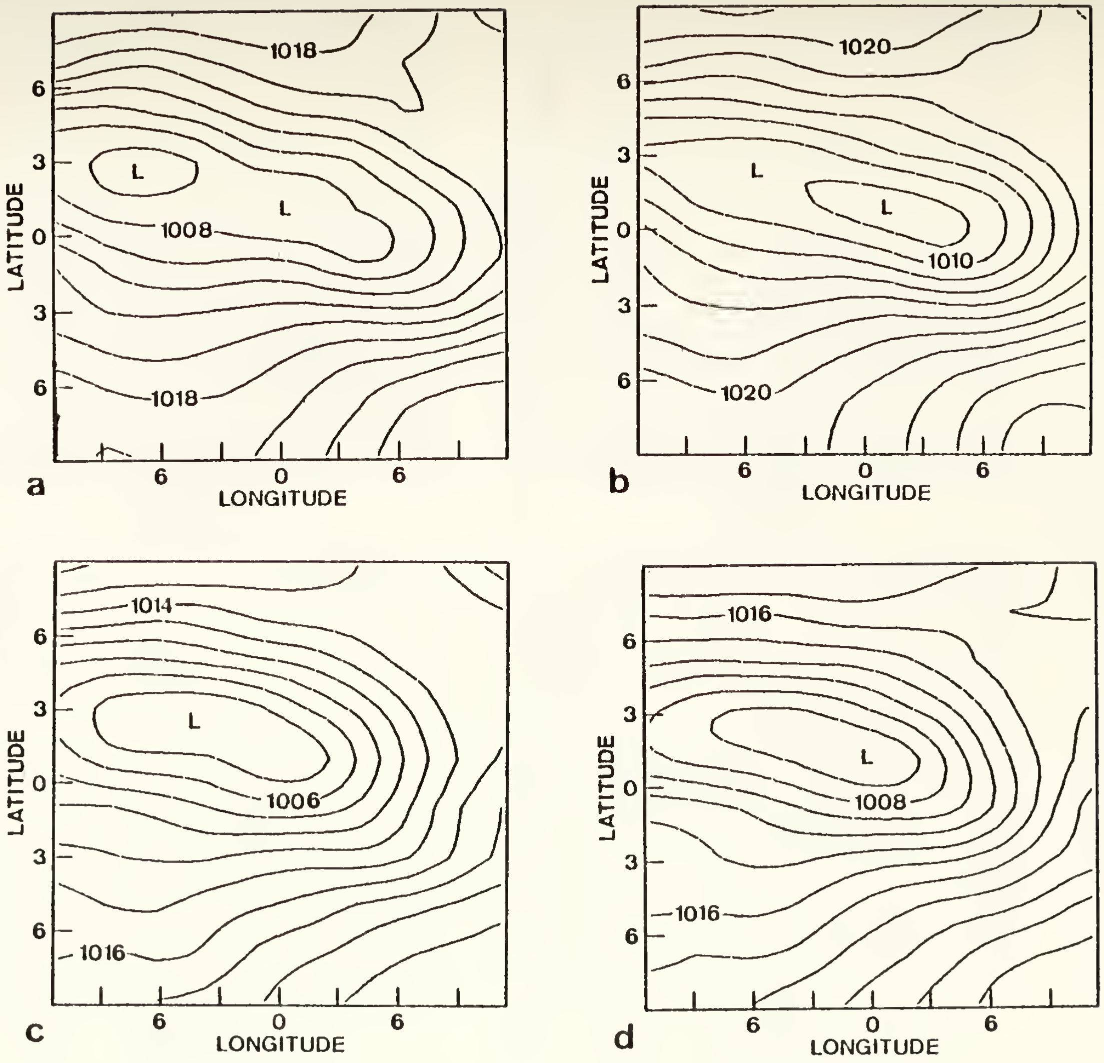
1018
6
3
L
L
1008
0
3
6
1018
6
0
6
LONGITUDE
LATITUDE
a
1020
L
L
1010
1020
b
1014
L
1006
1016
c
1016
L
1008
1016
d

Figure 5-2. Expanded surface pressure maps of the secondary low for Case A at day 6 in the fall hemisphere for a. D, b. D-FS, c. D-FQ and d. D-FSQ. Contour interval 2 mb.

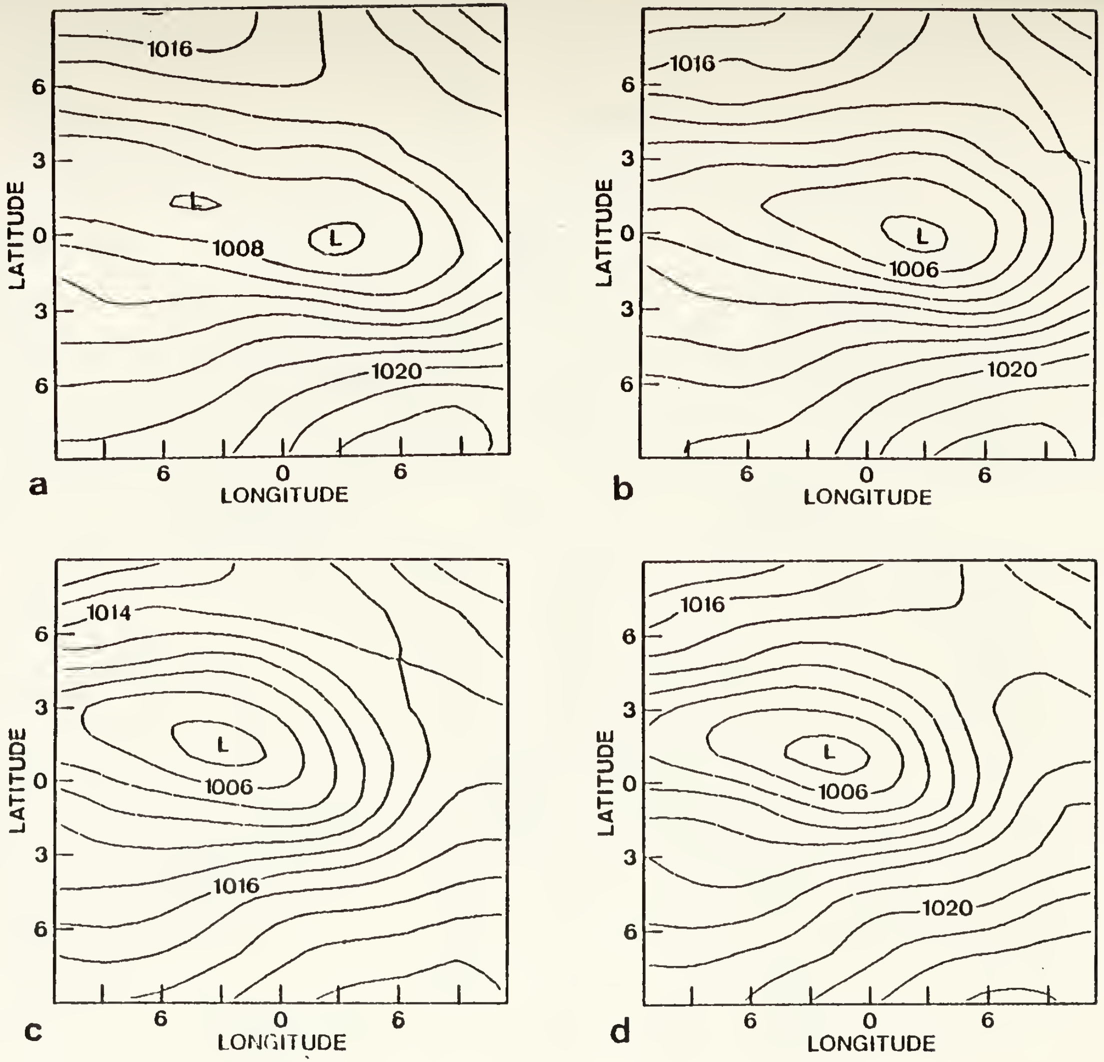

Figure 5-3. As in Fig. 5-2 except for day 6.25.

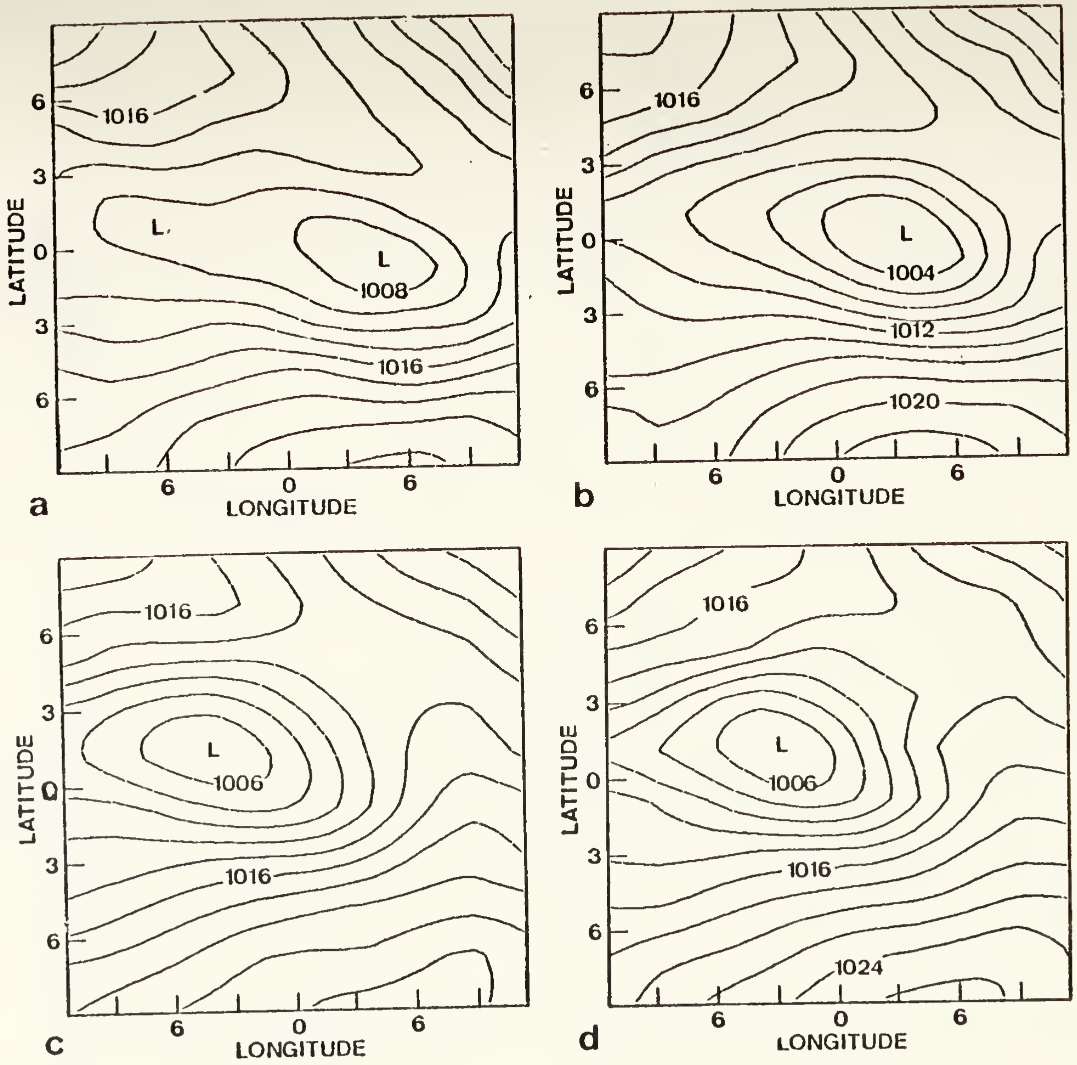
a
LATITUDE
6
3
0
3
6
1016
L
L
1008
1016
6
0
6
LONGITUDE
b
LATITUDE
1016
L
1004
1012
1020
c
LATITUDE
1016
L
1006
1016
d
LATITUDE
1016
L
1006
1016
1024

Figure 5-4. As in Fig. 5-2 except for day 6.5.

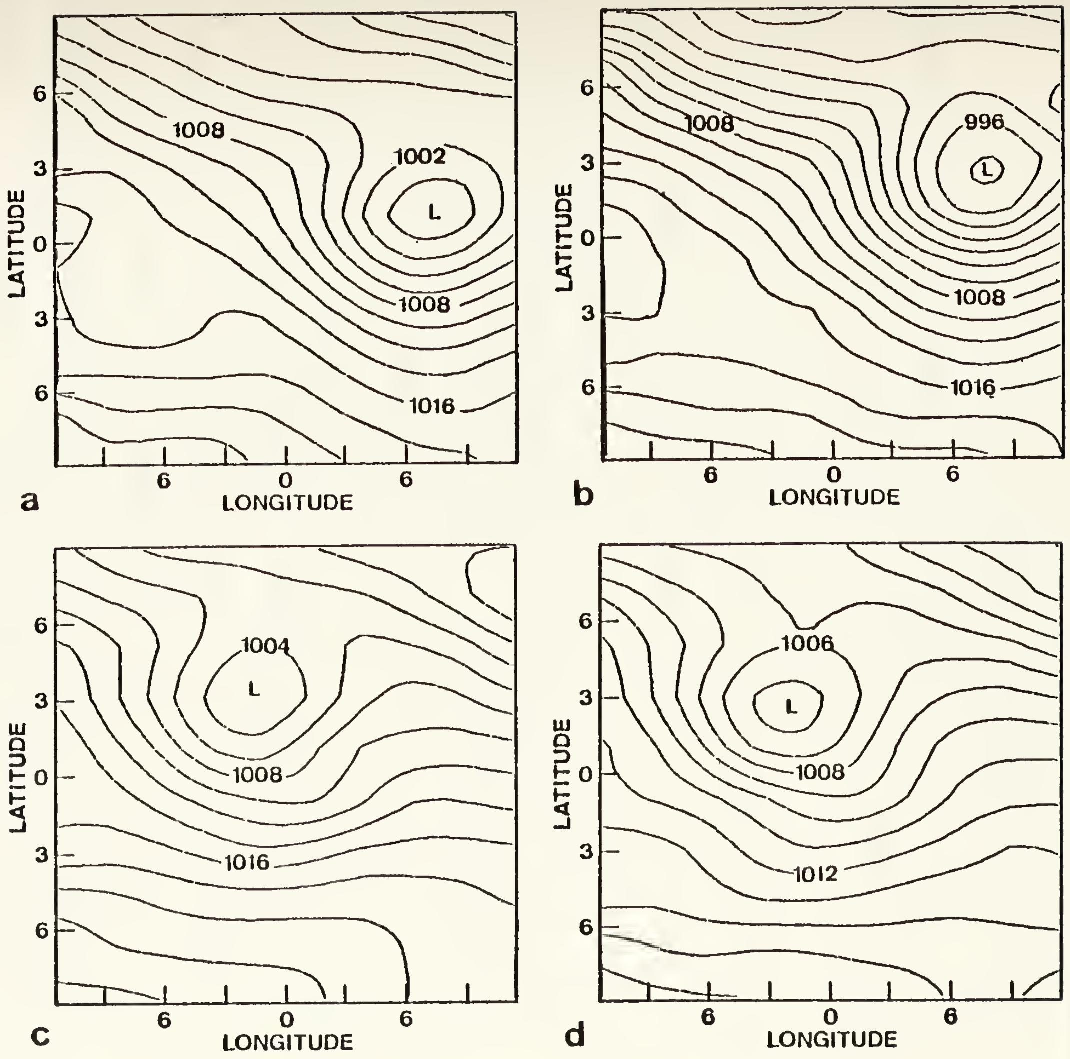

Figure 5-5. As in Fig. 5-2 except for day 8.

modification of the fluxes can result in a greatly different evolution in the atmosphere on a time scale of three to four days. In this case, the large differences are due more to selection of a different perturbation, rather than being due to significant differences in intensification rates.

The major differences in development occur in response to the low-level temperature advection and the release of latent heat. The low develops within a strong baroclinic zone (see Figs. 5-6 a-d) with the strongest temperature gradient and thermal advection located to the east of the low. The low-level temperature gradient is largest in D-FSQ (no surface flux) and smallest in D (full diabatic).

Precipitation is restricted to the region east of the secondary lows in all of the experiments (see Figs. 5-7 a-b and 5-8 a-d). At day 6 (Fig. 5-7), the precipitation rate associated with the developing secondary low in D and D-FS is up to 11 cm/day, although this rate decreases slightly at day 6.25 (Fig. 5-8). The precipiation rate in D-FQ and D-FSQ is less than 2 cm/day at day 6 (not shown) and increases slightly to 2 and 5 cm/day, respectively, at day 6.25. The maximum precipitation occurs over the region of maximum horizontal temperature advection (Fig. 5-6) in all experiments. Convective precipitation is less than 20% of the total precipitation in all cases. The low-level specific humidity fields at day 6 (Fig. 5-9 a-d) reflect the loss of the surface moisture flux in D-FSQ and D-FQ. Specific humidity is approximately 30% higher in the region of maximum precipitation in

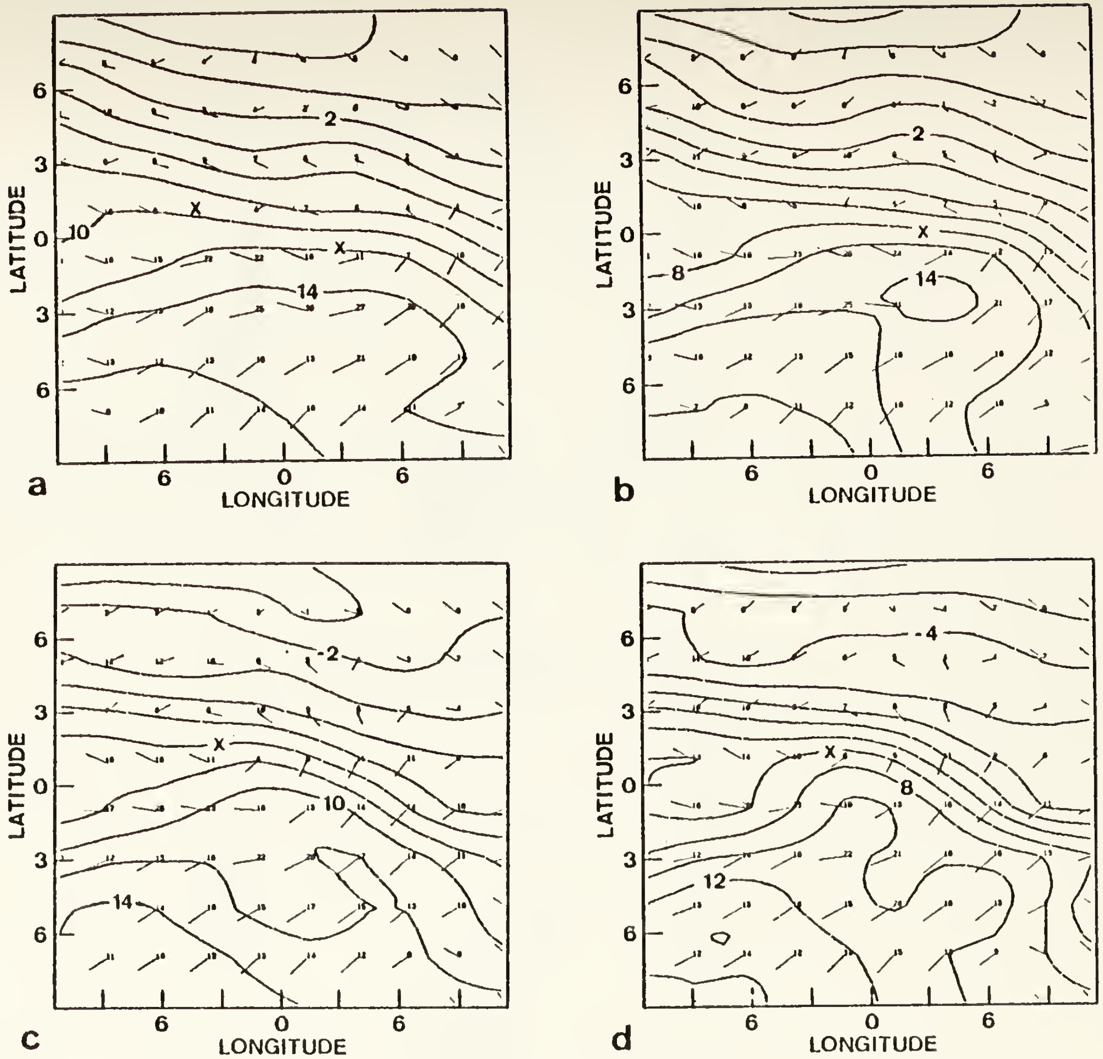

Figure 5-6. Temperature field with vector winds at lowest sigma level (900 mb) for day 6.25 using the expanded region as in Fig. 5-3 for a. D, b. D-FS, c. D-FQ and d. D-FSQ. Contour interval 2°C. X indicates position of secondary low. Vector length proportional to square root of wind speed. Speed also given at vector head (m/s). Direction of vector toward wind speed value.

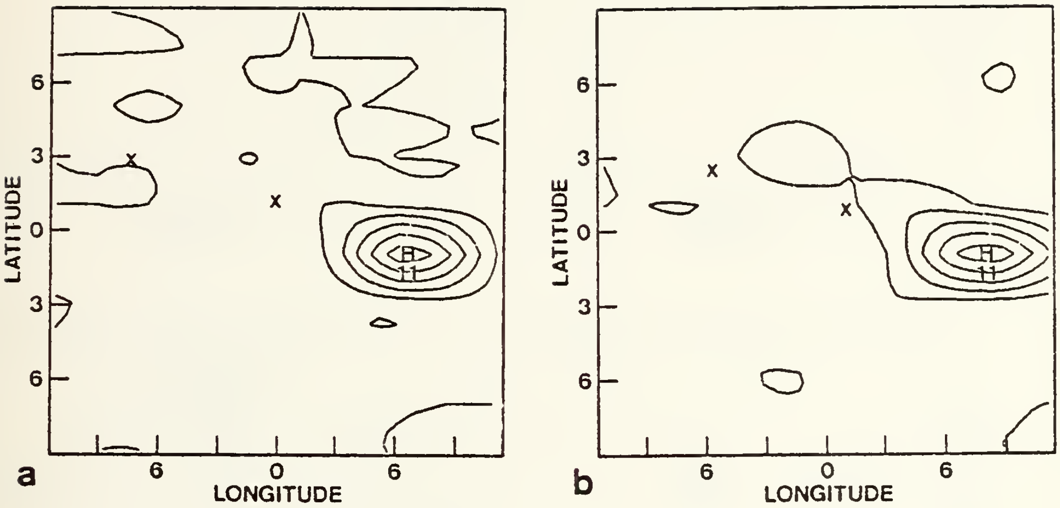

Figure 5-7. Precipitation rate for day 6 and expanded region as in Fig. 5-2 for a. D and b. D-FS. Contour interval 2 cm/day. Experiments D-FQ and D-FSQ not shown as rate less than 2 cm/day.

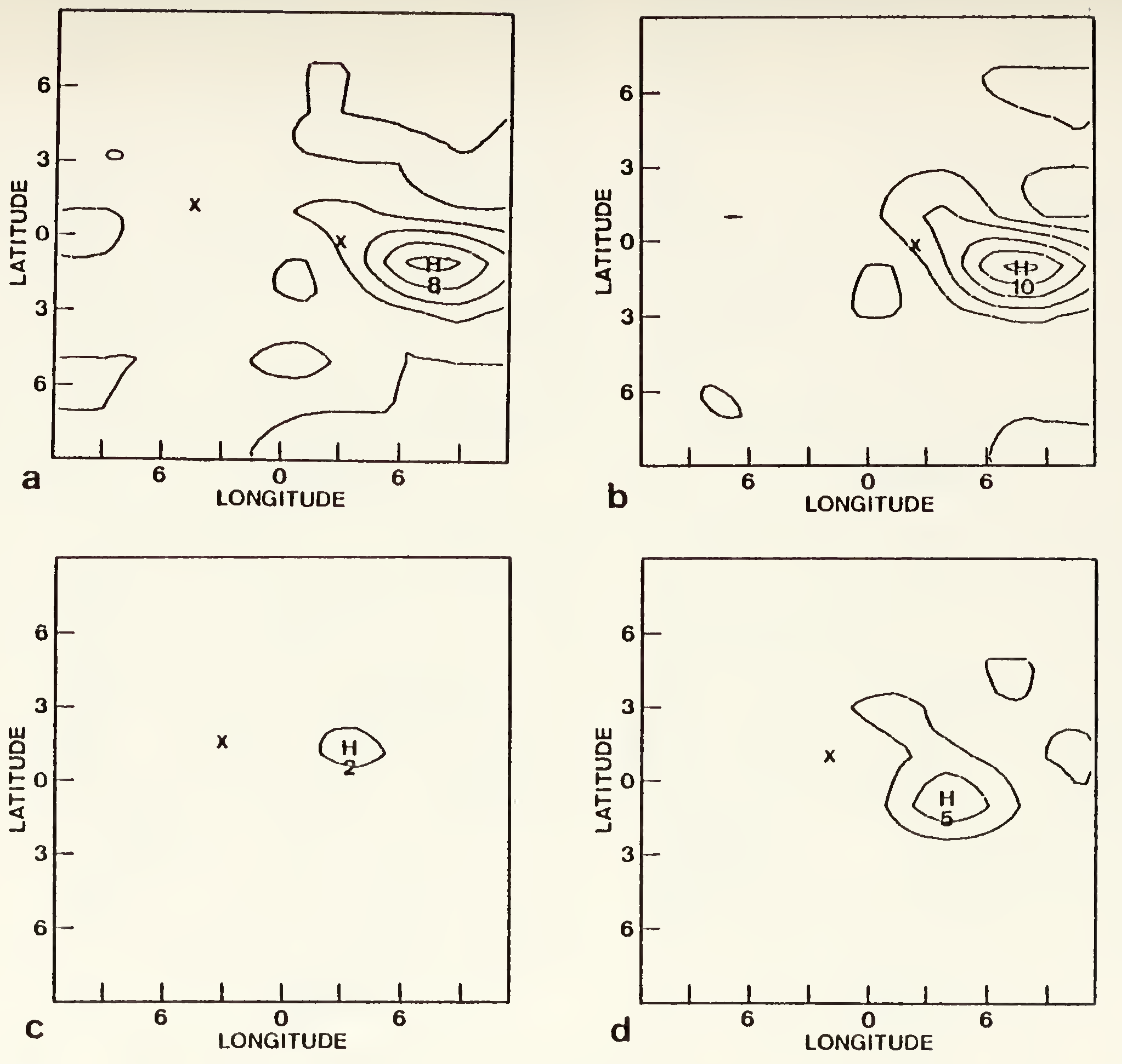

Figure 5-8. Precipitation rate for day 6.25 and expanded region as in Fig. 5-3 for a. D, b. D-FS, c. D-FQ and d. D-FSQ.

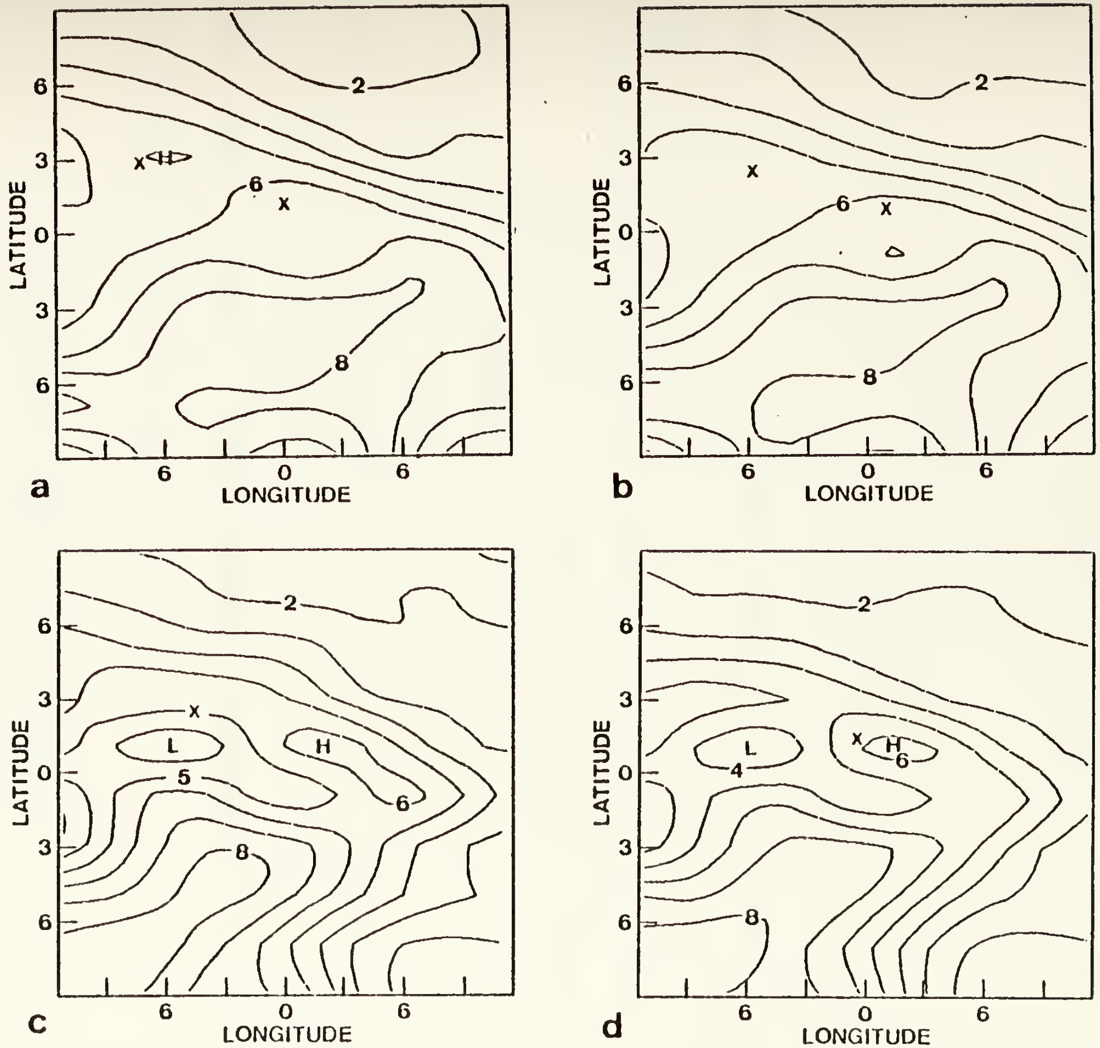

Figure 5-9. Specific humidity at the lowest model sigma level (900 mb) for day 6 and expanded region as in Fig. 5-2 for a. D, b. D-FS, c. D-FQ and d. D-FSQ. Contour interval 1 g/kg.

D and D-FS. The pattern of maximum specific humidity, and also the low-level wind field seems to indicate strong moisture advection from the southwest of the secondary low. In D-FQ and D-FSQ only, a region of relatively low specific humidity is present in the western quadrant of the secondary low.

The direction of motion of the secondary low is toward the southeast in all of the experiments. This is toward the maximum low-level thermal gradient, the area of highest precipitation and largest low-level moisture. The implication is that the development is brought about by low-level thermal processes as noted by Petterssen _et al._, (1962), and that the surface fluxes of sensible heat and moisture significantly modify this development.

To investigate the relative importance of the surface fluxes in the development of the secondary cyclone, the thermal terms of Petterssen's development equation (Petterssen, 1956) are evaluated. Petterssen's development equation derived in a sigma coordinate system is:

$$\underbrace{\frac{\partial \zeta_{g0}}{\partial t}}_{A} = \underbrace{\frac{\partial \zeta_{gu}}{\partial t}}_{B} - \underbrace{\frac{g}{f} \nabla^2 \frac{\partial h}{\partial t}}_{C} , \qquad (5\text{-}1)$$

where:

ζ_g = geostrophic vorticity

g = acceleration of gravity

f = coriolis parameter, and

h = thickness from level 0 to level u.

Here, term A represents the local change in geostrophic vorticity at the surface, term B is the local change in geostrophic vorticity at an upper level and term C is the change in thermal vorticity due to a change in thickness caused by warming or cooling the column of air.

Terms A and B can be inferred from the surface pressure fields and upper-level wind fields. Term C can be expanded to evaluate the contributions of the individual thermodynamic processes as follows:

$$g\frac{\partial h}{\partial t} = R\int_{\sigma_u}^{\sigma_0}\{\underbrace{-\mathbb{V}_H\cdot\nabla_\sigma T}_{D} + \underbrace{\dot{\sigma}\left(\frac{\alpha}{C_p}\pi-\frac{\partial T}{\partial\sigma}\right)+\frac{\alpha}{C_p}\sigma\frac{d\pi}{dt}}_{E}$$

$$+\underbrace{\frac{1}{C_p}\frac{dH}{dt}}_{F}\}\,\delta(\ln\sigma)\ , \qquad (5\text{-}2)$$

where:

$\mathbb{V}_H$ = horizontal wind on a sigma surface

∇_σ = horizontal gradient operator on a sigma surface

T = temperature

π = surface pressure

α = specific volume

C_p = specific heat at constant pressure

σ = p/π where p is pressure on a sigma surface

$\dot{\sigma}$ = $d\sigma/dt$

dH/dt = heating rate due to diabatic effects such as radiation and latent heat release, and

R = gas constant for dry air.

Here, term D represents the change in thickness due to temperature advection, term E the change due to dynamic warming or cooling and term F the change due to diabatic heating. In general, warm advection and precipitation (terms D and F) tend to enhance low-level vorticity, whereas the compensating upward vertical motion (term E) tends to oppose development.

Certain assumptions are necessary to evaluate the terms of the above equations. The upper level is chosen as sigma level 4 which is approximately 500 mb. Only a very weak disturbance in essentially straight flow exists at this level. The equations were also evaluated at one of the time periods using sigma level 5 as the upper level (approximately 700 mb) and yielded qualitatively the same results. The lowest model layer contains an idealized planetary boundary layer. Calculations in this layer are performed using an average of the sigma level 6 (900 mb) values and the surface values (19.5 m for wind values), rather than recalculate the complete boundary layer formulation.

Term B of the Petterssen development equation represents the contribution to low-level vorticity due to the change in upper-level vorticity. Comparison of sigma level 4 (500 mb) winds from D and D-FQ at days 5.5, 6 and 6.25 revealed nearly identical (± 1 m/s) winds with a small dual trough located vertically above the surface secondary lows in both experiments. The contribution to the secondary development from term B appears to be minor and in any case should be similar in the two experiments.

Term D represents the change in thickness due to horizontal temperature advection. The region of strongest advection is discussed above in terms of the low-level temperature and wind fields (Fig. 5-6). Term D (see Figs. 5-10 a-d) gives the thickness change in the lower model atmosphere produced by the horizontal temperature advection. The smallest thickness increases east of the secondary lows occur in D, and the largest in D-FSQ. The area of positive thickness increases is also much larger in D-FS, D-FQ and D-FSQ (no surface flux). This maximum thickness increase occurs five degrees westward in D-FQ and D-FSQ (no surface moisture flux experiments). This is consistent with the development of the western perturbation in these experiments.

Term E (Figs. 5-11 a-d) represents the dynamic cooling of the rising air and acts as a braking term to oppose development. This term is influenced both by the lapse rate of the environmental air and by the magnitude of the vertical motion--either larger upward motion or a smaller lapse rate leads to

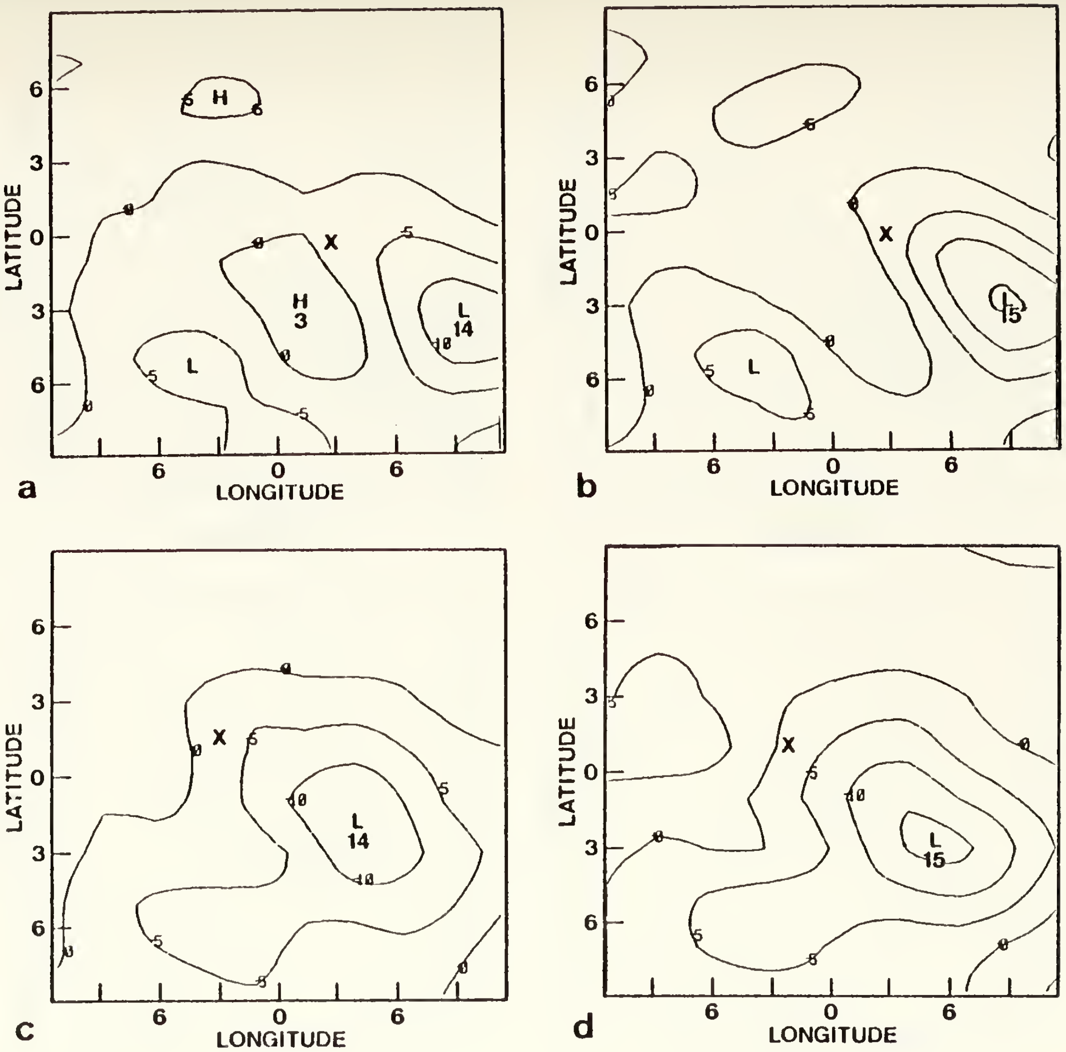
a
b
c
d
LATITUDE
LONGITUDE
6
3
0
3
6
H
L
14
L
H
3
15
L
14
15
X
5
10
0

Figure 5-10. Term D of the Peterssen development equation for day 6.25 and an expanded region as in Fig. 5-3 for a. D, b. D-FS, c. D-FQ and d. D-FSQ. Contour interval 5 x 10^{-5} °C/s (4.3 °C/day). Position of secondary low indicated by X. See text for discussion.

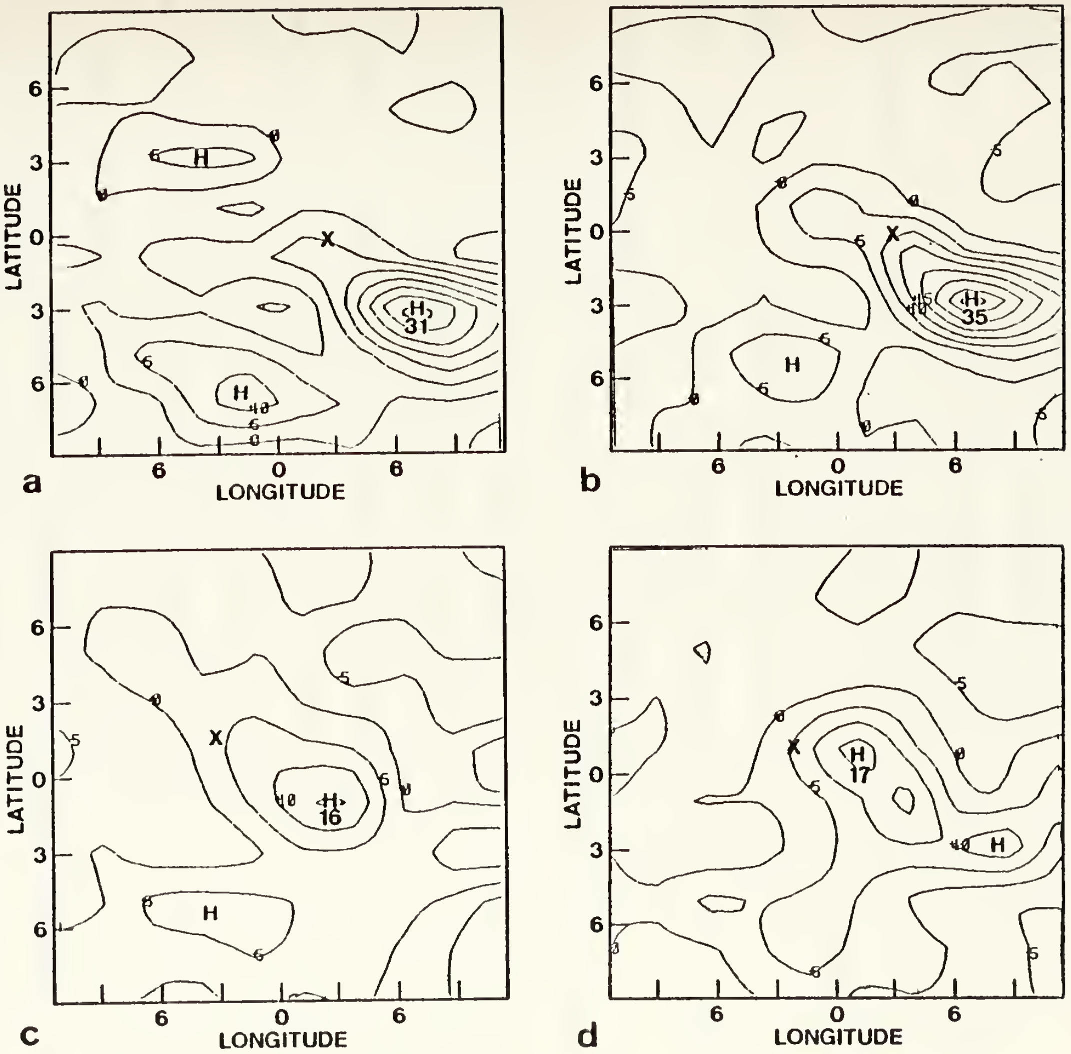

Figure 5-11. As in Fig. 5-10 except for term E.

greater braking. D and D-FS have very large values of term E. The secondary low in D has the highest central pressure at day 6.25 (see Fig. 5-3), and yet the magnitude of term E is twice that of D-FQ and D-FSQ. As discussed in the initial growth experiments, this is associated with vertical velocities that are two to three times larger in D and D-FS.

Term F (Fig. 5-12 a-d) represents the warming/cooling of the column of air through the diabatic processes of radiation, precipitation (latent heat release) and surface sensible heat flux. The greater warming in D-FS relative to D seems to be related to the 20% greater precipitation (see Fig. 5-7) in D-FS at day 6.25. This difference obscures the influence of the surface sensible heat flux between D and D-FS.

Diabatic heating (term F) contributes more to the development of the secondary low than does thermal advection (term D). However the mechanism for lifting the air and causing the diabatic heating is clearly the thermal advection. This is because of the near colocation of the maxima in these fields in Fig. 5-10 and Fig. 5-12 (also see Figs. 5-6 and 5-8). The loss of the surface fluxes of sensible heat and moisture lead to a larger contribution from thermal advection. The loss of the surface moisture flux, however, has a much greater effect, because it influences both the location of phasing as well as the intensity of the development. The total contribution of the thermal processes (term C) to the thermal vorticity (Fig. 5-13) is several times larger in the experiments with surface

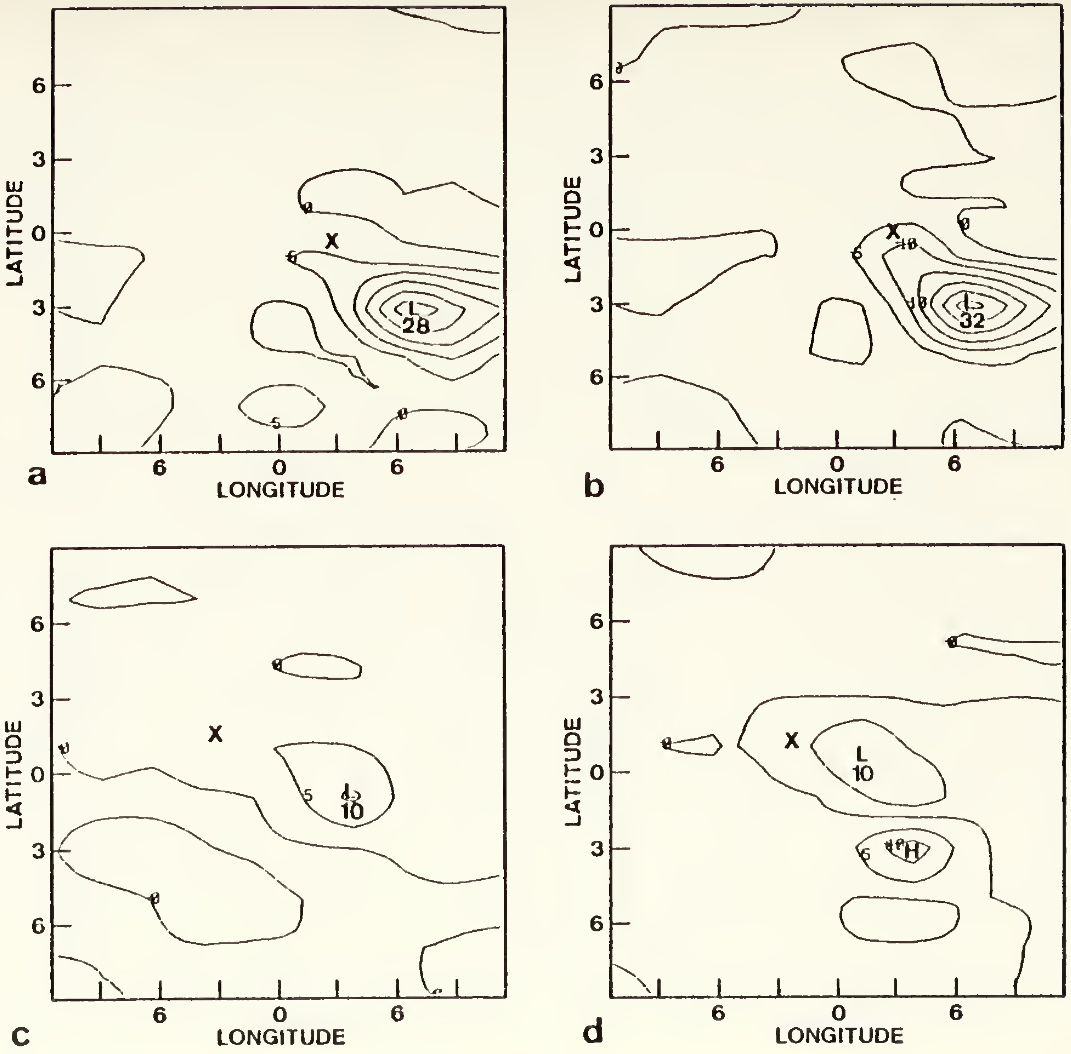

Figure 5-12. As in Fig. 5-10 except for term F.

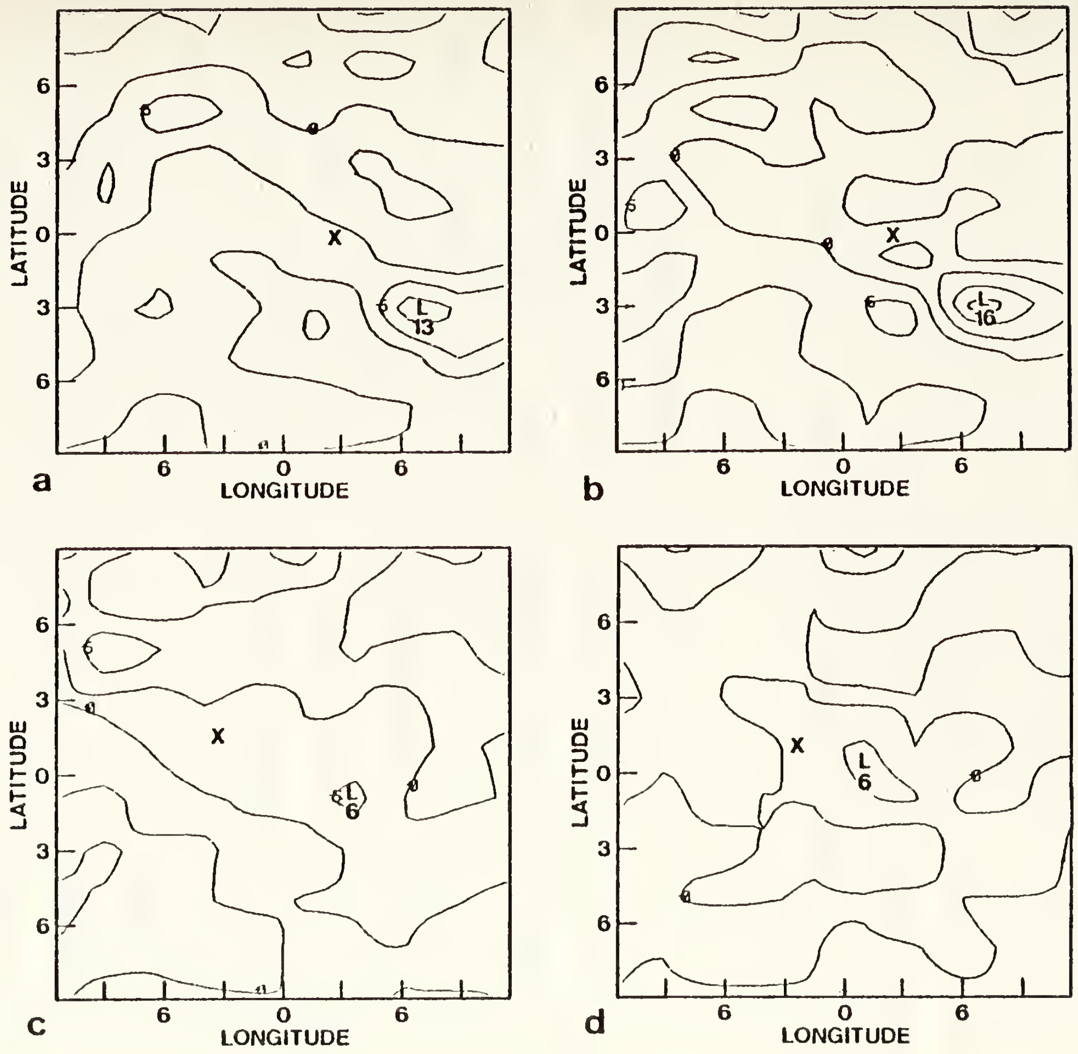

Figure 5-13. As in Fig. 5-10 except for term C. Contour interval 5×10^{-9}.

moisture flux. This process appears to be the reason why the secondary lows continue to develop in D and D-FS while they slowly dissipate in D-FQ and D-FSQ.

Although there is some deep convection, precipitation caused by large-scale lifting appears to be responsible for the development of the secondary lows in D and D-FS. This lifting is caused by warm advection and occurs in a region of strong moisture gradient. This moisture gradient is maintained by the advection of moisture and by the surface moisture flux and results in much greater precipitation in D and D-FS.

B. CASE B--FALL HEMISPHERE DAYS 10-12

The secondary development in this case is similar to the one examined in Case A. Model versions D-FS, D-FQ and D-FSQ are also initialized with fields from D at day 9. A 1008 mb secondary low first appears at approximately day 10 in all model versions. At day 10.5, 1.5 days after initialization, the secondary low enters the southwest quadrant of the primary low (see Fig. 5-14 a-d and also Fig. 5-1b) with approximately the same central pressure, 1007 mb ± 1 mb, and location in all the experiments. During the next 18 h, the secondary low develops (see Figs. 5-15 a-d and 5-16 a-d) much more rapidly in D and D-FS, and becomes the primary low by day 12. In D-FQ and D-FSQ (no surface moisture flux) the secondary low slowly dissipates after day 11. Also the phase speed of the secondary low is less in D-FQ and D-FSQ. This results in a

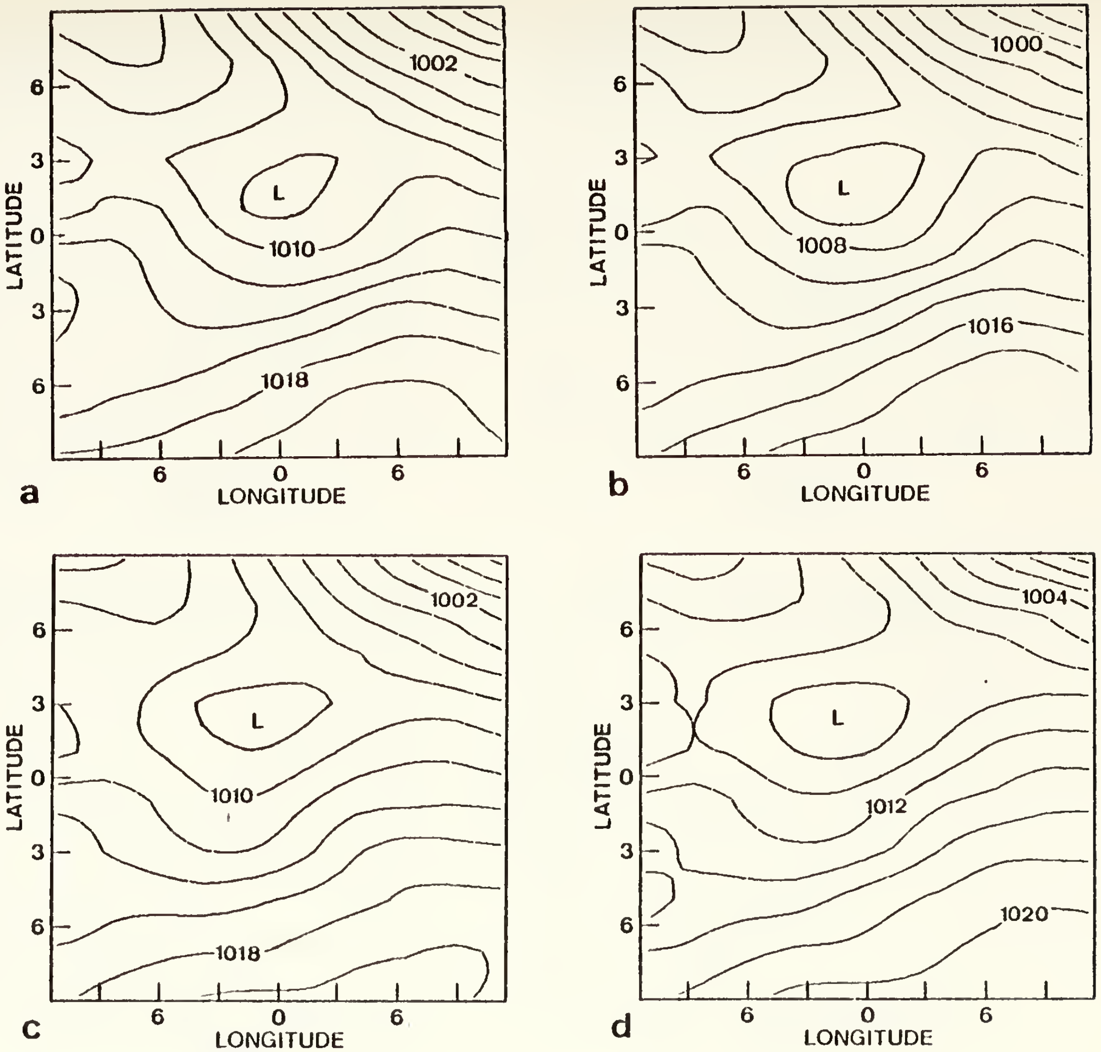

Figure 5-14. Expanded surface pressure maps of the secondary low for Case B at day 10.5 in the fall hemisphere for a. D, b. D-FS, c. D-FQ and d. D-FSQ. Contour interval 2 mb.

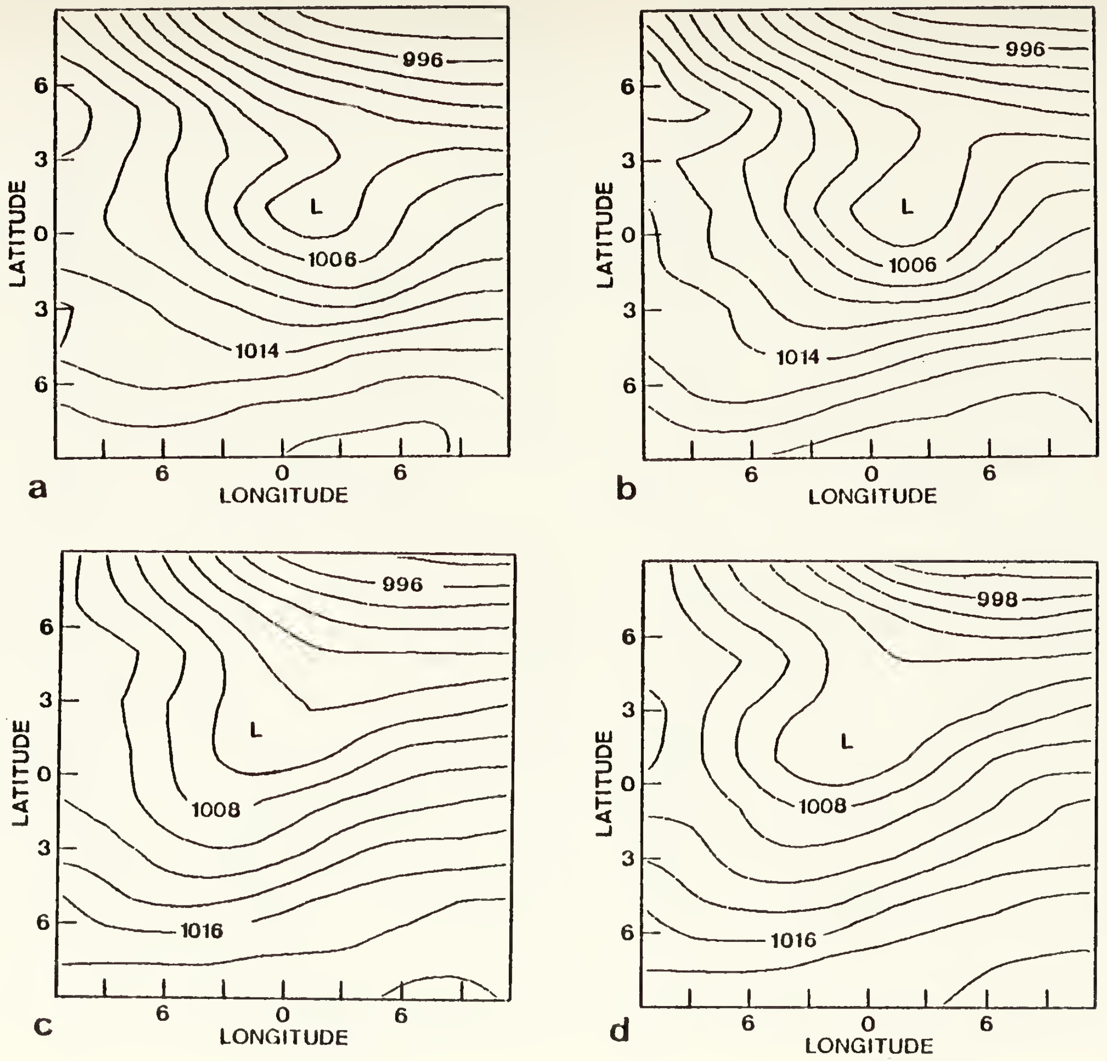

Figure 5-15. As in Fig. 5-14 except for day 11.

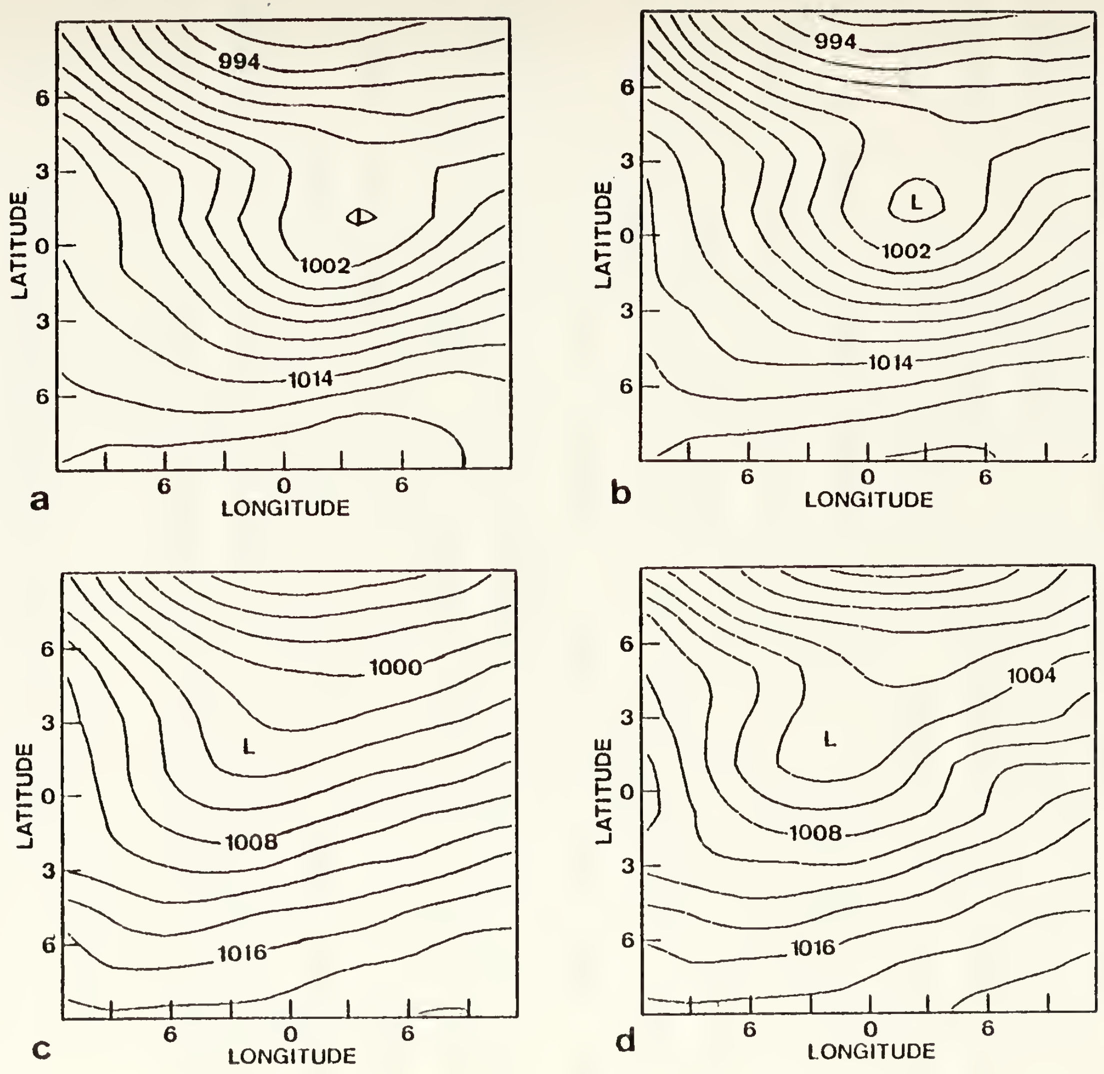

Figure 5-16. As in Fig. 5-14 except for day 11.25.

phase lag of 6° long relative to the secondary low in D during the period from day 10.5 to day 11.25.

Case B closely parallels Case A. To simplify the discussion, only the contributions of terms D, E, and F in the Petterssen development equation will be presented. Term D (Fig. 5-17 a-d) yields similar contributions as in Case A. D-FS and D-FSQ (no surface sensible heat flux), have larger contributions to development than the experiments with sensible heat flux, D and D-FQ, respectively. Term E (Fig. 5-18 a-d) again represents a much larger braking in D and D-FS due to the larger vertical motions associated with the secondary low. The diabatic heating term (term F, Fig. 5-19 a-d), represents the largest contribution to the thickness increase. The sum of terms D and F is not offset by term E in D and D-FS, which allows the secondary low to develop in D and D-FS, but dissipate in D-FQ and D-FSQ. The thermal advection term contributes to larger development in D-FS relative to D and less dissipation in D-FSQ than in D-FQ. Lifting due to warm advection is clearly the dominant mechanism in producing precipitation, and thermal advection is promoted by the absence of the surface sensible heat flux.

C. CASE C--SPRING HEMISPHERE DAYS 10-12

Case C is an example of a secondary low that fails to deepen. As in Case B, model versions D-FS, D-FQ and D-FSQ are initialized with fields from D at day 9. A secondary low is evident in all model versions about day 10.5, or 1.5 days

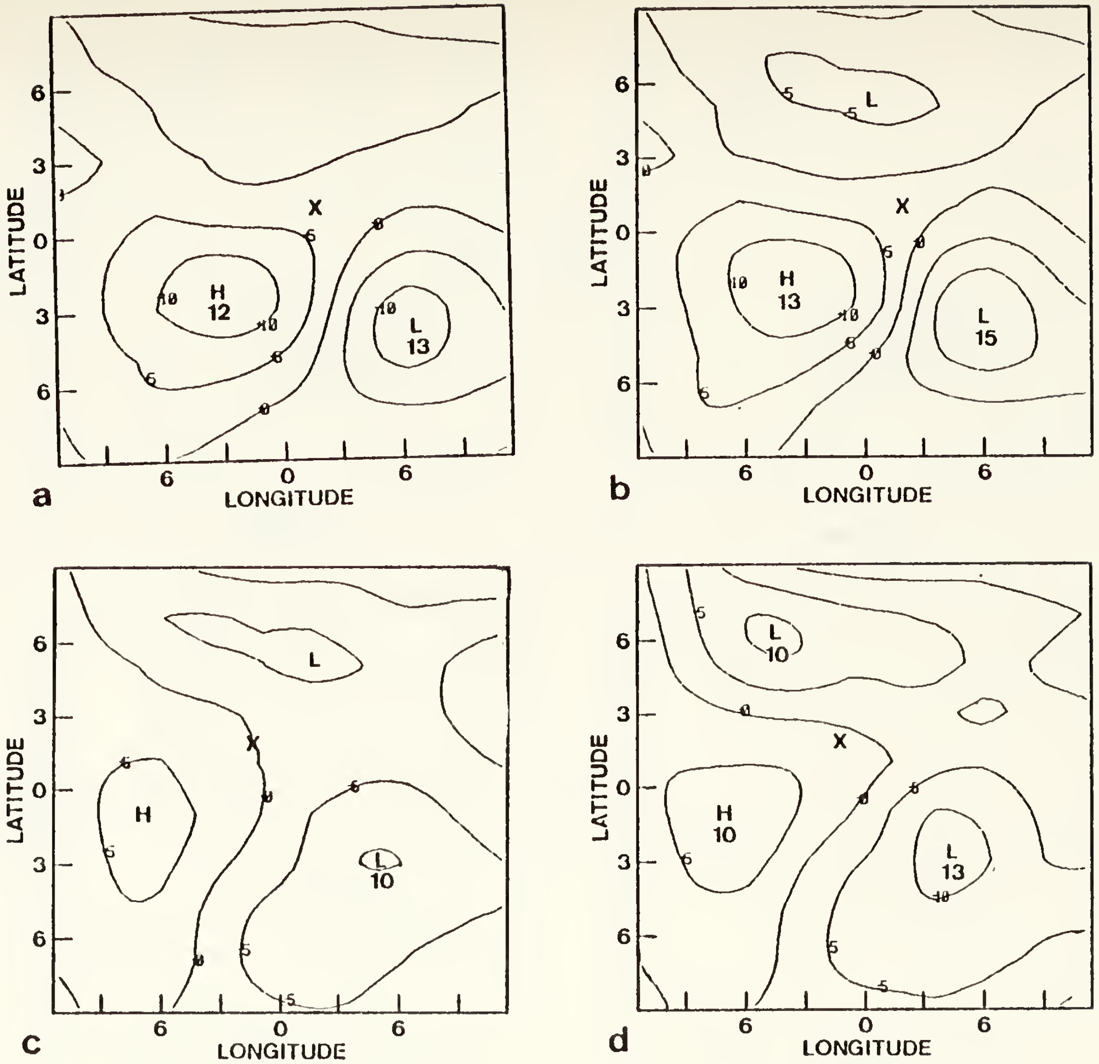

Figure 5-17. Term D of the Petterssen development equation for day 11 and an expanded region as in Fig. 5-15 for a. D, b. D-FS, c. D-FQ and d. D-FSQ. Contour interval 5 x 10^{-5} °C/s.

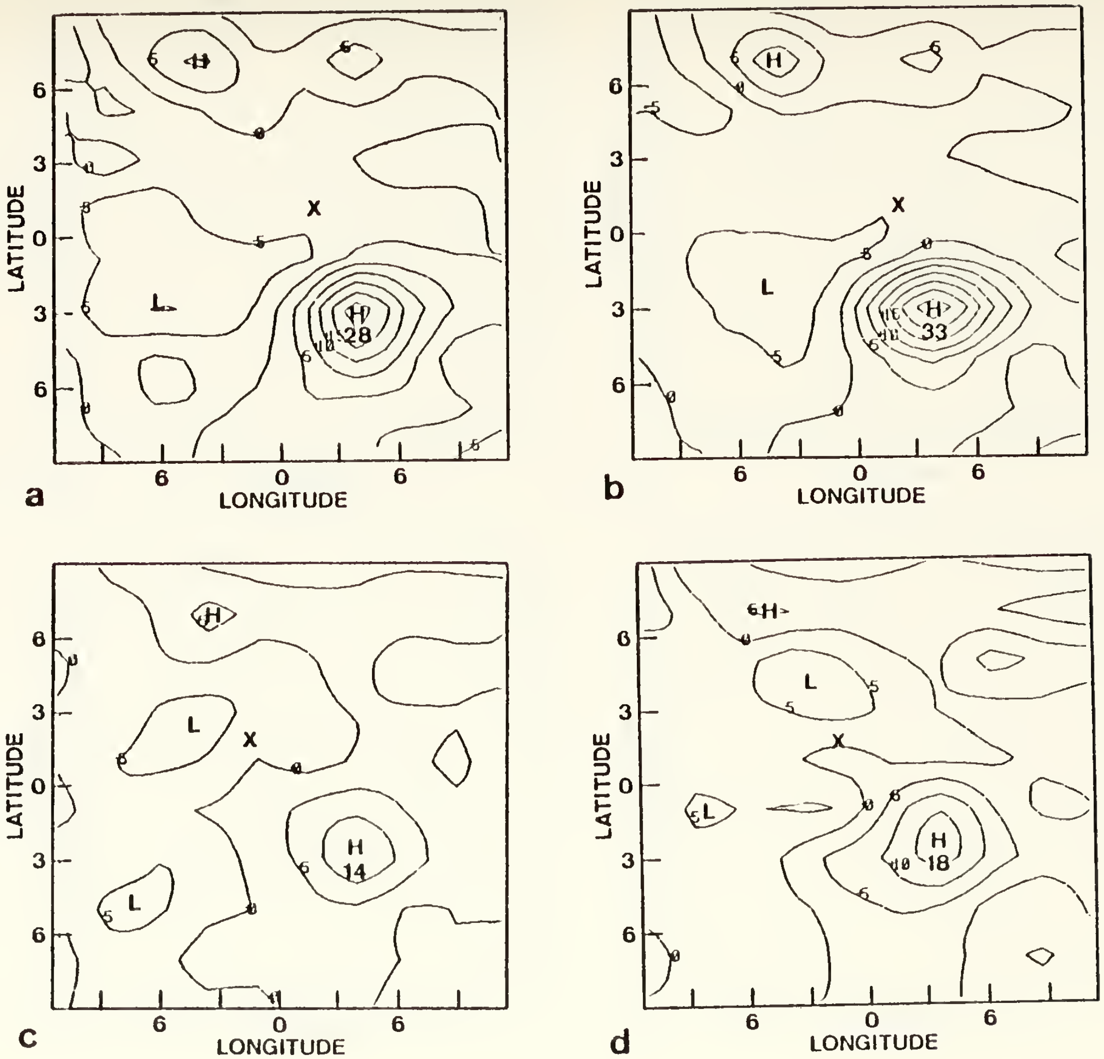

Figure 5-18. As in Fig. 5-17 except for term E.

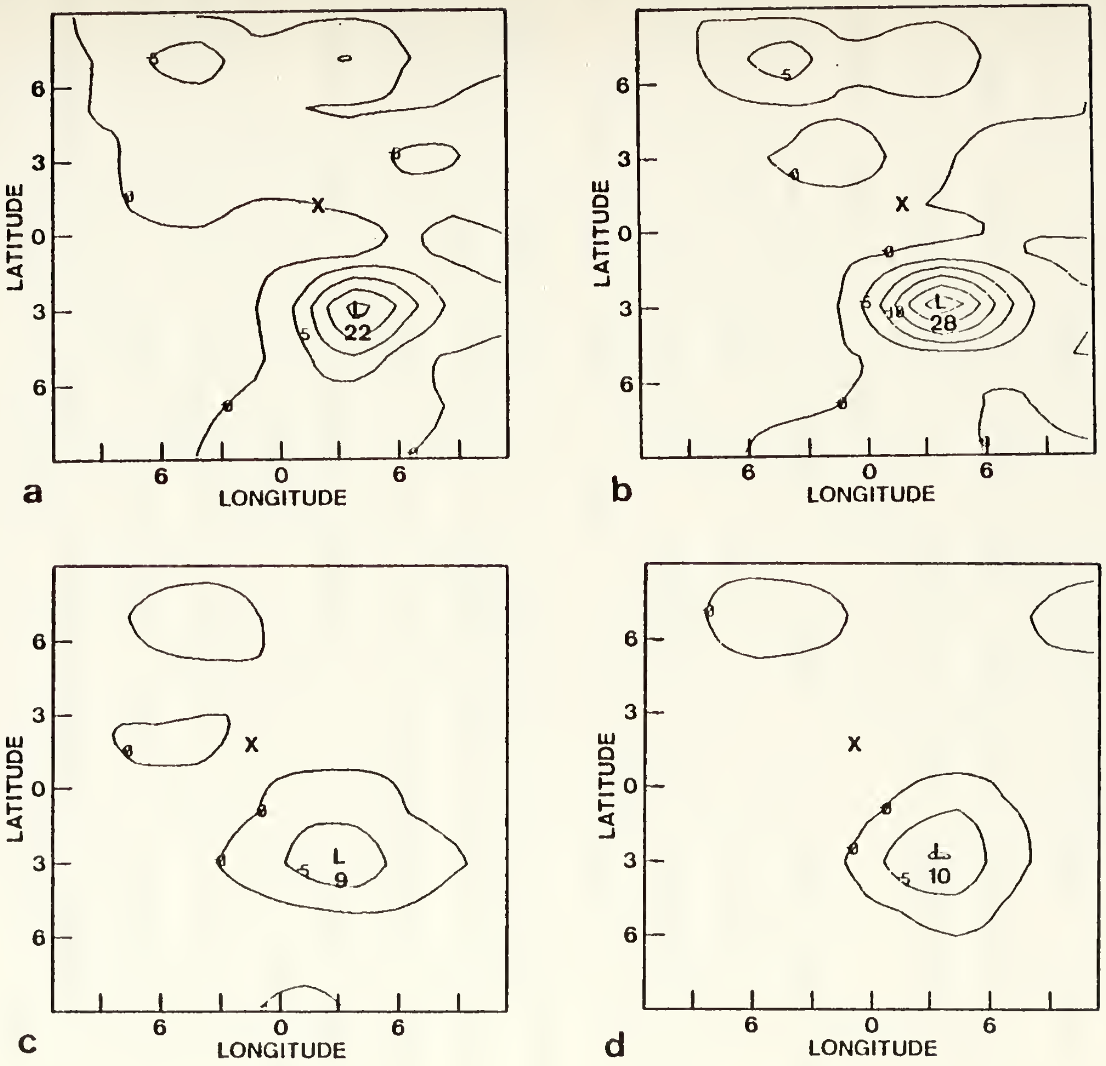

Figure 5-19. As in Fig. 5-17 except for term F.

after initialization. The low is in approximately the same location (see Fig. 5-20 a-d and Fig. 5-1c) with only small differences in initial intensity. The secondary low moves through the region southwest (would be northeast if plotted normally) of the primary low, which corresponds to the locations of the developments that occurred in Cases A and B. In this case, however, the low merely maintains the same intensity for approximately 12 h, and then slowly dissipates in all model versions (Figs. 5-21 and 5-22).

The Petterssen development equation terms have been evaluated for Case C at day 10.75 (Figs. 5-23, 5-24 and 5-25). Term D (Fig. 5-23) reflects a somewhat weaker thermal advection contribution than in Cases A and B, although the decrease in Case C is less than 10% for D and D-FS. It is the secondary lows in these two model versions which develop strongly in Cases A and B. Term F (Fig. 5-25) demonstrates a decrease of 60% to 80% in the diabatic warming of Case C from Cases A and B (Figs. 5-12 and 5-19) in experiments D and D-FS. The maximum values of the diabatic heating in Case C are only of the same order as those in D-FQ and D-FSQ of Cases A and B. The secondary low in D-FQ and D-FSQ dissipated eventually in both Cases A and B. The implication here is that a large contribution from diabatic heating, term F, is required for the secondary low to continue to develop.

D. CASE D--SPRING HEMISPHERE DAYS 9-11

This case differs from the previous three cases in that the secondary low develops in the poleward flow in the eastern

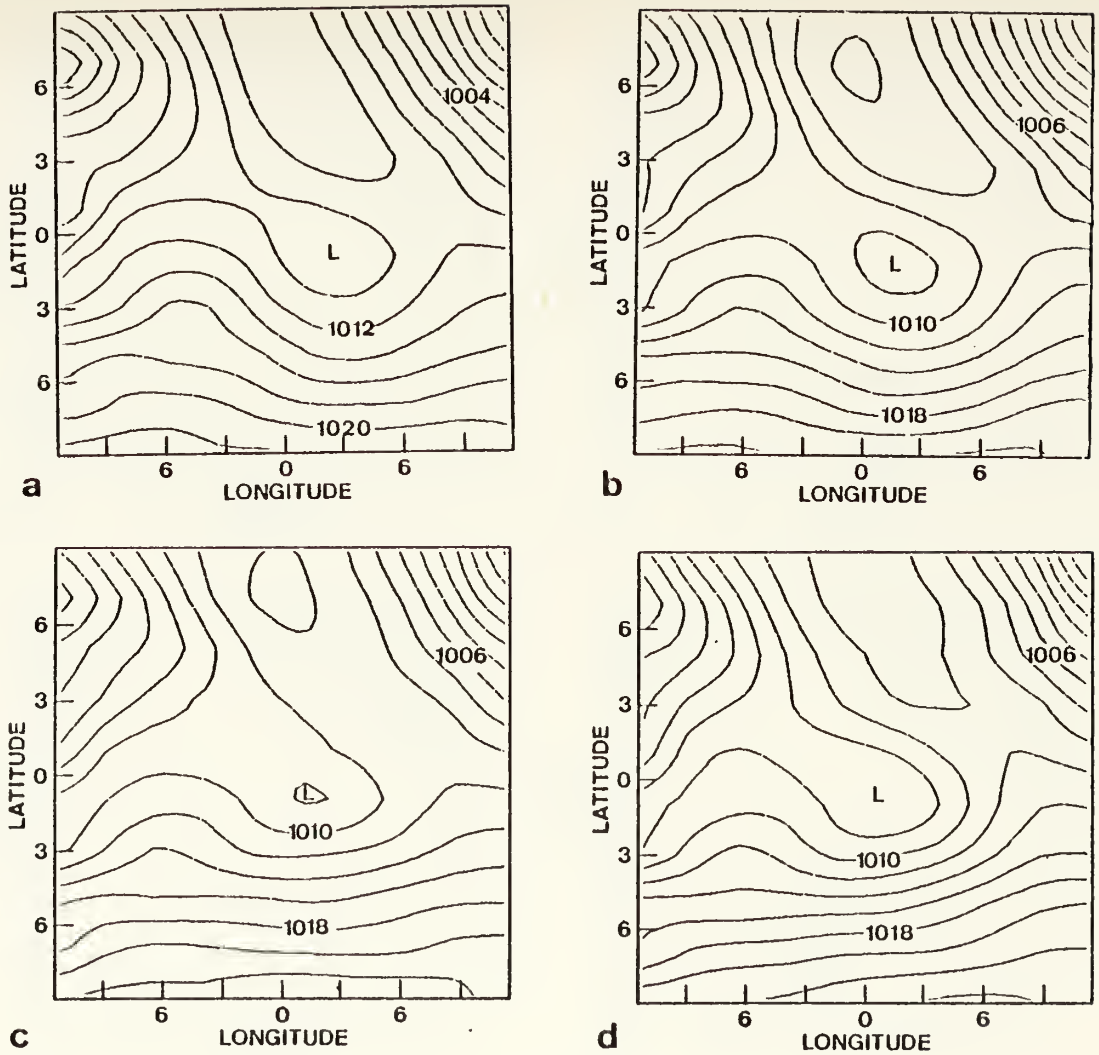
a
b
c
d
LATITUDE
LONGITUDE
6
3
0
3
6
6
0
6
L
1004
1012
1020
1006
1010
1018

Figure 5-20. Expanded surface pressure maps of the secondary low for Case C at day 10.5 in the spring hemisphere for a. D, b. D-FS, c. D-FQ and d. D-FSQ. Contour interval 2 mb.

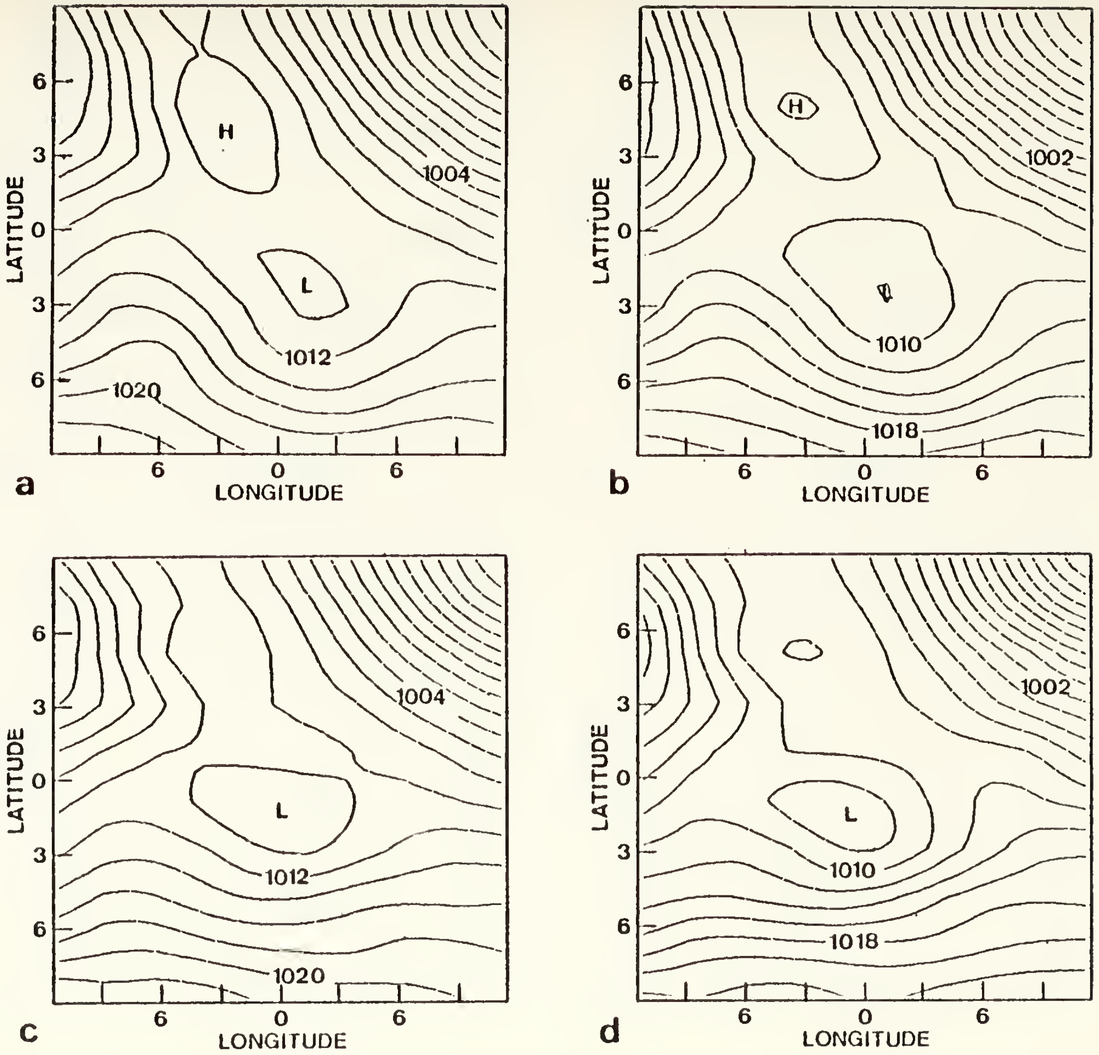

Figure 5-21. As in Fig. 5-20 except for day 10.75.

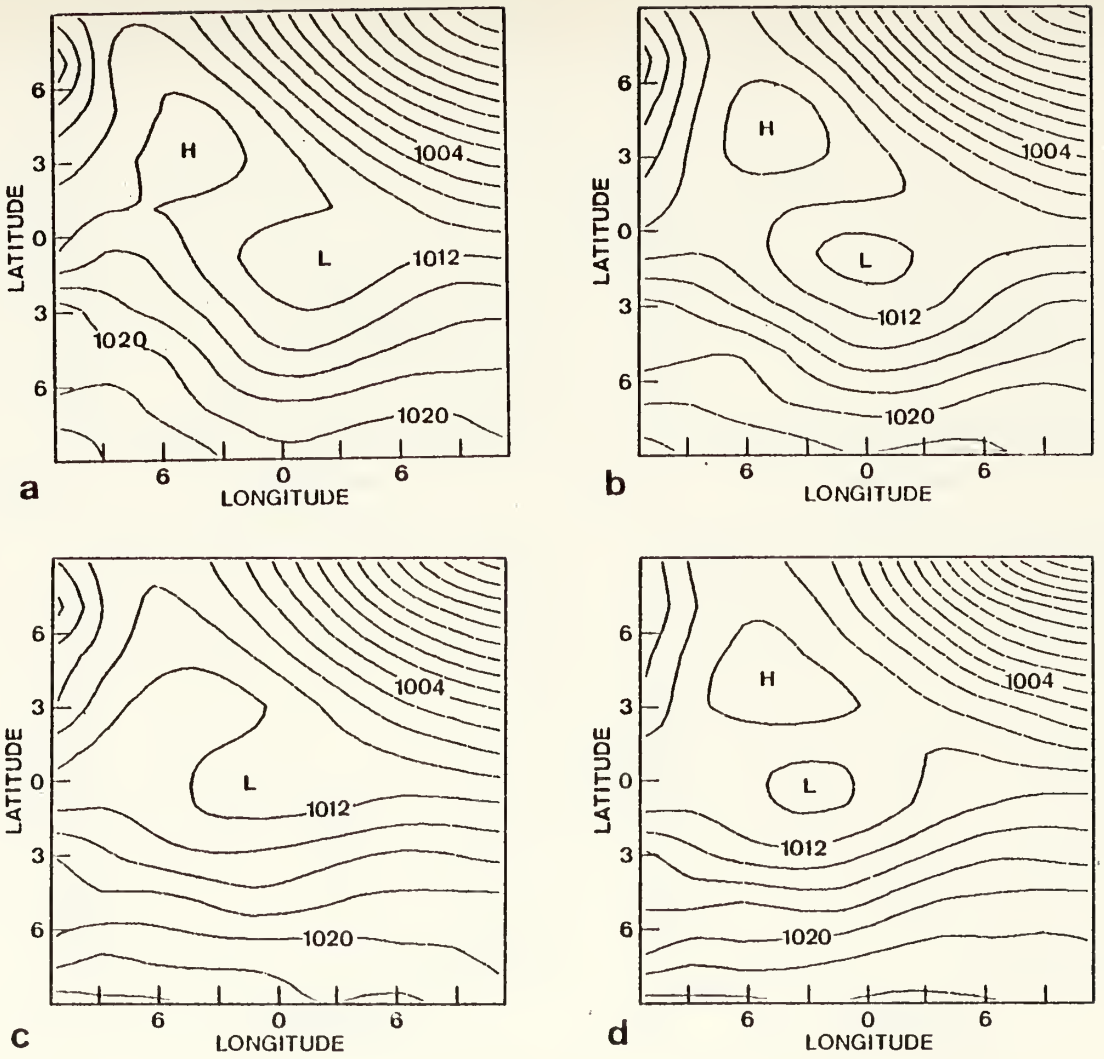

Figure 5-22. As in Fig. 5-20 except for day 11.

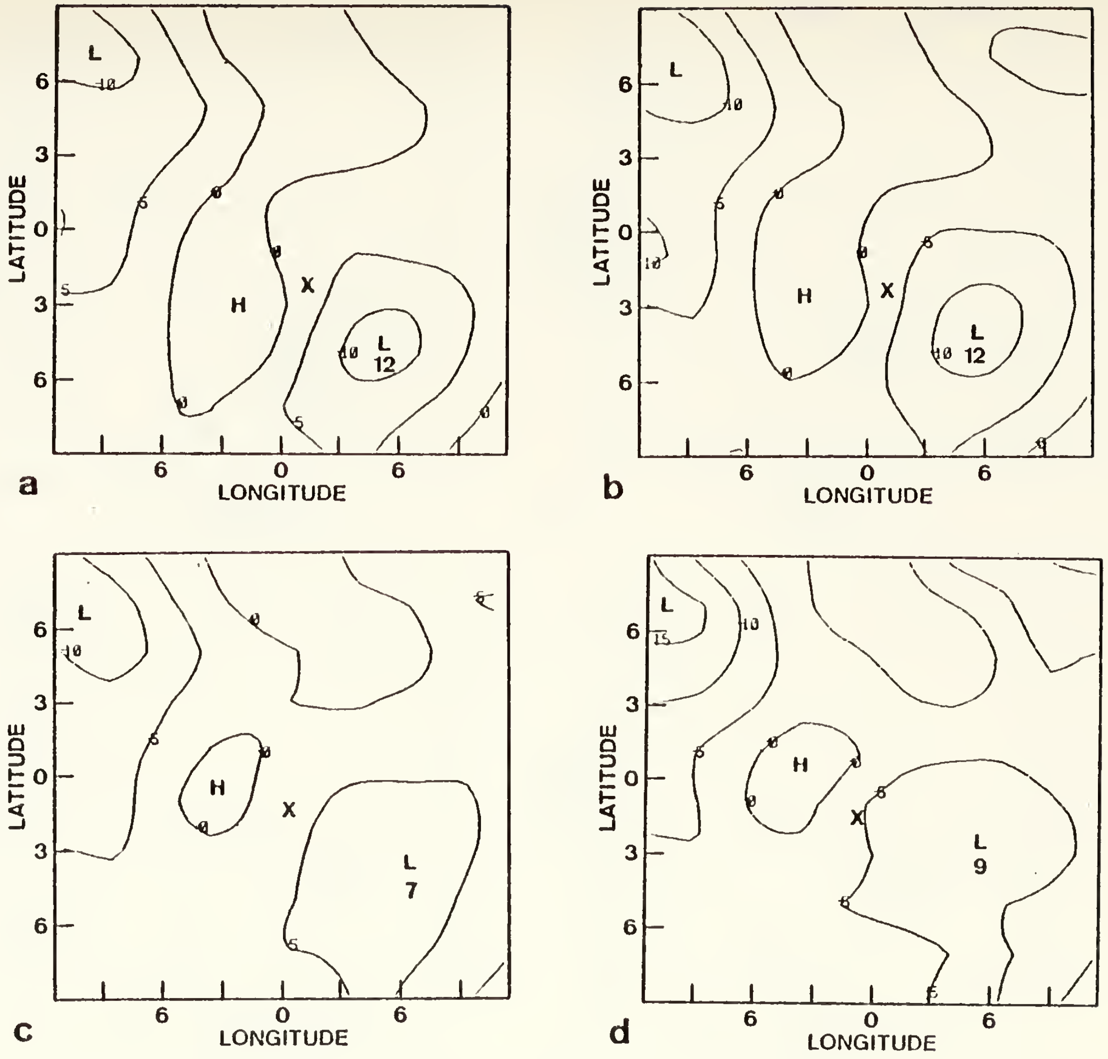

Figure 5-23. Term D of the Petterssen development equation for day 10.75 and an expanded region as in Fig. 5-21 for a. D_ζ b. D-FS, c. D-FQ and d. D-FSQ. Contour interval 5 x 10^{-5} °C/s.

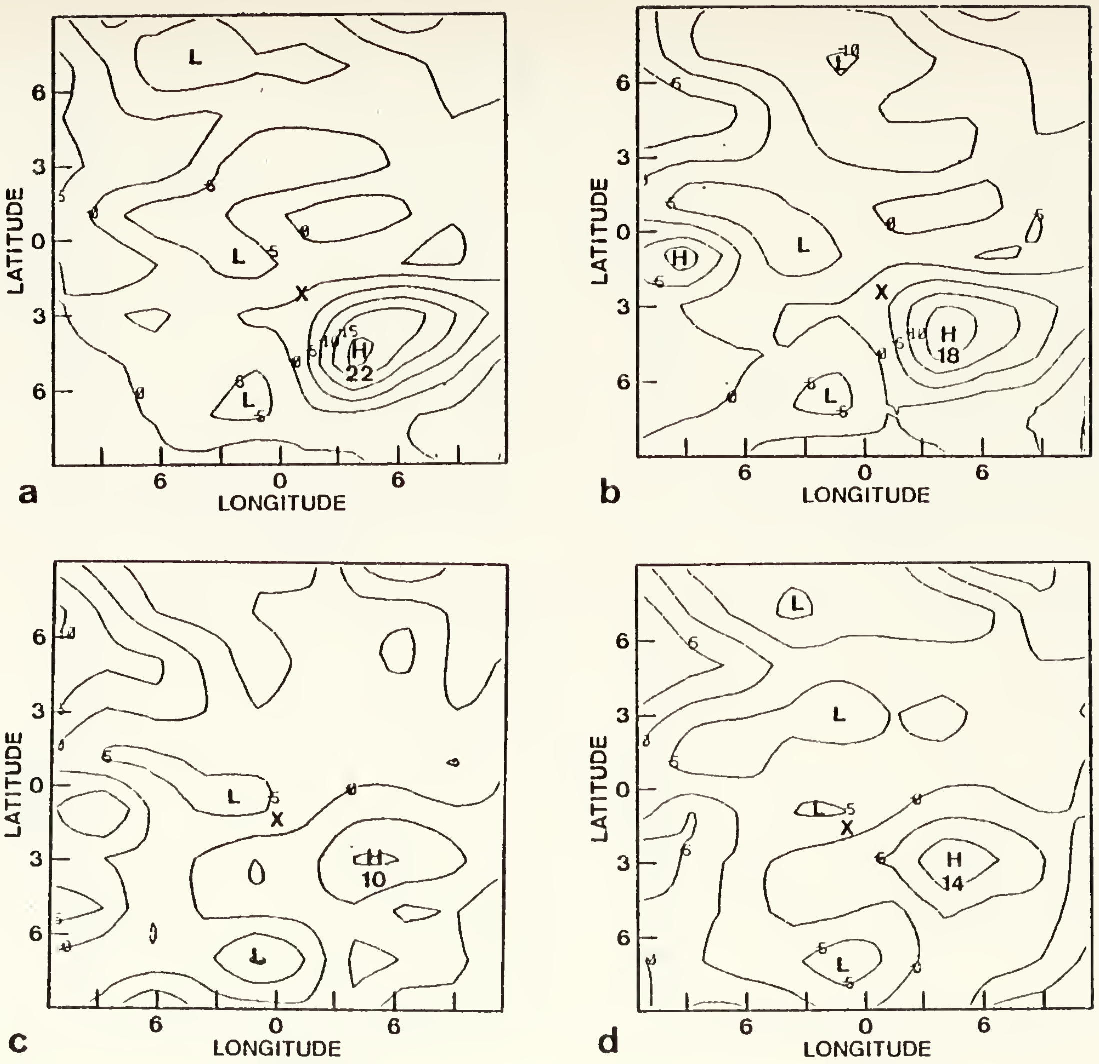

Figure 5-24. As in Fig. 5-23 except for term E.

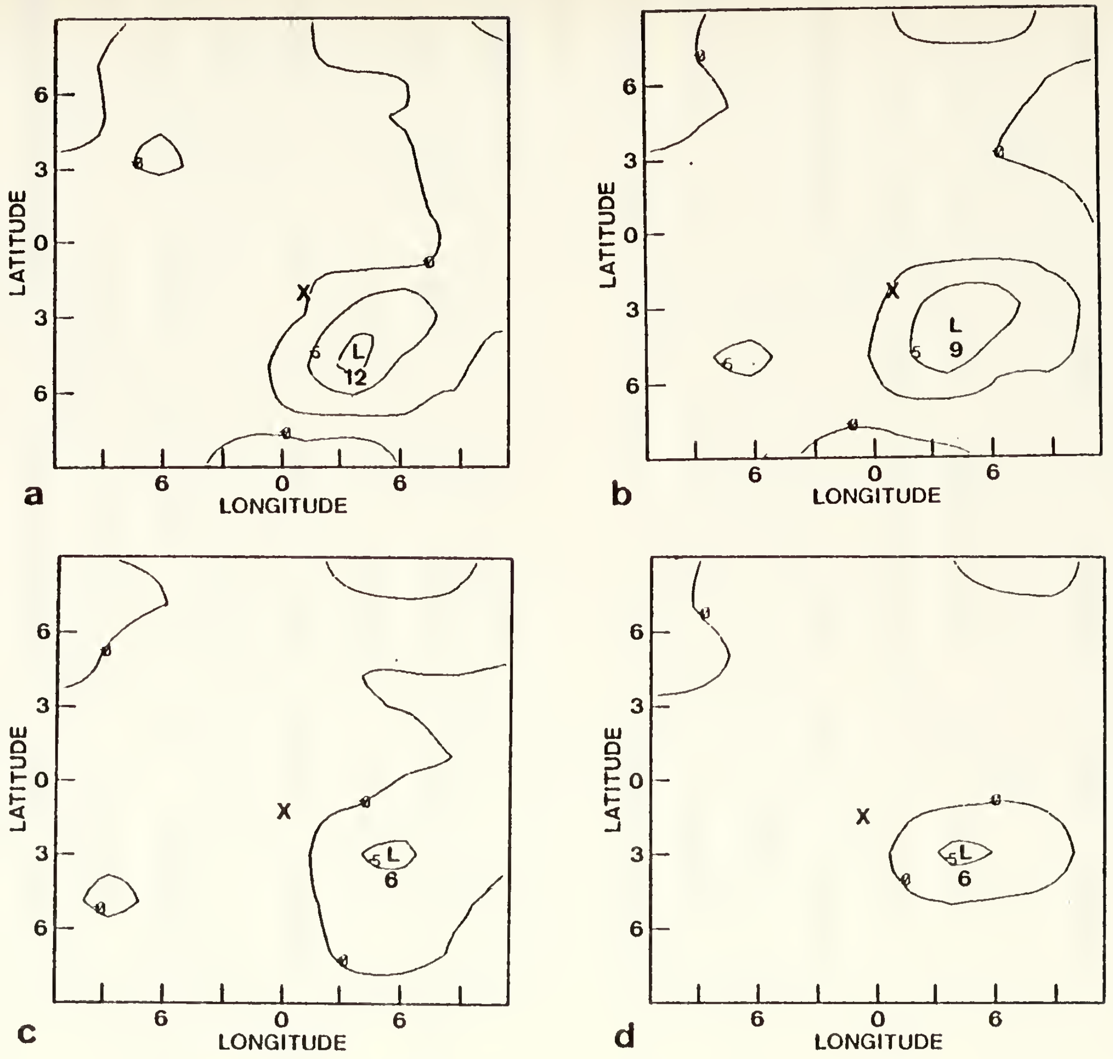

Figure 5-25. As in Fig. 5-23 except for term F.

quadrant of the primary cyclone (see Fig. 5-1d). Also, in apparent contradiction to the first three cases and the results discussed in Chapter III, the largest development occurs in the adiabatic experiment, F, with the least development in D.

Figs. 5-26 a-b present the expanded surface pressure maps for F corresponding to those presented in Figs. 5-20 a-d and 5-22 a-d for the diabatic experiments. The secondary low reaches its maximum intensity between days 10.5 and 11 in all experiments, prior to entering the region of strong equatorward flow where development occurs in Cases A and B. At this time, day 10.5, the secondary low is deepest in F, followed by D-FSQ, and with the highest central pressure occurring in D.

Temperature fields for experiments D and F (see Figs. 5-27 a-b) reveal a much larger low-level temperature gradient to the east of the primary cyclone in F than D. The gradients for D-FSQ, D-FS and D-FQ (not shown), respectively, are also larger than D and the secondary lows are correspondingly more intense (see Figs. 5-20 a-d). Expanded plots of the low-level temperature fields (Figs. 5-28 a-b) reveal a temperature gradient in F approximately twice that in D. Thus, the indication is that low-level temperature advection is responsible for the difference in development in this case.

In terms of the Petterssen development equation, the secondary low developing in F (adiabatic) has no contribution from diabatic heating (term F), yet it develops more

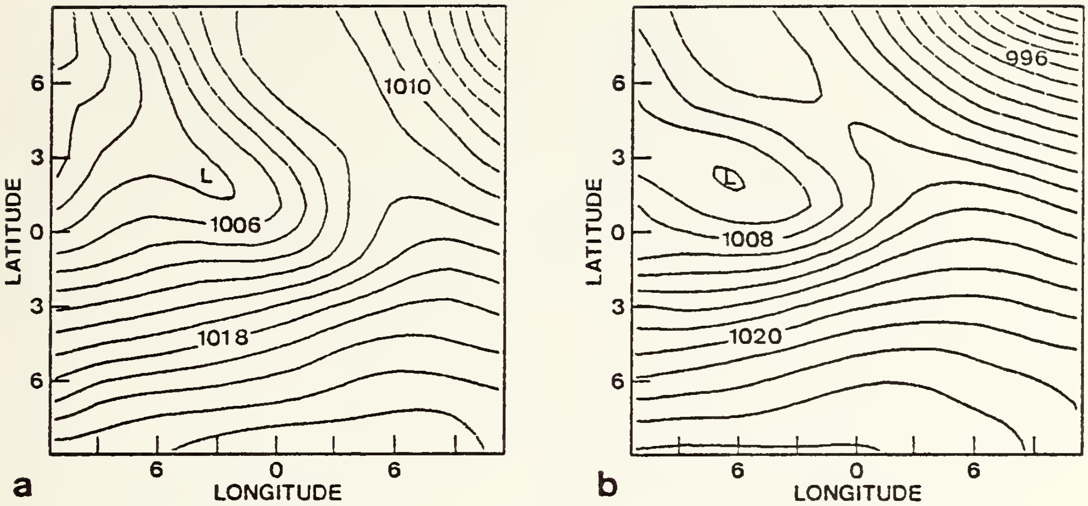

Figure 5-26. Expanded surface pressure maps of secondary low in F in the spring hemisphere for a. day 10.5 and b. day 11. Region as in Figs. 5-20 and 5-22, respectively. Contour interval 2 mb.

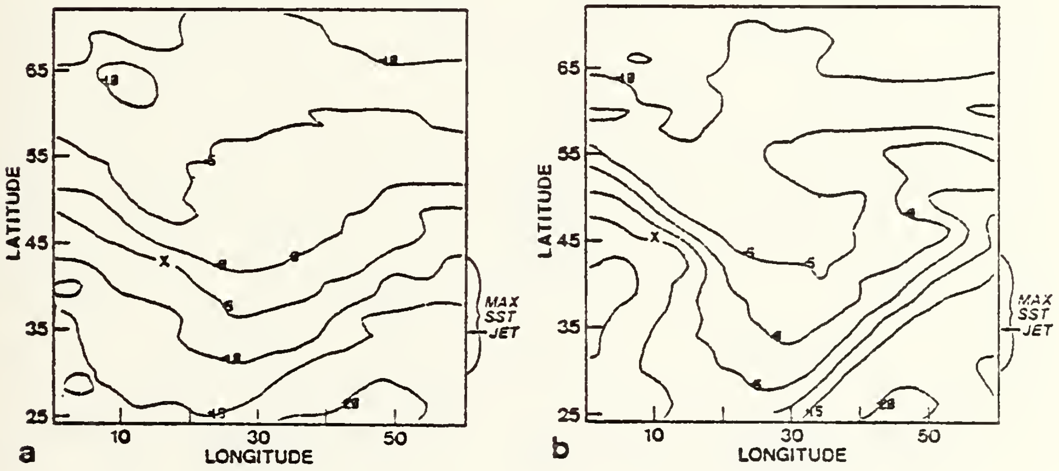

Figure 5-27. Southern hemisphere temperature fields at sigma level 6 (900 mb) at day 10.5 for a. D and b. F. Contour interval 5°C. Location of secondary low indicated by X.

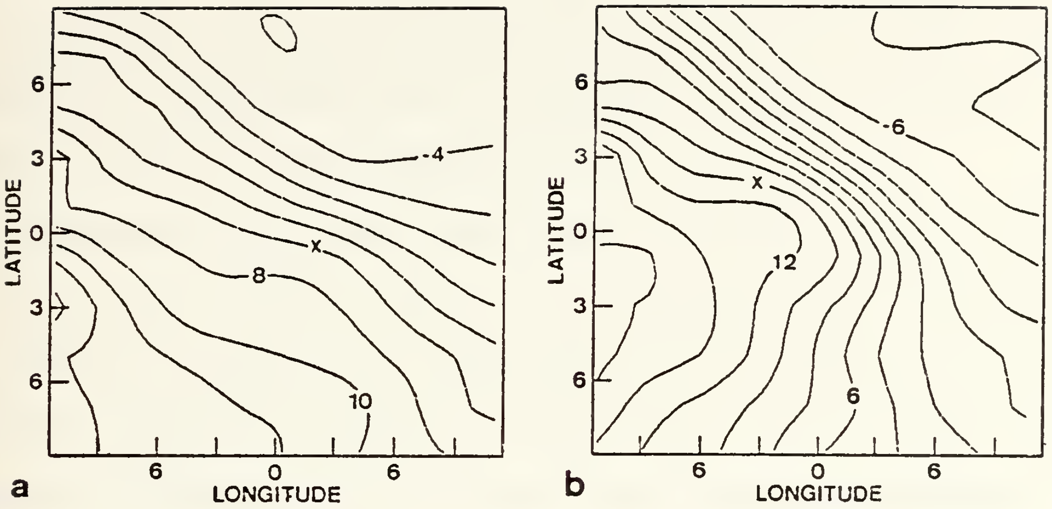

Figure 5-28. As in Fig. 5-27 except for expanded region as in Fig. 5-26a. Contour interval 2°C.

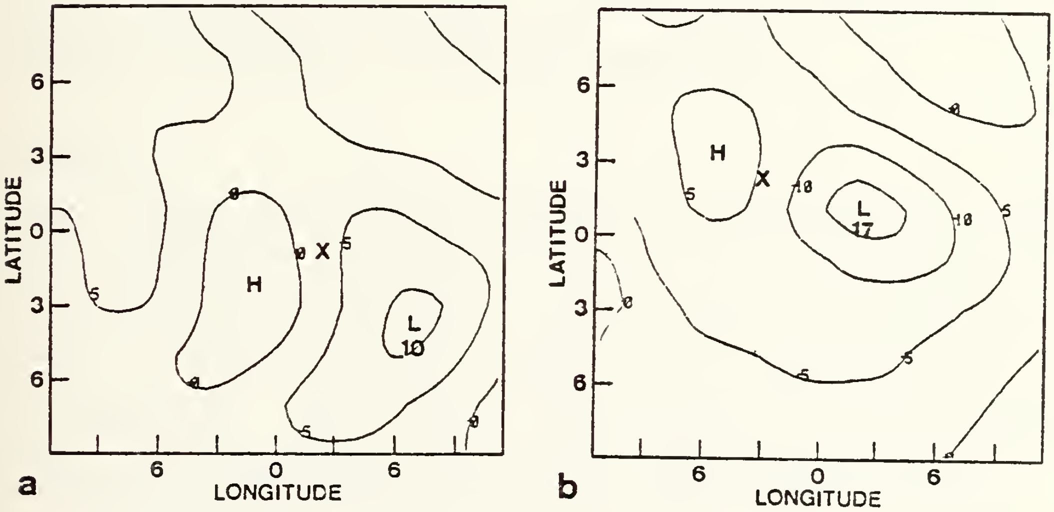

Figure 5-29. Term D of the Petterssen development equation for day 10.5 and an expanded region as in Fig. 5-26a for a. D and b. F. Contour interval 5 x 10^{-5} °C/s.

than the secondary low in D. Figs. 5-29 a-b give the contribution of the low-level temperature advection (term D) to development of the secondary low at day 10.5. The region of positive thickness change (negative values in figure) is larger as well as more intense in F.

Developments of this type (Case D) in the eastern quadrant of the primary cyclone occur in both hemispheres, although the intensity changes are generally not as marked as in this example. These situations, in which the air-sea fluxes and diabatic effects appear to hinder the cyclone development, are more common and more marked in the coarse-mesh model experiments. It appears that the relative role of the physical processes is changed in the different resolutions. In the northern or fall hemisphere, the larger diabatic effects in experiments D and D-FS tend to mask the contribution of the stronger low-level temperature advection.

E. SUMMARY

These cases clearly demonstrate the sensitivity of the model development of secondary lows to both the surface fluxes of sensible heat and moisture and to the baroclinicity of the model atmosphere. The loss of the surface sensible heat flux contributes to a greater low-level temperature gradient in both the spring and fall hemispheres. This contributes to an increase in low-level temperature advection, and leads to a greater development in the experiments with no sensible heat flux. The surface moisture flux is responsible for much

larger differences in the development of secondary lows. Here the physical mechanism is the latent heat release triggered by vertical velocities induced by the low-level temperature advection.

In the fall hemisphere with the weaker jet, the secondary low develops rapidly in the experiments with a surface moisture flux, and eventually replaces the primary, large-scale cyclone. In the experiments without surface moisture flux, the secondary lows slowly dissipate. In addition, there is a six-to-ten degree phase lag of the secondary lows in these experiments relative to those which had surface moisture fluxes. This phase lag occurs primarily during the 12 to 18 h period in which the secondary lows develop most rapidly.

In sharp contrast, in the spring hemisphere with the stronger jet and lower sea-surface temperatures, the secondary lows dissipated after one or two days, without intensifying greatly. The low-level temperature advection in this hemisphere is only about 10% less than in the experiments in which the secondary lows develop strongly in the fall hemisphere. The contribution from the diabatic heating, however, is much less in the spring hemisphere experiments with surface moisture flux, and is comparable to the experiments in which the secondary low dissipated in Cases A and B.

Reed (1979) concluded that the polar lows in the eastern North Pacific Ocean were predominately a baroclinic phenomena with possible contributions from thermal and barotropic processes. Rasmussen (1979), in a similar study of eastern North

Atlantic Ocean polar lows, concluded that they were predominately a thermal instability phenomena. The results of the model experiments presented here demonstrate that both of the above situations could exist in the marine atmosphere. The instability process which dominates in any given instance is sensitive to the surface fluxes of sensible heat and moisture, as well as to the degree of baroclinic instability present in the atmosphere. In these experiments, the surface fluxes are critically important on a time scale of two to four days, which is well within the predictability of the real atmosphere.

VI. CONCLUSIONS

The objective of this research is to use a numerical model to examine the role of the air-sea fluxes in extratropical cyclogenesis over the open ocean. The method employed is to specify analytic initial atmosphere and ocean conditions which are typical of fall and spring conditions in the real atmosphere. A state-of-the-art atmospheric prediction model is used to examine the contributions of the surface fluxes of moisture and sensible heat. This is accomplished by selectively removing the surface flux parameterizations from the model and comparing the results with a control run generated with the complete diabatic model. Consequently, this research emphasizes the role of the individual processes in the model and in the atmosphere rather than the response of the model to small changes in the sea-surface temperatures (e.g., Spar and Atlas, 1975).

The surface fluxes make a significant contribution in these simulations of cyclone evolution. In the fall hemisphere with a weaker upper-level jet and higher sea-surface temperature, the removal of the surface fluxes results in a large reduction in the initial growth rate of the model cyclones. In the presence of the more intense jet and lower sea-surface temperature of the spring hemisphere, removal of the surface fluxes has a smaller impact on the model cyclone growth. The contribution of the surface fluxes to the growth

of a pre-existing, large-scale cyclone is found to be relatively small as expected from previous studies.

The smaller-scale secondary cyclones respond rapidly to the removal of the model surface fluxes. Removal of the surface moisture flux prevents the development of secondary lows which might otherwise eventually replace the primary cyclone, as occurs in the complete diabatic model. Removal of the surface sensible heat flux results in the development of more intense cyclones although the overall evolution of the cyclone is not altered from that in the complete diabatic experiment. The result that different perturbations eventually become the primary cyclone after three to four days is significant. One may conclude that extending the usefulness of numerical model forecasts of open-ocean cyclones beyond the present limit of two to three days will require accurate specification of the air-sea fluxes.

The experimental technique of removing the surface-flux parameterizations from the model has no real world analog. The modelled results can not be verified with observations and indicate only the sensitivity of the model cyclones to the air-sea fluxes. The ability to perform experiments within a controlled, but admittedly idealized, environment can provide insights, however, that would otherwise require very large, detailed statistical studies. These results do suggest why some disturbances over the ocean develop while other, seemingly similar, disturbances do not develop.

The surface fluxes of moisture and sensible heat act to reduce the large gradients of low-level temperature and moisture in the model atmosphere. These gradients occur in regions of strong equatorward (poleward) advection associated with the primary cyclone, especially over the zone of largest sea-surface temperature gradient. Large-scale lifting produced by the low-level temperature advection triggers the release of latent heat as hypothesized by Petterssen et al., (1962). These two processes jointly lead to a large increase in vertical motion and, therefore, cyclone development. Removal of the surface sensible heat flux allows a larger low-level temperature gradient, resulting in enhanced vertical motions and in increased development of the cyclones. Removal of the surface moisture flux results in a large decrease in precipitation or latent heat release and, therefore, a large decrease in cyclone development.

Previous studies have focused on the region behind, or westward, of the cyclone, where the strongest fluxes occur. The cooperative effect of lifting produced by low-level temperature advection and the release of latent heat, however, results in the largest cyclone response occurring ahead, or eastward, of the cyclone. The results of these experiments indicate that the magnitude of the surface fluxes in terms of the amount of energy transferred across the air-sea interface is not as important as the location in which they occur. This resolves the apparent contradiction found by Wei (1979) and

also implies that accurate specification of the sea-surface temperature distribution is crucial to the evolution of open-ocean cyclones, at least on a medium range time scale of three to five days.

This experiment addresses open-ocean conditions with fixed sea-surface temperatures and moderate values of surface moisture and sensible heat fluxes. A variety of cyclone evolutions similar to those observed by Nitta and Yamamoto (1974), Reed (1979) and others is produced in the model integrations. Much more intense over-ocean cyclogenesis has been observed (Sanders and Gyakum, 1980; Pyke, 1965) in association with land-sea and ice-sea boundaries where the atmosphere is far from equilibrium with the ocean surface fluxes. Further research is necessary to investigate more fully the role of the surface fluxes in these cases of more intense cyclogenesis. Numerical experiments of the type described here can be helpful in understanding the physical processes involved in these cases, and will hopefully lead to improved prediction of extratropical cyclones over the oceans.

LIST OF REFERENCES

Arakawa, A., and V. Lamb, 1977: Computational design of the basic dynamical processes of the UCLA general circulation model. Methods in Computational Physics, 17, 173-265, Academic Press, New York.

Arakawa, A., and W. Schubert, 1974: Interaction of a cumulus cloud ensemble with the large-scale environment, part I. J. Atmos. Sci., 31, 674-701.

Baker, D. J., 1979: Ocean-atmosphere interactions in high southern latitudes. Dynamics of Atmospheres and Oceans, 3, 213-229.

Blumen, W., 1979: On short-wave baroclinic instability. J. Atmos. Sci., 36, 1925-1933.

Carleton, A. M., 1981: Monthly variability of satellite-derived cyclonic activity for the southern hemisphere winter. J. of Climatology, 1, 21-38.

Danard, M. B., and G. E. Ellenton, 1979: Physical influences on east coast cyclogenesis. Atmosphere-Ocean, 18(1), 65-82.

Deardorff, J. W., 1972: Parameterization of the planetary boundary layer for use in general circulation models. Mon. Wea. Rev., 100, 93-106.

Gall, R. L., 1976: Structural changes of growing baroclinic waves. J. Atmos. Sci., 33, 374-390.

Gambo, K. 1976: The instability of medium-scale disturbances in a moist atmosphere. J. Meteor. Soc. Japan, 5, 191-207.

Gyakum, J. R., 1980: On the evolution of the QE II storm. Preprints Eighth Conference on Weather Forecasting and Analysis, Denver, Colo., Amer. Meteor. Soc., 23-28.

Haltiner, G., 1967: The effects of sensible heat exchange on the dynamics of baroclinic waves. Tellus, XIX, 183-198.

Haltiner, G. 1971: Numerical Weather Prediction. John Wiley and Sons, Inc., New York, 309 pp.

Haltiner, G., and R. T. Williams, 1980: Numerical Prediction and Dynamic Meteorology. John Wiley and Sons, Inc., New York. 477 pp.

Hoskins, B., 1978: Linear and Nonlinear baroclinic instability on a sphere. *The General Circulation: Theory, Modeling, and Observations*. Notes from NCAR Colloquim; Summer 1978. 116-143.

Katayama, A., 1972: A simplified scheme for computing radiative transfer in the troposphere. Tech. Report No. 6, Dept. of Meteor., University of California, Los Angeles.

Laevastu, T., 1965: Daily heat exchange in the North Pacific, its relations to weather and its oceanographic consequences. *Soc. Sci. Fennica*, *Commentationes Phys.-Math.*, *31*, No. 2, 1-53.

Lord, S. J., 1978: Development and observational verification of a cumulus cloud parameterization. Ph.D. Thesis, Dept. of Atmos. Sci., University of California, Los Angeles.

Mechoso, C. R., M. J. Suarez and A. Arakawa, 1978: July simulation by the UCLA general circulation model. *Preprints Fourth Conference on Numerical Weather Prediction*, *Amer. Meteor. Soc.*, 282-289.

Mullen, S., 1979: An investigation of small synoptic-scale cyclones in polar air streams. *Mon. Wea. Rev.*, *107*, 1636-1647.

Nitta, T., and J. Yamamoto, 1974: On the observational characteristics of intermediate scale disturbances generated near Japan and vicinity. *J. Meteor. Soc., Japan*, *52*, No. 1, 11-31.

Oort, A. H., and E. R. Rassmussen, 1971: Atmospheric circulation statistics. NOAA Prof. Paper 5. (U.S. Govt. Printing Office, Stock No. 0317-0045, c55.25:5.)

Paine, S. L., 1980: Preliminary results of a comparison of the Navy northern hemisphere primitive equation model with the NEPRF/UCLA global forecast system. *Preprints Eighth Conference on Weather Forecasting and Analysis*, Denver, Colo., *Amer. Meteor. Soc.*, 496-500.

Palmen, E., and C. W. Newton, 1969: *Atmospheric Circulation Systems*. Academic Press, 603 pp.

Petterssen, S., 1956: *Weather Analysis and Forecasting*, Vol. 1, McGraw-Hill Book Co., New York.

Petterssen, S., D. Bradbury and K. Pedersen, 1962: The Norwegian cyclone models in relation to heat and cold sources. *Geofys. Publor.*, *24*, 243-280.

Pyke, C., 1965: On the role of air-sea interaction in the development of cyclones. *Bull. Am. Meteor. Soc.*, *46*, 4-15.

Randall, D. A., 1976: The interaction of the planetary boundary layer with large-scale circulations. Ph.D. Thesis, Dept. of Atmos. Sci., University of California, Los Angeles.

Rao, V. B., and N. J. Ferreira, 1979: Stability properties of medium-scale disturbances in a balance model. Instituto de Pesquisas Espaciais, Conselho Nacional de Desenvolimento Cientifico e Technologico, Sao Paulo, Brasil. 20pp.

Rassmussen, E., 1979: The polar low as an extratropical CISK disturbance. Quart. J. Roy. Meteor. Soc., 105, 531-549.

Reed, R. J., 1979: Cyclogenesis in polar air streams. Mon. Wea. Rev., 107, 38-52.

Robinson, M., K., 1976: Atlas of North Pacific Ocean Monthly Mean Temperatures and Mean Salinities of the Surface Layer. Naval Oceanographic Office, Ref. Pub. No. 3, Washington, D.C.

Sanders, F., and J. R. Gyakum, 1980: Synoptic-dynamic climatology of the "bomb". Mon. Wea. Rev., 108, 1589-1606.

Schlesinger, M. E., 1976: A numerical simulation of the general circulation of the atmospheric ozone. Ph.D. Thesis, Dept. of Atmos. Sci., University of California, Los Angeles.

Simmons, A. J., and B. J. Hoskins, 1976: Baroclinic instability on spheres: normal modes of the primitive and quasi-geostrophic equations. J. Atmos. Sci., 33, 1454-1477.

Simmons, A. J., and B. J. Hoskins, 1977: Baroclinic instability on the sphere: solutions with a more realistic tropopause. J. Atmos. Sci., 34, 581-588.

Simmons, A. J., and B. J. Hoskins, 1978: The life cycles of some nonlinear baroclinic waves. J. Atmos. Sci., 35, 414-432.

Simpson, J., 1969: On some aspects of sea-air interaction in middle latitudes. Deep-Sea Res., Supp. to vol. 16, 233-261.

Spar, J., and R. Atlas, 1975: Atmospheric response to variations in sea-surface temperature. J. Appl. Meteor., 14, 1235-1245.

Staley, D. O., and R. L. Gall, 1977: On the wavelength of maximum baroclinic instability. J. Atmos. Sci., 34, 1679-1688.

Wei, M., 1979: The energy budgets of a developing cyclone over the East China Sea during the 1975 Air Mass Transformation Experiment. OU AMTEX Contribution No. 79-1, University of Oklahoma. 136pp.

Williams, R. T., 1965: Nonlinear, non-geostrophic effects in a baroclinic atmosphere. J. Atmos. Sci., 22, 388-401.

Winston, J. S., 1955: Physical aspects of rapid cyclogenesis in the Gulf of Alaska. Tellus, 7, 481-500.

INITIAL DISTRIBUTION LIST

		No. Copies
1.	Defense Technical Information Center Cameron Station Alexandria, VA 22314	2
2.	Library, Code 0142 Naval Postgraduate School Monterey, CA 93940	2
3.	Chairman (Code 63Rd) Department of Meteorology Naval Postgraduate School Monterey, California 93940	1
4.	Chairman (Code 68Mr) Department of Oceanography Naval Postgraduate School Monterey, California 93940	1
5.	Director Naval Oceanography Division Naval Observatory 34th and Massachusetts Avenue, NW Washington, D.C. 20390	1
6.	Commander Naval Oceanography Command NSTL Station Bay St. Louis, MS 39522	1
7.	Commanding Officer Naval Oceanographic Office NSTL Station Bay St. Louis, MS 39522	1
8.	Commanding Officer Fleet Numerical Oceanography Center Monterey, California 93940	1
9.	Commanding Officer Naval Ocean Research and Development Activity NSTL Station Bay St. Louis, MS 39522	1
10.	Commanding Officer Naval Environmental Prediction Research Facility Monterey, California 93940	1

11. Chairman, Oceanography Department 1
U.S. Naval Academy
Annapolis, MD 21402

12. Chief of Naval Research 1
800 N. Quincy Street
Arlington, VA 22217

13. Office of Naval Research (Code 480) 1
Naval Ocean Research and
Development Activity
NSTL Station
Bay St. Louis, MS 39522

14. Professor R. L. Elsberry (Code 63Es) 3
Department of Meteorology
Naval Postgraduate School
Monterey, California 93940

15. Lt. Scott A. Sandgathe (Code 63Ss) 2
Department of Meteorology
Naval Postgraduate School
Monterey, California 93940

16. Associate Professor R. L. Haney (Code 63Hy) 1
Department of Meteorology
Naval Postgraduate School
Monterey, California 93940

17. Associate Professor C. P. Chang (Code 63Cp) 1
Department of Meteorology
Naval Postgraduate Schol
Monterey, California 93940

18. Assistant Professor R. W. Garwood 1
(Code 68Gd)
Department of Oceanography
Naval Postgraduate School
Monterey, California 93940

19. Professor G. H. Jung (Code 68Jg) 1
Department of Oceanography
Naval Postgraduate School
Monterey, California 93940

20. Associate Professor A. L. Schoenstadt 1
(Code 53Zh)
Department of Mathematics
Naval Postgraduate School
Monterey, California 93940

21.	Assistant Professor C. H. Wash (Code 63Wy) Department of Meteorology Naval Postgraduate School Monterey, California 93940	1
22.	Dr. John R. Gyakum Department of Meteorology Massachusetts Institute of Technology Cambridge, MA 02139	1
23.	LCDR Donald E. Hinsman, Code 63 Department of Meteorology Naval Postgraduate School Monterey, California 93940	1
24.	Capt. John L. Hayes, Code 63 Department of Meteorology Naval Postgraduate School Monterey, California 93940	1

Thesis 194468
S1635
Sandgathe
c.1
A numerical study
of the role of air-sea
fluxes in extratropical
cyclogenesis.

The
S16
c.1

Thesis 194468
S1635 Sandgathe
c.1 A numerical study
of the role of air-sea
fluxes in extratropical
cyclogenesis.

thesS1635
A numerical study of the role of air-sea
3 2768 001 97732 5
DUDLEY KNOX LIBRARY